AD-A066 752 UNITED TECHNOLOGIES RESEARCH CENTER EAST HARTFORD CONN F/G 9/5
APPLICATION OF THE PSK DIODE-CORRELATOR FOR PROGRAMMABLE FREQUE--ETC(U)
APR 78 T W GRUDKOWSKI, T M REEDER N00173-76-C-0373
UNCLASSIFIED UTRC/R78-922667-18 NL

| OF |
ADA
066752

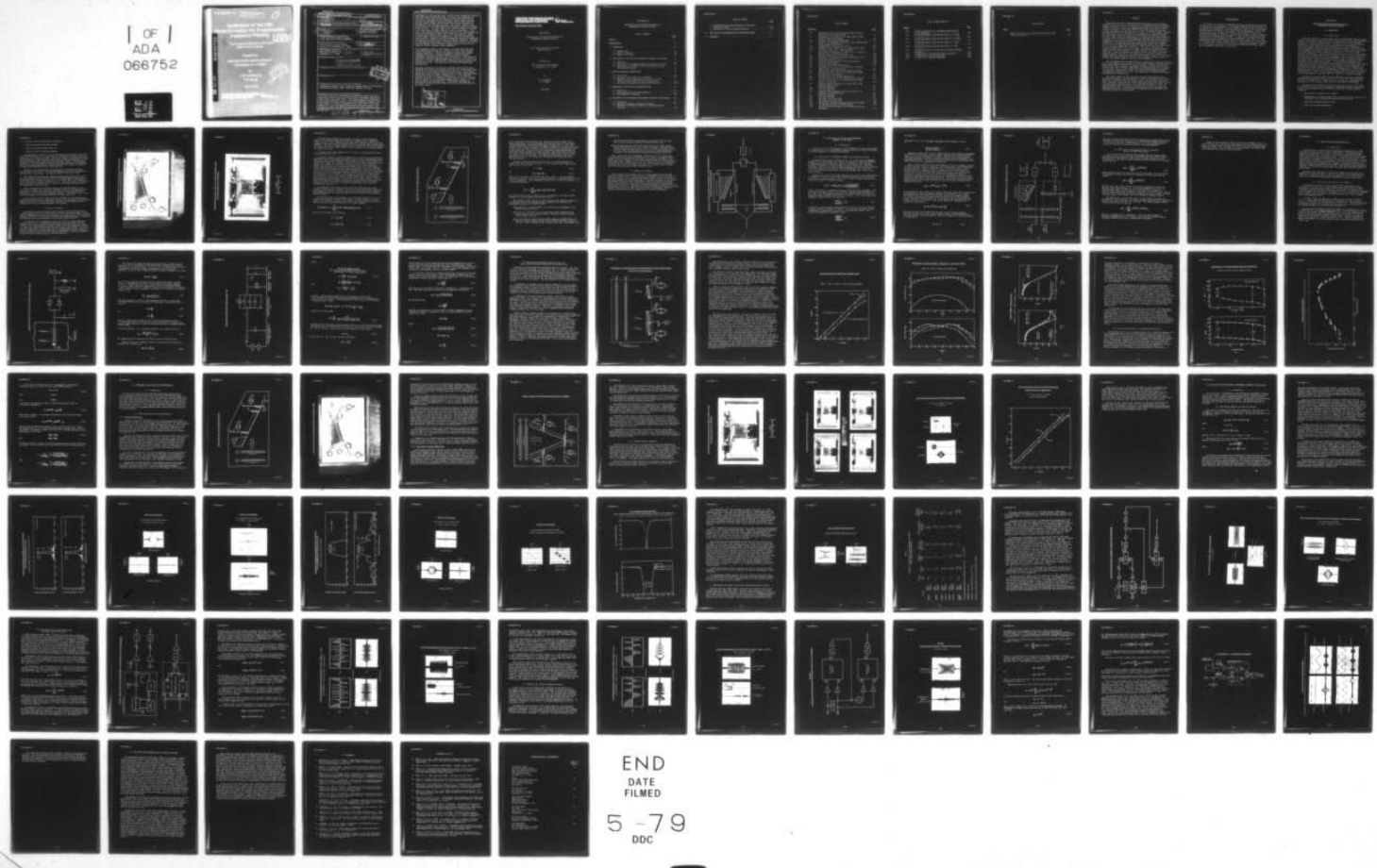

END
DATE
FILMED
5-79
DDC

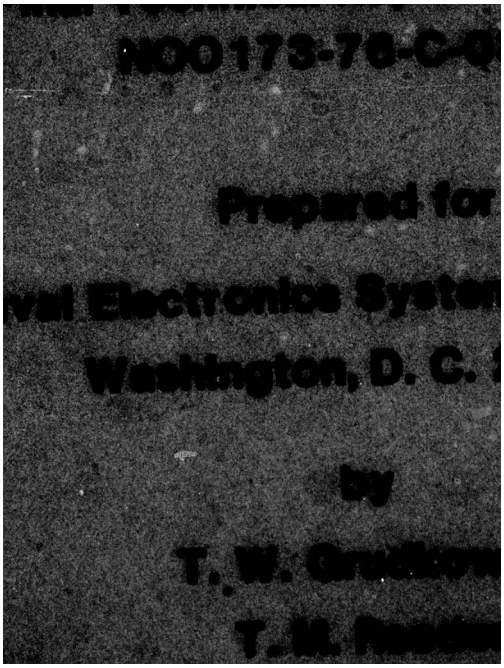

UNCLASSIFIED

SECURITY CLASSIFICATION OF THIS PAGE (When Data Entered)

(14) UTRC

REPORT DOCUMENTATION PAGE

READ INSTRUCTIONS BEFORE COMPLETING FORM

1. REPORT NUMBER: R78-922667-18	2. GOVT ACCESSION NO.
3. RECIPIENT'S CATALOG NUMBER: (9)	
4. TITLE (and Subtitle): (6) Application of the PSK Diode-Correlator to for [redacted] Programmable Frequency Filtering.	5. TYPE OF REPORT & PERIOD COVERED: Final Report. Oct. 1, '76-Apr. 28, '78. 1 Oct 76-28 Apr 78
	6. PERFORMING ORG. REPORT NUMBER
7. AUTHOR(s): (10) T. W./Grudkowski, T. M./Reeder	8. CONTRACT OR GRANT NUMBER(s): (15) N00173-76-C-0373
9. PERFORMING ORGANIZATION NAME AND ADDRESS: United Technologies Research Center, Silver Lane, East Hartford, Connecticut	10. PROGRAM ELEMENT, PROJECT, TASK AREA & WORK UNIT NUMBERS
11. CONTROLLING OFFICE NAME AND ADDRESS: Naval Electronics Systems Command, Crystal City, Washington, D.C. 20360	12. REPORT DATE: (11) 28 Apr [redacted] 1978
	13. NUMBER OF PAGES
14. MONITORING AGENCY NAME & ADDRESS (if different from Controlling Office): Naval Research Laboratory, 4555 Overlook Avenue, S.W., Washington, D. C. 20375 (12) 88p.	15. SECURITY CLASS. (of this report): Unclassified
	15a. DECLASSIFICATION/DOWNGRADING SCHEDULE

16. DISTRIBUTION STATEMENT (of this Report)

This document has been approved for public release and sale; its distribution is unlimited.

17. DISTRIBUTION STATEMENT (of the abstract entered in Block 20, if different from Report)

18. SUPPLEMENTARY NOTES

19. KEY WORDS (Continue on reverse side if necessary and identify by block number)

Programmable Frequency Filter, Correlation Matched Filter, PSK Correlation, Surface Acoustic Waves, Signal Processing, Integrated Circuits

20. ABSTRACT (Continue on reverse side if necessary and identify by block number)

This report describes an experimental and theoretical study of nonlinear tapped delay lines for use as an electronically programmable amplitude and phase weighted transversal filter. The Surface Acoustic Wave (SAW) delay line device studied here, which is called the Programmable Frequency Filter Module (PFFM), is a hybrid, integrated circuit device which utilizes SAW tapped delay lines and attached microelectronic diode and resistor arrays. The PFFM is based on the UTRC PSK Diode Correlator which underwent basic

DD FORM 1 JAN 73 1473 EDITION OF 1 NOV 65 IS OBSOLETE

UNCLASSIFIED

SECURITY CLASSIFICATION OF THIS PAGE (When Data Entered)

development as a 128 tap Phase Shift Key (PSK) signal encoder and correlator under NESC Contract N00014-75-C-0978. While the signal processing capabilities of the single acoustic channel PSK Diode Correlator rely on discrete tap programming in 0 and 180 degree relative phase increments, the dual acoustic channel PFFM described here utilizes continuous tap programming in both amplitude and phase. Each acoustic channel of the device consists of a P diode-tapped signal processing region and two input transducer ports. The input signal and cw reference voltages are applied to the input ports at center frequency f_1 and f_2, respectively. A low power, wide bandwidth nonlinear mixing process occurs at each diode tap and the difference frequency signals from all taps are summed at a common electrode comprising the filter output port. Rapid tap amplitude and biphase coding is achieved by controlling magnitude and polarity applied to the diode mixers located at each delay line tapping transducer. Continuous tap amplitude and phase coding of the dual acoustic channel filter results from the addition of the difference frequency outputs of the real and imaginary channels combined in phase quadrature.

The Programmable Frequency Filter Module, as a generalized transversal filter having equal tap spacing, is capable of a wide range of signal processing operations. These include adaptive bandpass and bandstop frequency filtering with variable bandshape and center frequency, programmable encoding and matched filter correlation of a wide variety of phase and/or amplitude coded waveforms such as PSK and chirp signals, and operation as a Chirp Z Transform (CZT) processor having an electronically variable chirp slope. These operations are studied and demonstrated experimentally.

The design, fabrication and testing of prototype 128 tap devices and a matched 64 tap PFFM pair are described which utilize lithium niobate delay lines and silicon on sapphire diode and resistor arrays. These devices operate with signal and output frequencies near 70 and 30 MHz respectively and have delay line tap spacing corresponding to a filter sampling frequency of 9.8 MHz. An improved balanced mixer tap design is utilized which is capable of a tap programming dynamic range in excess of 40 dB while minimizing the tap phase error. Perturbation techniques are described for eliminating the residual phase errors associated with the tap circuit design.

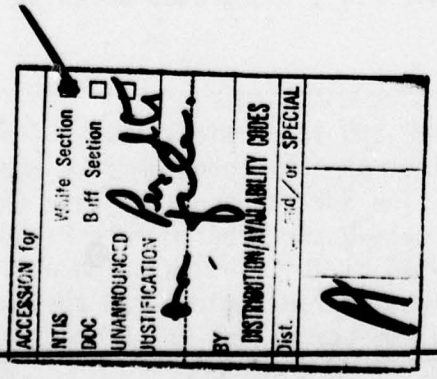

UNITED TECHNOLOGIES
RESEARCH CENTER

East Hartford, Connecticut 06108

R78-922667-18

Application of the PSK Diode-Correlator for Programmable Frequency Filtering

Final Technical Report on Contract
N00173-76-C-0373

Prepared for

Naval Electronics System Command
Washington, D. C. 20360

by

T. W. Grudkowski
T. M. Reeder

April 1978

R78-922667-18

Application of the PSK Diode-Correlator for Programmable Frequency Filtering

TABLE OF CONTENTS

TABLE OF CONTENTS

LIST OF FIGURES

LIST OF FIGURES (Cont'd)

LIST OF TABLES

ABSTRACT

This report describes an experimental and theoretical study of nonlinear tapped delay lines for use as an electronically programmable amplitude and phase weighted transversal filter. The Surface Acoustic Wave (SAW) delay line device studied here, which is called the Programmable Frequency Filter Module (PFFM), is a hybrid, integrated circuit device which utilizes SAW taped delay lines and attached microelectronic diode and resistor arrays. The PFFM is based on the UTRC PSK Diode Correlator which underwent basic development as a 128 tap Phase Shift Key (PSK) signal encoder and correlator under NESC Contract N00014-75-C-0978. While the signal processing capabilities of the single acoustic channel PSK Diode Correlator rely on discrete tap programming in 0 and 180 degree relative phase increments, the dual acoustic channel PFFM described here utilizes continuous tap programming in both amplitude and phase. Each acoustic channel of the device consists of a P diode-tapped signal processing region and two input transducer ports. The input signal and CW reference voltages are applied to the input ports at center frequency f_1 and f_2, respectively. A low power, wide bandwidth nonlinear mixing process occurs at each diode tap, and the difference frequency signals from all taps are summed at a common electrode comprising the filter output port. Rapid tap amplitude and biphase coding is achieved by controlling magnitude and polarity applied to the diode mixer located at each delay line tapping transducer. Continuous tap amplitude and phase coding of the dual acoustic channel filter results from the addition of the difference frequency outputs of the real and imaginary channels combined in phase quadrature.

The Programmable Frequency Filter Module, as a generalized transversal filter having equal tap spacing, is capable of a wide range of signal processing operations. These include adaptive bandpass and bandstop frequency filtering with variable bandshape and center frequency, programmable encoding and matched filter correlation of a wide variety of phase and/or amplitude coded waveforms such as PSK and chirp signals, and operation as a Chirp Z Transform (CZT) processor having an electgronically variable chirp slope. These operations are studied theoretically and demonstrated experimentally.

The design, fabrication and testing oof prototype 128 tap devices and a matched 64 tap PFFM pair are described which utilize lithium niobate delay lines and silicon on sapphire diode and resistor arrays. These devices operate with signal and output frequencies near 70 MHz and 30 MHz, respectively, and have delay line tap spacing corresponding to a filter sampling frequency of 9.8 MHz. An improved balanced mixer tap design is utilized which is capable of a tap programming dynamic range in excess of 40 dB while minimizing the tap phase error. Perturbation techniques are described for eliminating the residual phase errors associated with the tap circuit design.

ACKNOWLEDGMENTS

The authors are pleased to acknowledge the many contributions made by others during the course of the program. The successful construction and performance of the deliverable programmable filters and diagnostic devices constructed during the program are due in large part to the microelectronic expertise of B. Bujnarowski who fabricated these devices. The prototype 128 tap programmable filters, constructed under a prior program, were expertly fabricated by E. Branciforte. Detailed measurements of the device parameters were carried out with the competent assistance of W. Sheades and D. Kleeberg. R. Rukus provided valuable assistance in the construction of peripheral electrical components. The authors have also appreciated and have benefited from discussions with D. Webb of the U. S. Naval Research Laboratories and L. Sumney of the U. S. Naval Electronics Systems Command. A. J. DeMaria and M. Gilden have provided their enthusiasm and support. Thanks are also sincerely expressed to the Illustrations and Word Processing Groups for help in assembling this report in final form.

Application of the PSK Diode-Correlator for Programmable Frequency Filtering

1.0 INTRODUCTION

1.1 Program Scope

This report describes an exploratory research and development program directed toward the development of a state-of-the-art Surface Acoustic Wave (SAW) Programmable Frequency Filter Module (PFFM) for use as an electronically variable bandpass, bandstop and correlation matched filter. The PFFM is based on the UTRC PSK Diode-Correlator, a unique SAW device that utilizes nonlinear mixing phenomena in a hybrid semiconductor tapped delay line configuation. The basic development of a 128 tap programmable PSK Diode-Correlator/Encoder Module which could be cascaded to process biphase code lengths of 1024 chips or more at 10 MHz chip rates was carried out at UTRC under NESC Contract N00014-75-C-0978 (Ref. 1). While the signal processing capabilities of the PSK Diode-Correlator relied on discrete tap programming in 0 and 180 degree relative phase increments, the dual acoustic channel PFFM described here utilizes continuous tap programming in both amplitude and phase. A much wider range of signal processing applications results, including the encoding and matched filter correlation of a wide variety of phase and amplitude coded waveforms such as PSK and chirp signals. As a generalized transversal filter having equal tap spacing, the PFFM is also capable of adaptive bandpass and bandstop filtering with separate control of the filter bandwidth and center frequency. A third application area involves the use of the PFFM as a Chirp Z Transform (CZT) processor. The CZT is performed by programming the PFFM taps as a chirp filter whose response is related to the discrete Fourier transform of the video modulation applied at an input port. By electronically varying the chirp slope, the rate of the CZT response may be altered to best suit a particular system's requirement.

The signal processing capabilities of the PFFM take advantage of a powerful nonlinear mixing process occurring at each of the filter taps. The output from each tap of a single acoustic channel device is electronically programmable in amplitude over a 40 dB dynamic range and in 0 or 180 degree relative phase.

Continuous phase programming is achieved in the dual acoustic channel PFFM by combining the outputs from the separately programmable channels in phase quadrature. The resulting processor configuration offers the following important advantages:

* High processor bandwidth (10 to 100 MHz),
* Programmable tap control by application of mA range dc bias currents to the integrated circuit, biphase mixer associated with each tap,
* High tap reprogramming speed (<1 μsec),
* Small size and power dissipation,

* Low cost hybrid microelectronic construction,

* Long code processing by module cascade,

* Large input/output dynamic range, and

* Accurate signal processing performance.

These advantages, coupled with the diverse applications mentioned previously, offer significant potential for satisfying the requirements of present and future communication and navigation systems. The present program has been directed toward the development of a module having 64 amplitude and biphase programmable taps (32 complex tap weights) with 10 MHz processing bandwidth. However, straightforward development of the hybrid SAW/integrated circuit configuration would considerably extend the processing capability to 100 MHz bandwidths, well above the capability of competitive programmable charge transfer devices.

The goal of the program has been to demonstrate the important advantages and operational capabilities of the UTRC Programmable Frequency Filter Module as a general purpose filter module. The program consisted of two major tasks:

Task I was directed toward the detailed characterization and utilization of the two Government Furnished Property (GFP) 128 tap PSK Diode-Correlator modules developed under the previous Navy contract as a prototype PFFM. A photograph of one of these 128 tap modules is shown in Fig. 1-1. Under this task, a new balanced mixer tap design was developed which extended the tap programming dynamic range while reducing the tap phase error.

Task II considered the design and operation of a matched PFFM pair, each consisting of 64 amplitude and biphase programmable taps of the improved balanced mixer design. Complex tap coefficient values were achieved by the quadrature combination of two 32 tap real and imaginary channels. A photograph of one of the four 32 tap channels of the matched PFFM pair is shown in Fig. 1-2.

The program successfully demonstrated that the PFFM could be configured and operated as a state-of-the-art generalized transversal filter capable of programmable bandpass and bandstop frequency filtering, dispersive and nondispersive signal encoding and correlation, and programmable CZT processing.

1.2 Method of Approach

The nonlinear interaction between surface acoustic waves propagating within a diode-coupled tapped delay line has been utilized for achieving a number of high speed, programmable signal processing functions. Early applications of the nonlinear phenomena have included electronically variable radar signal convolution, correlation, and real time Fourier transformation of video input signals (Ref. 2-7).

The application as a programmable transversal filter for biphase PSK coded signals resulted from an improved diode mixer tap configuration (Ref. 8) which permitted electronically controlled phase reversal of the nonlinear output signal at a given tap. These PSK Diode-Correlator devices have been developed in the form of 128 tap programmable modules under the previous Navy contract (Ref. 1) and have formed the basis for the present application to programmable frequency filtering. This more general application follows from the capability for electronic amplitude weighting as well as phase reversal at the PSK diode taps.

FIG. 1-1

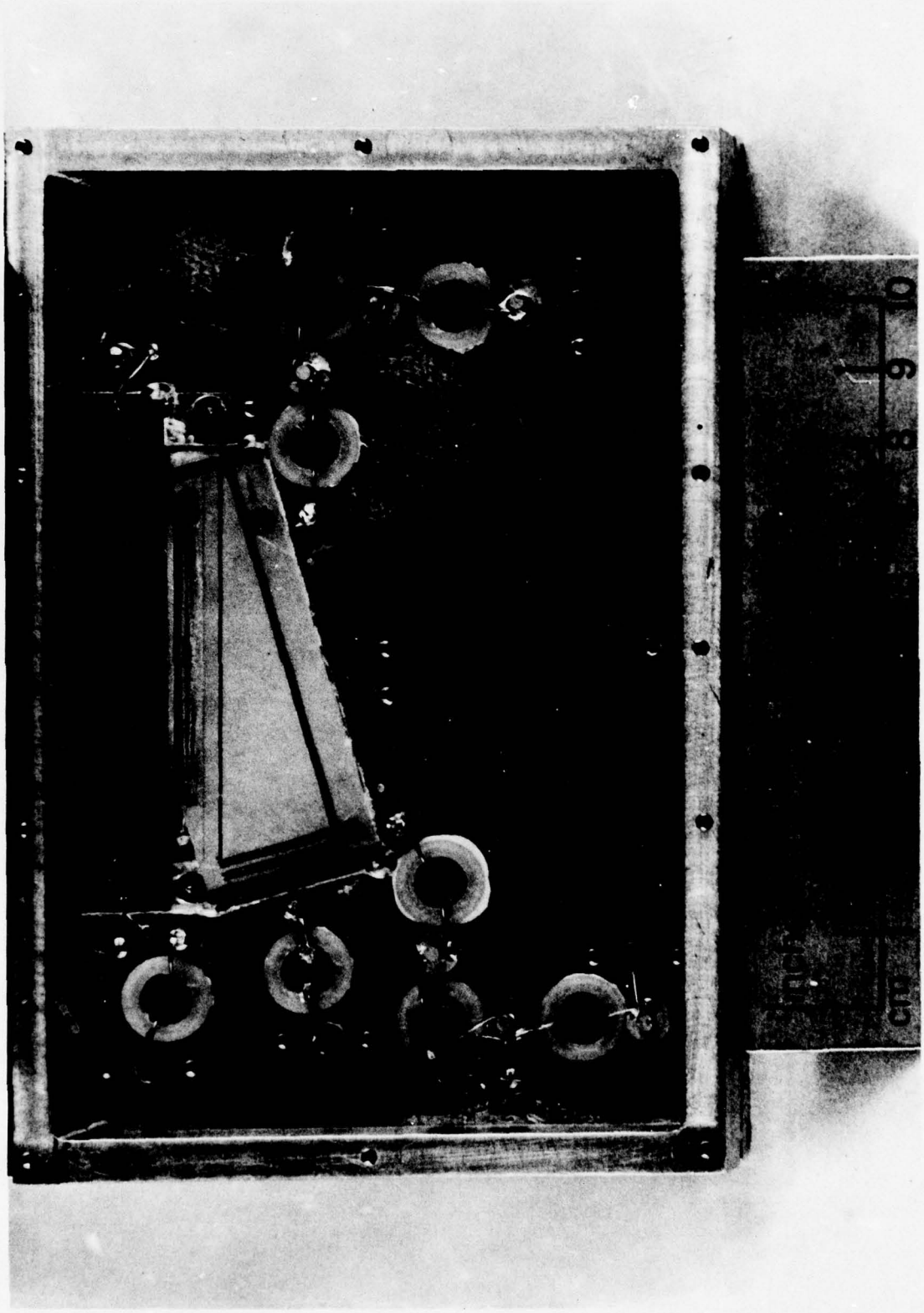

PHOTOGRAPH OF ONE OF TWO 128 TAP PSK DIODE CORRELATOR MODULES USED AS A PROTOTYPE PFFM

FIG. 1–2

PHOTOGRAPH OF ONE OF FOUR 32 TAP SINGLE CHANNEL PFFMs
DELIVERED UNDER THIS PROGRAM

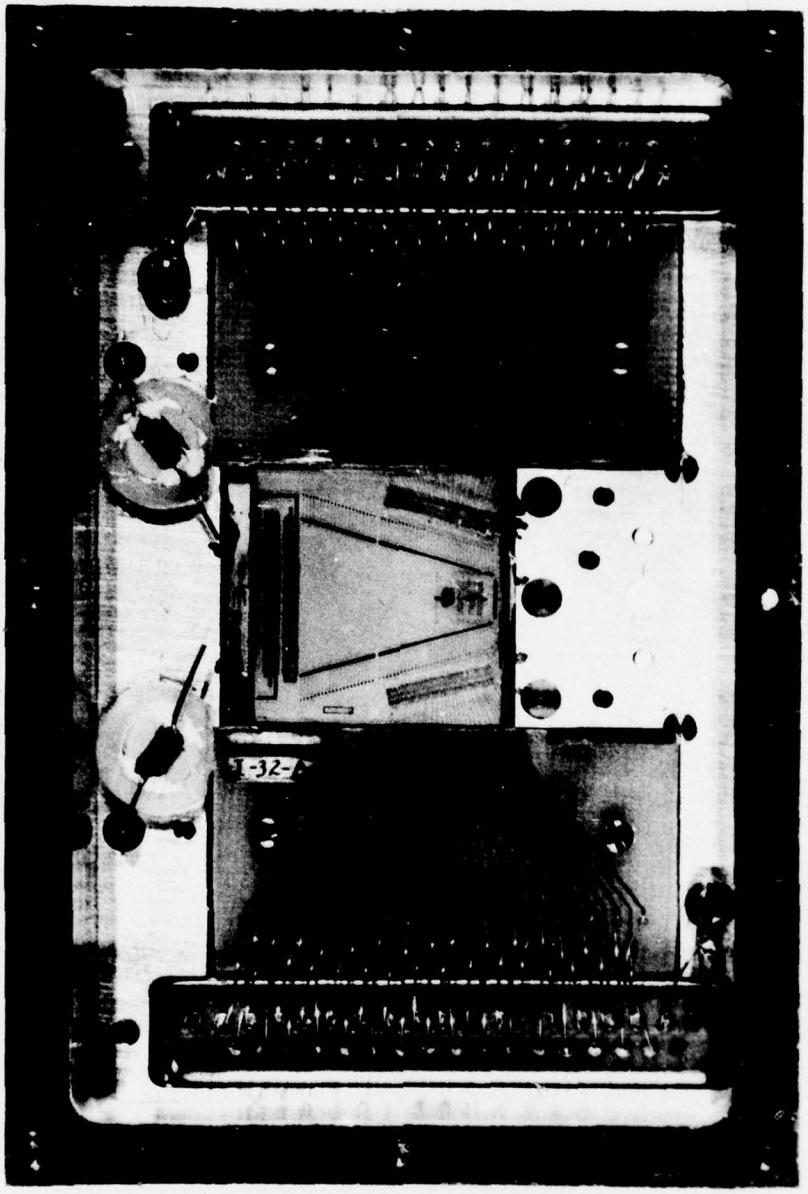

The PSK Diode-Correlator thus performs as a single channel Programmable Frequency Filter Module (PFFM) having positive and negative real coefficient values. As such, several important filter types may be realized including variable bandpass filters and correlation matched filters for amplitude and/or biphase coded waveforms. The filter synthesis capabilities are considerably extended by combining the output of two single channel PFFM's in phase quadrature thus providing complex tap coefficient values.

The basic single channel PFFM structure is that of the PSK Diode-Correlator shown schematically in Fig. 1-3.

The device is based on the hybrid combination of a high quality piezoelectric tapped delay line and an attached integrated circuit array of semiconductor diodes. Two surface acoustic wave transducers are provided on the LHS of the piezoelectric substrate for excitation of acoustic signals which are directly proportional to the applied input signal, $V_1(t)\exp(j\omega_1 t)$, and to a local oscillator reference signal, $V_2(t)\exp(j\omega_2 t)$. The two acoustic signals travel to the right toward a special inclined tapping and nonlinear signal processing array which consists of broad bandwidth SAW transducers and attached semiconductor diode pairs. As shown in Fig. 1-3, the diode pairs are arranged in antiparallel, and the P transducer-tap/diode-pair circuits are connected in parallel with an output port where a signal $V_3(t)\exp(j\omega_3 t)$ is to be received. The operation of the device is based upon the properties of small signal, product mixing obtained when voltages induced at a given tap due to the presence of acoustic waves 1 and 2 cause currents to flow through the diode-pair attached to the subject tap. Nonlinear mixing in the diode which is forward-biased produces a current and voltage with sum or difference frequency ($\omega_3 = \omega_2 \pm \omega_1$) which is accurately proportional to the product of waveforms $V_1(t)$ and $V_2(t)$.

By designing the individual tap circuits to have relatively high series impedance (say 1000 ohms), a sample of the product signal developed at a given tap can be supplied to the Port 3 output load circuit with a minimum of interference from loading and spurious signal excitation due to the other P-1 taps circuits in parallel at Port 3.

The PSK devices have been designed for use with input signals at $f_1 = \omega_1/2\pi$ = 70 MHz, local oscillator reference signal near f_2 = 100 MHz, and Port 3 output signal at the difference frequency, f_3 = 30 MHz. The voltage relationship at the three ports is well represented by the serial product expression

$$V_3(t)\exp(j\omega_3 t) = H_T \sum_{p=0}^{P-1} g_p V_1^*(t_1)\, V_2(t_2) \exp\left(j\omega_2 t_2 - j\omega_1 t_1\right) \qquad (1\text{-}1)$$

where the time variables are defined by

$$t_1 = t - t_{01} - p\Delta T \qquad (1\text{-}2)$$

$$t_2 = t - t_{02} - p\Delta T \qquad (1\text{-}3)$$

FIG. 1–3

PROTOTYPE 128 TAP PFFM CONFIGURATION

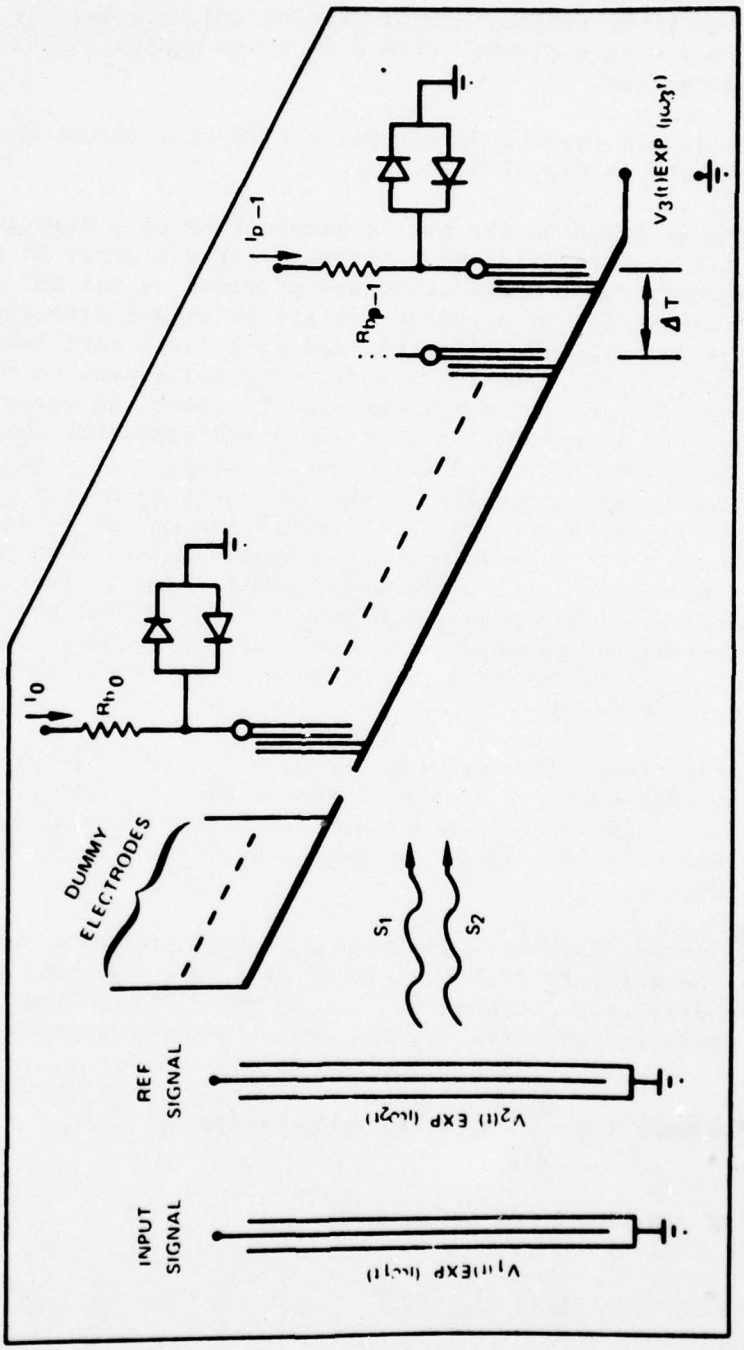

and t is the input time coordinant, t_{01}, t_{02} are the acoustic transit times between transducers 1 and 2 and interaction region tap 0, and ΔT is the transit time between adjacent interaction region taps. The factor H_T is a three port transfer function which represents the frequency reponse due to acoustic excitation at Ports 1 and 2 and due to acoustic detection at any one of the identical interaction region taps. The factor g_p is an electronically programmable weighting coefficient which represents the relative product term output from the pth tap. This factor can be adjusted over a wide amplitude range by adjusting the current I_{bp} applied to the pth diode-pair. The sign of g_p corresponds to the sign of applied bias current. It is convenient to define H_T so that g_p varies over the range $-1 \leq g_p < +1$.

In order to simplify analysis with Eq. (1-1), it is also convenient to redefine the input time frame so that t = 0 occurs when the input signal reaches tap 0. Thus, in this case,

$$t_1 = t - p\Delta T \tag{1-4}$$

and

$$t_2 = t - t_{OS} - p\Delta T \tag{1-5}$$

where t_{OS} is the offset time between input Ports 1 and 2. Since the reference signal $V_2(t)\exp(j\omega_2 t)$ is used as a CW local oscillator, we can define $V_2(t) = 1$ with no loss in generality. Then, remembering that $\omega_3 = \omega_2 - \omega_1$, Eq. (1-1) reduces to the waveform expression

$$V_3(t) = H_T' \sum_{p=0}^{P-1} g_p \exp(-j\omega_3 p\Delta T)\, V_1^*(t - p\Delta T) \tag{1-6}$$

where $H_T' = H_T \exp(-j\omega_2 t_{OS})$. Equation (1-6) is recognized as the serial product convolution of $g_p \exp(-j\omega_3 p\Delta T)$ with waveform $V^*_1(t)$.

The strikingly simple form of Eq. (1-6) reveals several important features of the PSK Diode-Correlator configuration which illustrate its usefulness as a Programmable Frequency Filter Module (PFFM):

- The factor $h_p = g_p \exp(-j\omega_3 p\Delta T)$ is an electronically programmable filter impulse response function,
- If $V_1(t)$ is a CW signal, Eq. (1-6) gives the Fourier transform of tap coefficients g_p and is therefore equal to the serial product frequency filter response function,
- If the interaction region taps are equally spaced (as assumed above), the time and frequency response of Eq. (1-6) is exactly the same as would be seen for a linear interdigital SAW transducer with time T equi-spaced taps

and electrode apodization corresponding to tap coefficients g_p, except that the output carrier frequency is shifted from f_1 to f_3,

- If the spacing between interaction region taps of the single acoustic channel PFFM shown in Fig. 1 were chosen to represent a nonlinear phase function versus tap time position t_p (i.e., a radar chirp variation, etc.), Eq. (1-6) could represent any type of dispersive or nondispersive SAW transducer - with electronically variable tap weighting coefficients.

Thus, the electronically programmable characteristics of a single Diode-Correlator PFFM will be quite general and can be utilized to synthesize a great variety of filter characteristics realizable using positive and negative real coefficient values. However, as will be described in Section 2, the dual acoustic channel PFFM, shown schematically in Fig. 1-4, provides both real and imaginary tap coefficient values, thus permitting dispersive or nondispersive filtering within the same equi-spaced tapped transversal filter.

1.3 Summary of the Report

The following report begins in Section 2 with a description of the PFFM operating principles and its applications as a programmable transversal filter. A theoretical analysis of the tap weighting characteristics is given in Section 3 which also compares the experimental amplitude and phase response of the prototype and optimized diode mixer tap configuations. Section 4 describes the design, fabrication, and characterization of the prototype 128 tap and the 64 tap dual acoustic channel devices. The signal processing performance of these devices is demonstrated in Section 5. Experimental results for bandpass and bandstop filtering, PSK and chirp matched filtering, and CZT processing are presented. Section 6 provides conclusions and gives recommendations for further development.

FIG. 1-4

SCHEMATIC OF PROGRAMMABLE TRANSVERSAL FILTER HAVING EQUALLY SPACED, COMPLEX COEFFICIENTS

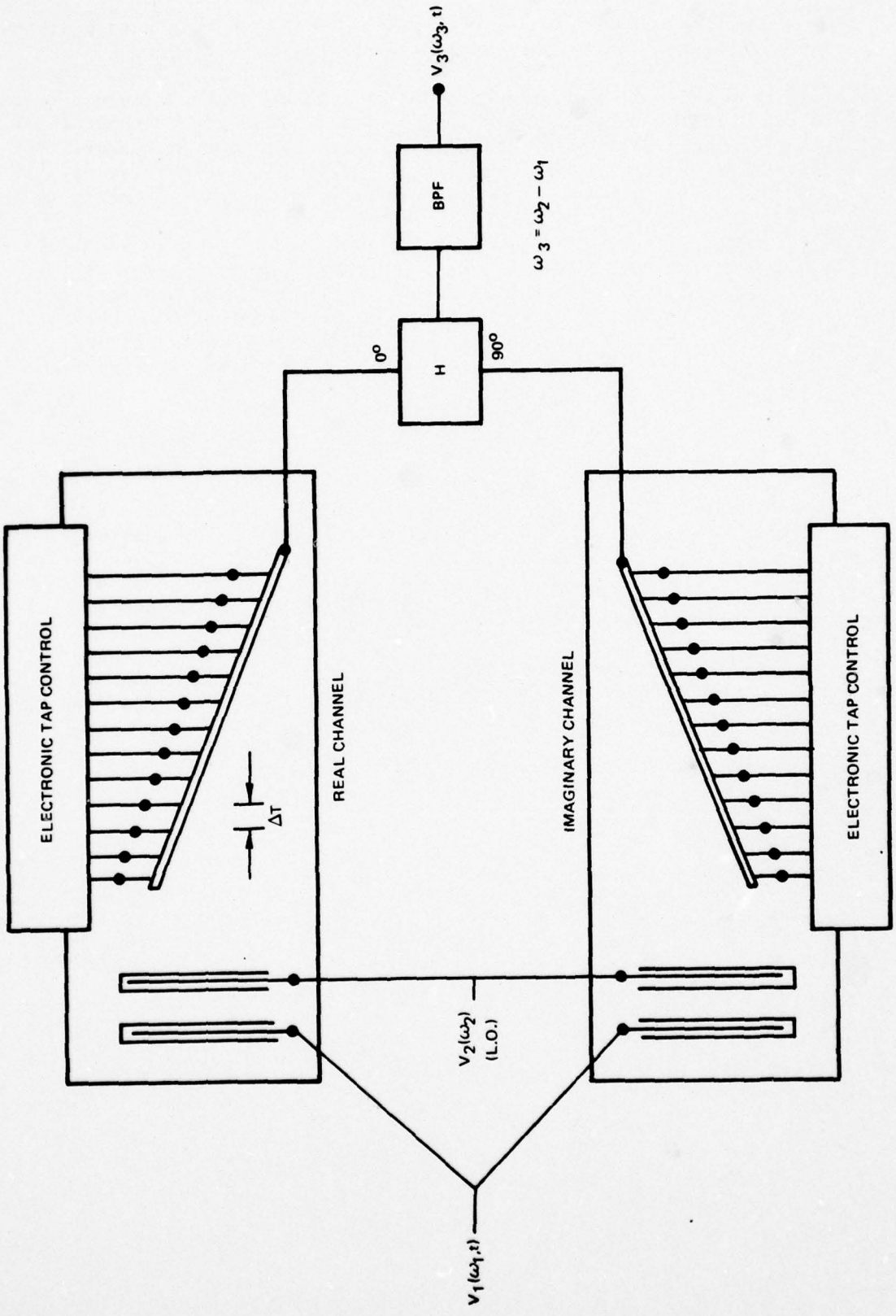

78-04-311-2

2.0 APPLICATIONS OF THE UTRC SAW PROGRAMMABLE FREQUENCY FILTER MODULE

2.1 Introduction

In this section, the applications of the Programmable Frequency Filter Module are summarized for use as a programmable bandpass, bandstop or correlation matched filter for dispersive or nondispersive waveforms.

2.2 Application to Programmable Bandpass and Bandstop Filtering

The PSK Diode-Correlator, as shown in Fig. 1-3, is basically a programmable bandpass filter which accepts input signals at frequency f_1, provides filtering by applying the acoustic signal to a series of P multiplier taps, and super heterodyne translates the filtered signal to output frequency f_3. The center frequency of the filter is tuned by simply adjusting the local oscillator frequency f_2, and the complex filter frequency response (bandshape, skirt selectivity, etc.) is controlled by adjusting the set of bias currents that control the tap coefficients g_p.

A simple way to assess the overall usefulness of a given P tap Diode-Correlator as a PFFM is to consider the CW signal frequency response when the tap coupling coefficients are equal (say $g_p=1$). The Port 1 to Port 3 transfer function then has a sin x/x type of frequency response,

$$V_3/V_1 = H'_T \exp\left[-j2(P-1)f_3/f_s\right]\left[\frac{\sin \pi P f_3/f_s}{\sin \pi f_3/f_s}\right] \qquad (2\text{-}1)$$

which is expected for a bandpass transversal filter with equal tap weights. The quantity f_s introduced in Eq. (2-1) is a device sampling frequency defined by $f_s = 1/\Delta T$. The 3 dB bandwidth obtained with the sin x/x filter is close to the minimum bandwidth obtainable with a given P tap filter. Thus, the minimum filter bandwidth is expected from (2-1) to be near

$$\begin{matrix}\text{minimum} \\ \text{bandwidth}\end{matrix} = f_s/P. \qquad (2\text{-}2)$$

In addition, the filter output described by Eq. (2-1) has a series of identical harmonics centered at multiples of f_s which can be selected by design of input transducers at frequencies f_1, f_2 and choice of output port filter. As a result, the maximum usable bandwidth is near

$$\begin{matrix}\text{maximum} \\ \text{usable} \\ \text{bandwidth}\end{matrix} = f_s. \qquad (2\text{-}3)$$

Consequently, the ratio of maximum programmable filter bandwidth is close to

$$\frac{\text{maximum bandwidth}}{\text{minimum bandwidth}} = P \qquad (2\text{-}4)$$

Obviously, a wide range of filter characteristics can be created by programming the PFFM tap coefficients to specific values. Tancrell (Ref. 9) has shown that a number of very useful bandpass filter response characteristics can be obtained with fixed interdigital electrode transducer filters by properly choosing the electrode tap coefficients. We can use these same coefficients in the Diode-Correlator PFFM by electronically programming the diode taps.

While the basic Diode-Correlator PFFM appears best suited to bandpass filtering, a similar configuration can be employed to provide convenient control of bandstop or notch filtering. Figure 2-1 shows how this is done using one of the PSK Diode-Correlators as a bandpass filter in combination with a second delay line. Alternatively, this could be done more effectively using a single SAW substrate. In Fig. 2-1 the input (f_1) and local oscillator (f_2) signals are applied to two parallel acoustic paths; one path has a P tap programmable interaction region identical to the bandpass PFFM discussed earlier, and the second path has a single output transducer with attached diode multiplier. After filtering, amplifying and combining the outputs of these two channels, we have produced a combined filter response of the form

$$V_3/V_1 = e^{-j\theta_P} H_P Q_P + e^{-j\theta_1} H_1 \qquad (2\text{-}5)$$

where subscripts P and 1 refer to the acoustic paths with P and 1 taps, respectively. Q_P represents the frequency dependent response of the bandpass filter channel. The combined input and multiplier tap transfer functions are denoted by H_P and H_1; these two functions can be made nearly identical by careful SAW transducer design. Moreover, the phase delays for the two delay paths can be made to differ by exactly π radians ($\theta_P = \theta_1 + \pi$). With careful design, the combined filter response will be given by

$$V_3/V_1 \cong e^{-j\theta_1} H_1 \left[1 - Q_P(f_3/f_s)\right]. \qquad (2\text{-}6)$$

This type of filter will provide high insertion loss at an output frequency which is a multiple of f_s, but can be designed to pass all other frequencies in the band with very little perturbation. Since the frequency of "notch" attenuation is controlled by

$$f_3 = f_2 - f_1, \qquad (2\text{-}7)$$

FIG.2-1

PROGRAMMABLE DUAL CHANNEL NOTCH FILTER

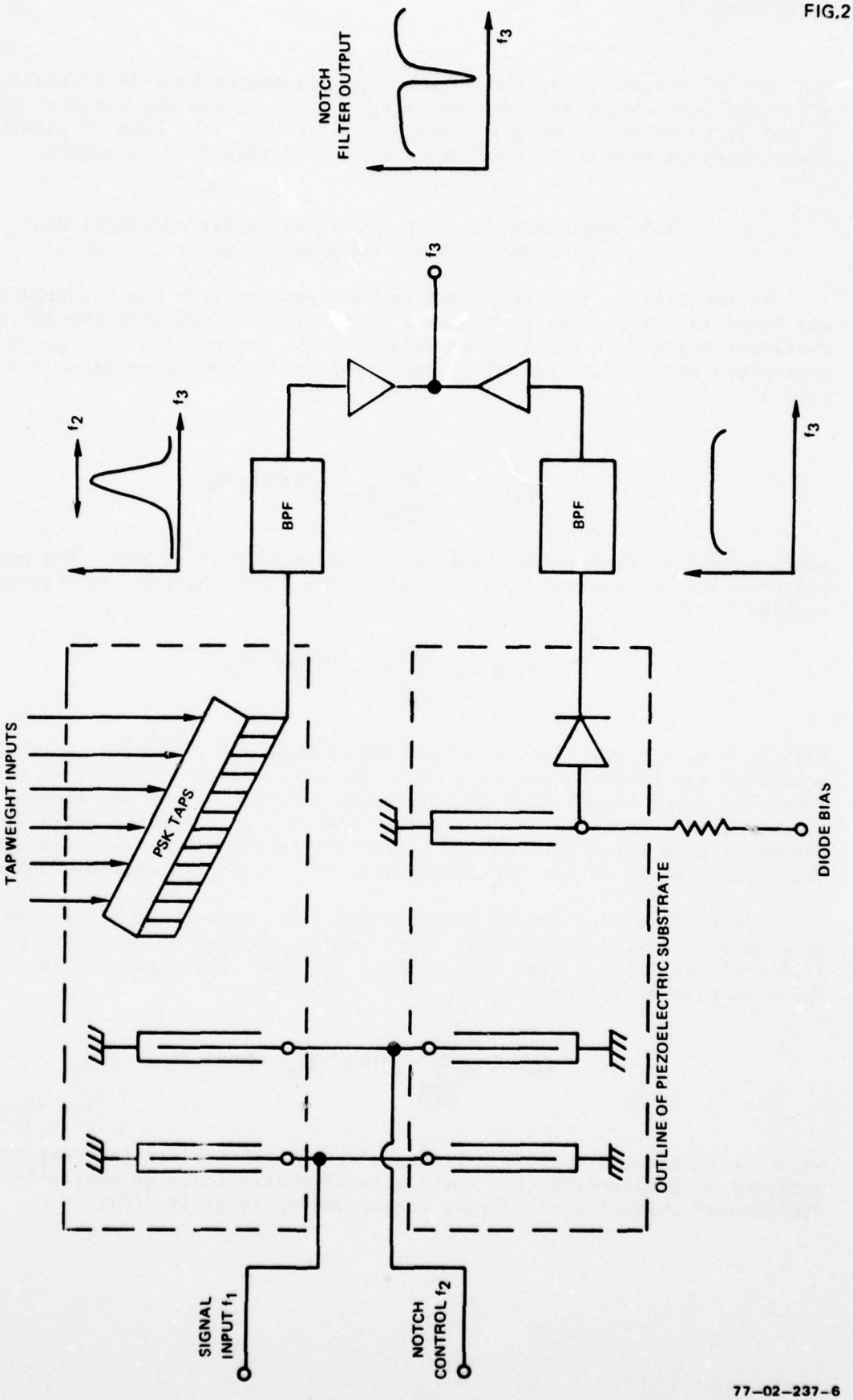

77-02-237-6

the "notch" frequency as seen in the input frequency band is controlled by simply adjusting local oscillator frequency f_2. By designing the bandpass response at f_1 and f_2 to be flat over a bandwidth equal to f_s, it should be possible to create very uniform notch characteristics over this same bandwidth.

2.3 Application as a Generalized Filter for Amplitude and/or Phase Modulated Signals

In the filters just described we have assumed that the P tapped region was fixed in tap spacing at the time of fabrication and that the desired PFFM characteristics were obtained by adjusting the tap coefficients g_p in some prescribed way. This type of filter provides an impulse response for equi-spaced taps of the form

$$V_3(t) = H'_T \sum_{p=0}^{P-1} g_p \, e^{-j2\pi p f_3/f_s} \tag{2-8}$$

where g_p may be positive or negative but must be real valued. The most general filter would, of course, have a similar form where the tap coefficients are complex:

$$V_3(t) = H'_T \sum_{p=0}^{P-1} C_p \, e^{-j2\pi p f_3/f_s} \tag{2-9}$$

with $C_p = A_p + j\,B_p$. Such a filter can be built by combining two precisely matched P tap Diode-Correlators as is illustrated schematically in Fig. 1-4. There the input signal (f_1) and the local oscillator (f_2) are applied to identical dual acoustic path transducers as was done for the notch filter, and the output of each P tap interaction region is combined in a hybrid coupler to provide the correct phase offset between "real" and "imaginary" component channels.

The PFFM in Fig. 1-4 has applications in a wide range of dispersive and nondispersive filter operation. For example, suppose a dispersive pulse compression filter of the Chirp-Z type (Ref. 10) is desired. The impulse response function for this type of filter is given by

$$V_3(t) = H'_T \sum_{p=0}^{P-1} e^{-j\pi p^2/P} \, e^{-j2\pi p f_3/f_s} \tag{2-10}$$

where it is assumed that $f_3 = (\text{integer}) f_s$. This very complex response is achieved by programming the "real" channel coefficients as $\cos(\pi p^2/P)$ and the "imaginary" channel coefficients corresponding to $\sin(\pi p^2/P)$.

Perhaps the most attractive feature of the device diagrammed in Fig. 1-4 is the fact that such a relatively simple module could be utilized as either an encoder or matched filter correlator for diverse and rapidly programmed system transmission modes. Thus, the same units could be equally well used for PSK, chirp, and many other types of signal modulation.

3.0 PFFM TAP WEIGHTING CHARACTERISTICS

3.1 Introduction

In this section, the theoretical and experimental dependence of the PFFM tap weights on tap dc control current is investigated. An equivalent circuit model of the diode mixer tap is used to develop the tap amplitude and phase weighting characteristics. This model is then ued for comparison with the experimental data for the tap configuration studied. In addition to the single sided diode mixer tap utilized in previous PSK diode correlator designs (Ref. 1), a new balanced mixer tap geometry is investigated. This new design is shown to overcome many of the previous tap weighting error sources by discriminating between the desired nonlinear output signal and the fundamental frequency and spurious signal components normally present at the output port. Good agreement between theory and experiment is found for the balanced mixer tap design over a 40 dB tap control dynamic range.

The phase of the tap output is found to vary slowly as a function of tap weighting in a predictable manner. While the 15 degree variation observed over a 35 dB control range represents a modest programming error, this error source is shown to be eliminated by using perturbed complex tap weighting coefficients.

3.2 Equivalent Circuit Model for the PFFM Tap

As described in Section 2, the most general PFFM configuration of Fig. 1-4 consists of a dual acoustic channel geometry which permits both continuous amplitude and continuous phase control of the dual channel tap outputs. This continuous weighting is provided by quadrature addition of the separately programmable real tap weights of each channel. The analysis of the single channel tap circuit which follows is thus quite general and applies directly to the case of complex filter tap weighting as well.

A schematic view of the pth tap of a single acoustic channel is shown in Fig. 3.1. Input signal and reference waves at frequencies f_1 and f_2, respectively, are detected by the pth interdigital transducer tap. The detected voltages, V_{g1} and V_{g2} are applied to an antiparallel diode pair which is in series with the tapping transducer and the output load resistance, R_L.

Nonlinear sum and difference frequency components at frequencies $f_3 = f_3 \pm f_1$ are generated within the forward biased diode (Refs. 1-8) and subsequently filtered to select the difference frequency component. Earlier nonlinear diode-coupled delay line devices have used a single bias dependent diode mixer to control the amplitude of the generated difference frequency signal. However, by using two diodes in the antiparallel connection shown in Fig. 3.1, both the amplitude and phase ($\pm$ 180 degrees) of the tap nonlinear output are controlled by the dc bias current, I_{bp}.

FIG. 3-1

SCHEMATIC VIEW OF THE p^{th} TAP OF A SINGLE CHANNEL PFFM

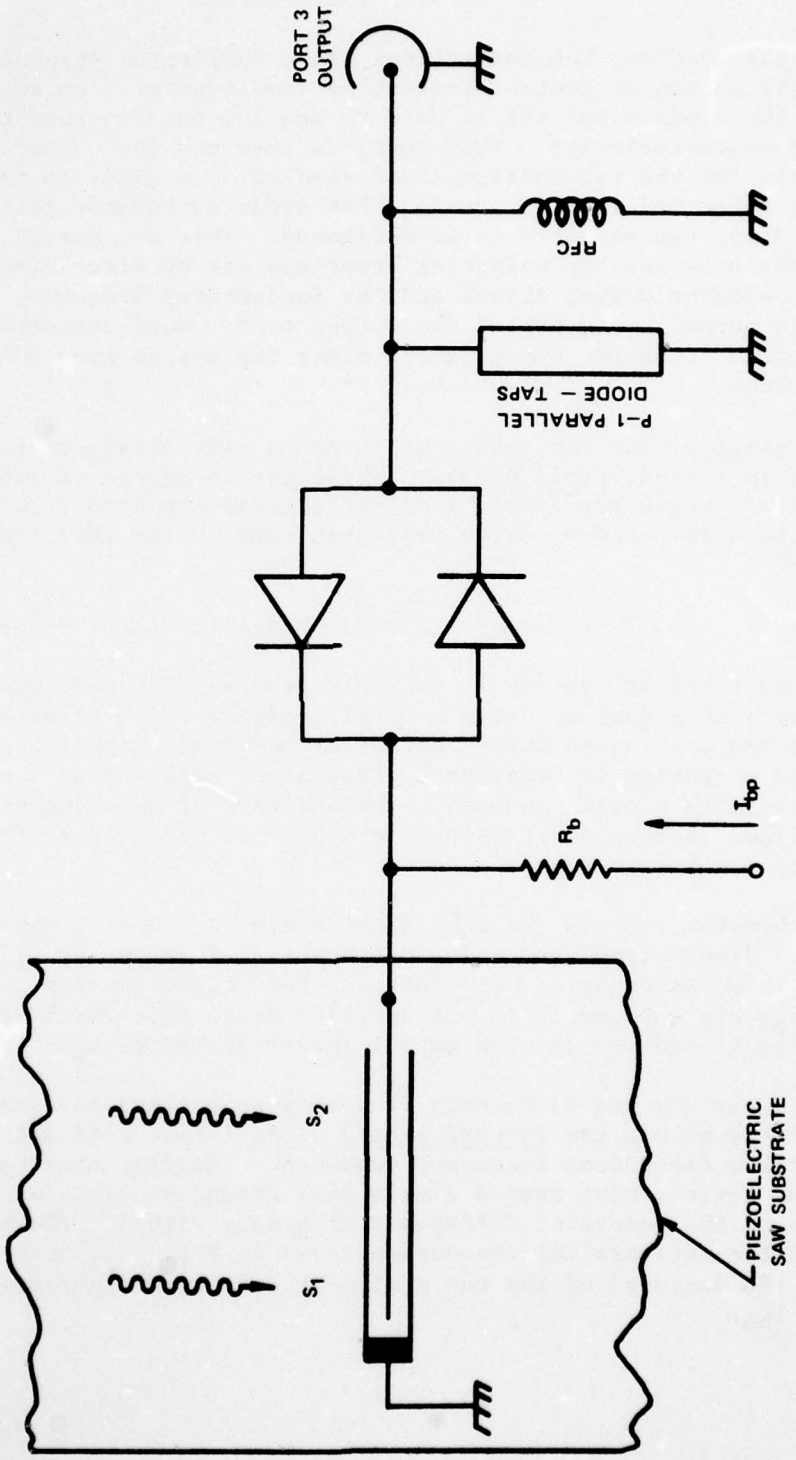

76-09-229-9

The relationship between the generated nonlinear output voltage from the pth tap and the dc bias applied to the diode mixer is determined by using the equivalent circuit representation of Fig. 3-2. The interdigital delay line tap is represented by voltage V_{g1} and V_{g2}, corresponding to tap excitation at frequencies f_1 and f_2, and a frequency dependent transducer impedance, Z_{gi}, given by

$$Zgi = Rai + \frac{1}{j\omega_i C_T} \tag{3-1}$$

R_{ai} is the tap radiation resistance and C_T is the tap capacitance. The subscript, i, corresponds to the value of these quantities at radian frequency $\omega_i = 2\pi f_i$. A shunt capacitance, C_{SH}, accounts for the fringing capacitance to ground resulting from wire connections and the tap bonding pads. The diode rf circuit includes a current independence resistance, R_s, in series with a parallel impedance, Z_b,

$$Z_{bi} = \frac{1}{G_b + j\omega_i (C_b + C_J)} \tag{3-2}$$

where the subscript, b, refers to bias dependent quantities., G_b and C_b are the forward biased diode rf conductance and capacitance, respectively (Ref. 11) given by

$$G_b = \frac{I_b}{V_q} \tag{3-3}$$

and

$$C_b = \frac{I_b \tau}{2V_q} \tag{3-4}$$

where V_q is the thermal voltage (equal to .040V at room temperature) and τ is the minority carrier lifetime. The fixed capacitance, C_J, represents the parasitic diode capacitance of the reverse biased diode which is assumed constant to first order

The current generator at the difference frequency, f_1, is given by (Ref. 5).

$$I_{g_3} = -\frac{[G_b + j\omega_3 C_b]}{2V_q} V_{D1}^* V_{D2} \tag{3-5}$$

The impedance $Z_p/(P-1)$ represents the effect of the (P-1) parallel taps.

The Port 3 voltage at frequency f_3 which is induced across R_L due to the pth diode-tap is found to be

$$V_{3p} = H_p V_{g1}^* V_{g2} \tag{3-6}$$

FIG. 3-2

EQUIVALENT CIRCUIT FOR A SINGLE DIODE-TAP

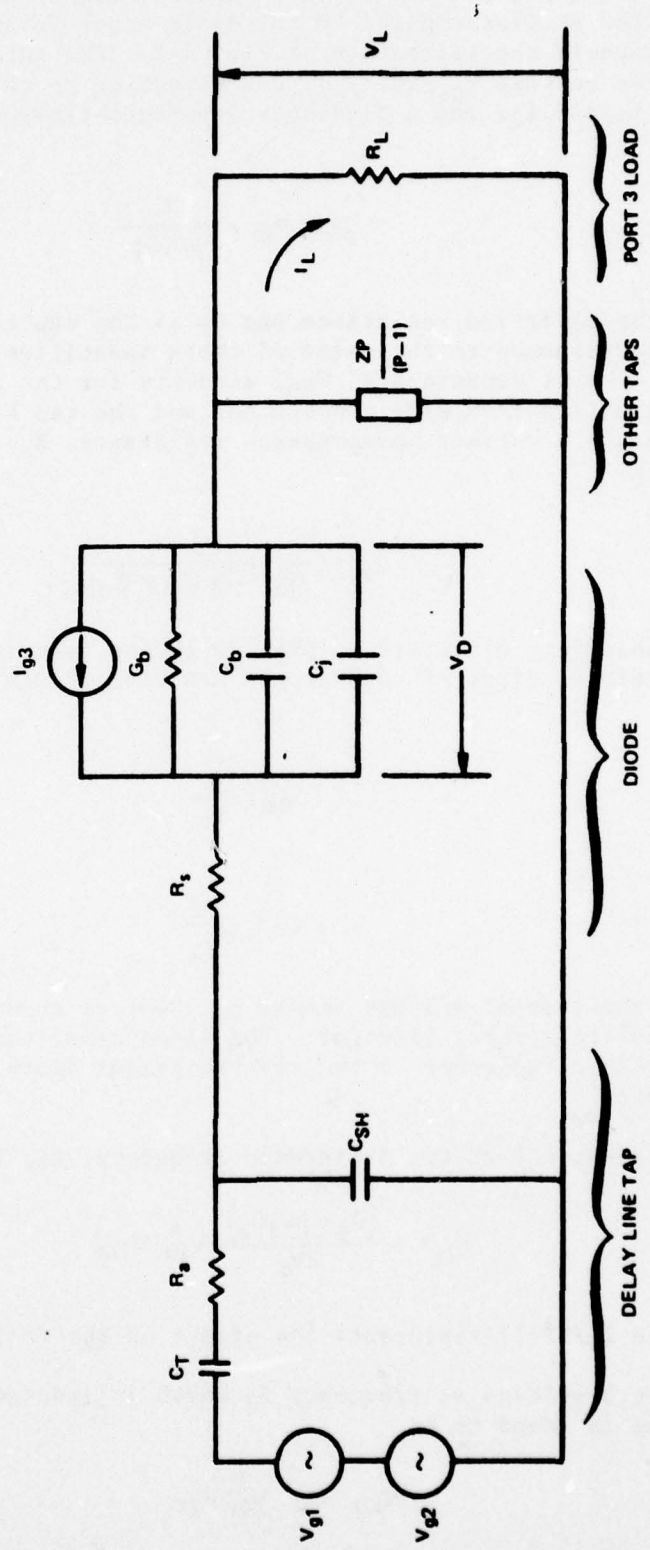

78-04-311-3

where

$$H_p = \frac{R_L\, Z_{b1}\, Z_{b2}\, Z_{b3}\left[G_b + j\omega_3 C_b\right]}{2V_q U_1 U_2 (Z_{p_1} + Z_{L_1})^* (Z_{p_2} + Z_{c_2})(Z_{p_3} + PR_L)}$$

$$U_i = \frac{C_{SH}}{C_T} + j\omega_i C_{SH} R_{ai} \qquad (3\text{-}7)$$

$$Z_{pi} = \left(\frac{R_{ai} + 1}{j\omega_i C_T}\right) \Big/ \left[U_i + R_s + Z_{bi}\right]$$

and

$$Z_{Li} = 1 \Big/ \left[\frac{(P-1)}{Z_{pi}} + \frac{1}{R_L}\right]$$

The Port 3 mixer transfer coefficient for the pth tap, H_p, given by Eq. (3-7) contains the desired amplitude and phase dependence of the tap output as a function of dc bias current. The bias dependence is more explicit if we consider a simplified case in which

$$G_b >> \omega_3 C_b;\ C_{SH} = 0 \quad \text{and,} \quad R_s,\ R_a,\ \frac{1}{\omega_i C_T} << \frac{1}{\omega_i C_J}$$

Equation (3-7) then becomes

$$H_p \approx \frac{R_L}{2V_g} \frac{R_b^2}{(R_b + jX_1)(R_b + jX_2)(R_b + PR_L)} \qquad (3\text{-}8)$$

where $R_b = 1/G_b = V_q/I_b$ is the diode resistance and $X_i = -1/\omega_i C_T$ is the tap reactance. The magnitude of H_p is maximum when the dc bias, I_b, approach the value I_{bo} for which $R_b \approx X_1, X_2$. For $I_b << I_{bo}$, we find a linear dependence on bias current;

$$H_b \alpha \pm I_b \qquad (3\text{-}9)$$

while, for $I_b >> I_{bo}$, we find a nonlinear dependence;

$$H_b \alpha \pm \left(\frac{1}{I_b}\right)^2 \qquad (3\text{-}10)$$

Both of these bias current ranges have been utilized experimentally to control the tap nonlinear output and therefore the filter tap weights over a broad dynamic range. The optimum range for experimental filter synthesis, as described later in this section and in Section 5, depends on second order phenomena which contribute to tap weighting errors at low output levels.

It is useful to express the voltage generators V_{gi} in terms of the available acoustic power that they represent. Since interdigital transducer-taps are bidirectional and we assume peak voltages in all equations, the relation between tap generator voltage and acoustic driving power is

$$P_{ai} = \frac{|V_{gi}|^2}{4 R_{ai}} \tag{3-11}$$

where R_{ai} is the tap radiation resistance at frequency f_i. Consequently, the Port 3 nonlinear output due to excitation at the pth tap can be written,

$$V_{3p} = 4 H_p \sqrt{R_{a1} R_{a2} P_{a1} P_{a2}} \tag{3-12}$$

and the output power

$$P_3 = \frac{|V_{3p}|^2}{2R_L} \tag{3-13}$$

Finally, for convenience, it will be helpful to define a relative tap output coefficient g_p which is normalized to unity at a specific value of tap bias current, I_{bo}. Thus,

$$V_{3p} = A_o g_p \tag{3-14}$$

where

$$A_o = 4 \sqrt{R_{a1} R_{a2} P_{a1} P_{a2}} H_o, \tag{3-15}$$

$$H_o = H_p(I_{bp} = I_{bo}) \tag{3-16}$$

and

$$g_p = \frac{H_p}{H_o} \tag{3-17}$$

3.3 Experimental Tap Weighting Characteristics for Single Sided and Balanced Diode Mixer Tap Configurations

Two basic tap designs have been investigated under this program. The first, a single sided mixer tap design, is that shown in Fig. 1-3 and was utilized in the construction of the 128 tap PSK Diode-Correlators (Ref. 1). This initial tap design has been shown to provide accurate PSK signal processing and has an advantage in construction simplicity since it requires only one antiparallel diode mixer pair per tap. A new balanced mixer tap design has been developed under this program and is shown to provide superior tap weighting performance, particularly for high dynamic range tap weights. The main properties of the balanced mixer tap include:

* Suppression of fundamental input frequency components at the tap output. This suppression should improve intertap isolation by reducing unwanted mixing of the fundamental signals at taps of an array other than that at which they are directly received. Re-excitation by other taps of the array will also be reduced. Fundamental frequency suppression will also relax the tolerance on the system bandpass filter located at the PFFM output difference frequency.

* Suppression of residual difference frequency signals which are either generated by means of the piezoelectric nonlinearity of the acoustic substrate or subharmonics of the input frequencies directly launched at the input transducers. This residual signal will introduce both amplitude and phase error in the nonlinear tap output. This is particularly significant at low tap weights where the bias controlled mixed component within the diode mixers is comparable to the residual fixed difference frequency component. Eventually, the residual signal would dominate, limiting the lower end of the output programming dynamic range and introducing phase error in the tap output.

Figure 3-3 shows a schematic diagram of the diagnostic y-z lithium niobate delay line used to compare the operation of the balanced mixer tap and the previously used single sided tap. Input signal and reference was at frequencies f_1 = 70 MHz and f_2 = 100 MHz, respectively, are launched by means of wide aperture interdigital transducers which, for simplicity, are represented by three quarter wavelength electrode lines. The actual transducer design used for f_1, f_2 was more complex; parallel segments having split eighth wavelength electrode design and low series resistance loss were used to achieve low conversion loss. The signal and reference input transducers had an acoustic length corresponding to N = 2 and 3 interdigital periods, respectively. The upper tap of Fig. 3-3 was identical to that used previously in the prototype PFFM module (Ref. 1) and consisted of N = 1/2 interdigital periods with eighth wavelength fingers at the tap center frequency of 85 MHz. At a single side of the transducer tap was located a silicon on sapphire antiparallel diode pair which provided mixing of the received signals at f_1 and f_2. Amplitude and biphase weighting of the mixed signal was provided by control of the amplitude and polarity of the dc bias current applied to the diode pair.

EXPERIMENTAL CONFIGURATION FOR COMPARISON OF SINGLE AND BALANCED MIXER TAP CHARACTERISTICS

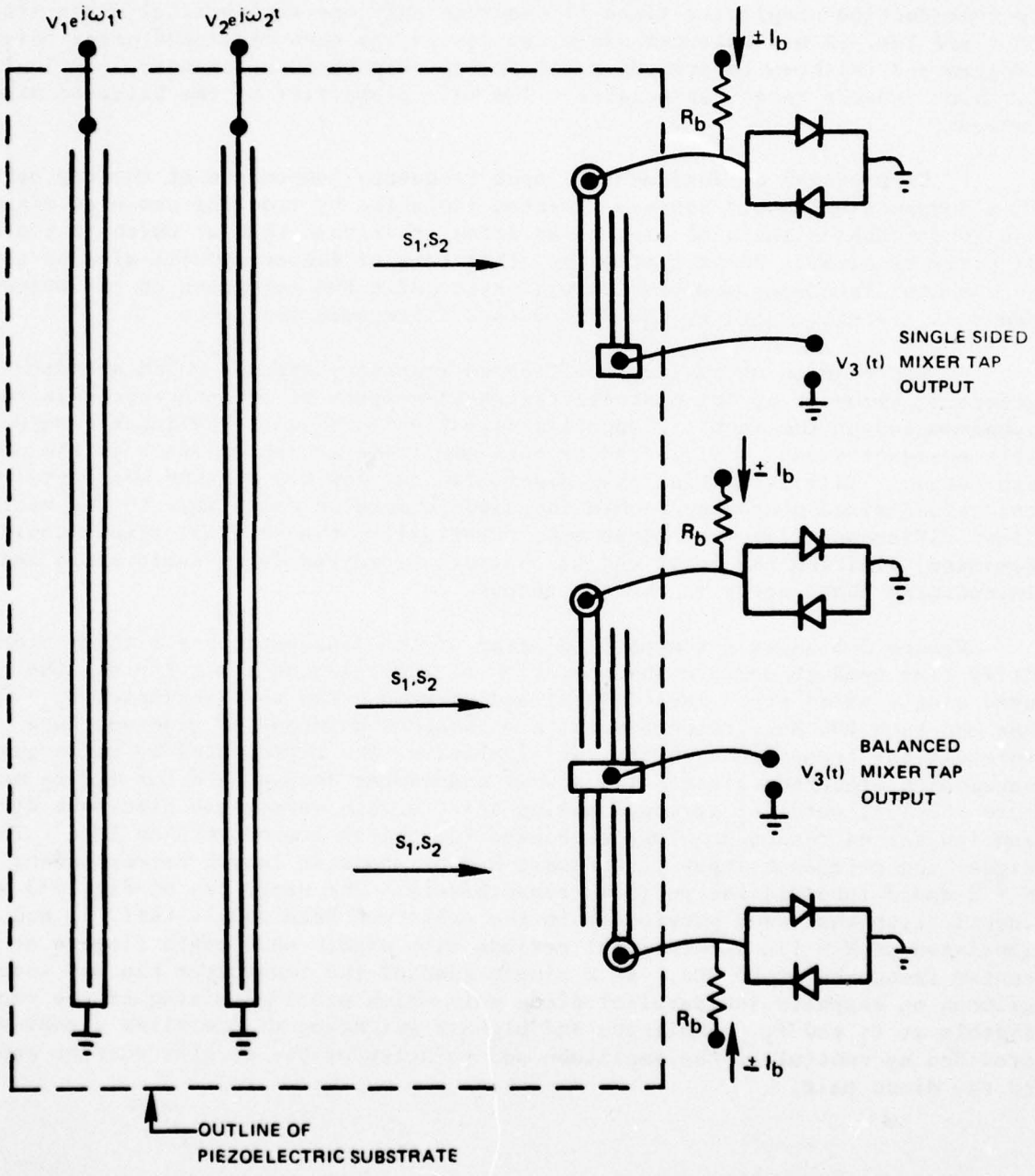

77-07-210-1

The balanced mixer tap is simply a parallel combination of two single sided taps having reversed interdigital finger location. The relative phase of the received signal is reversed at each side for equal bias applied to both diode pairs. However, since the received signals are multiplied within the diode pairs, their difference frequency outputs add in phase.

The difference frequency output power level versus input power to the delay line is plotted in Fig. 3-4 for both tap configurations. The 6 dB higher output of the balanced mixer tap results from the in phase addition of the mixed outputs from both sides. Saturation onset is observed for input power levels near $P_1 = P_2 = 14$ dB with the bilinear relationship satisfied over an output dynamic range of greater than 45 dB. The relatively low single tap input/output conversion efficiency results of course from the 7 to 1 ratio of input transducer to single tap transducer aperture of this diagnostic device.

Figure 3-5 shows the detected power levels of the input frequency components relative to the difference frequency output for both tap configurations. The pulsed measurements were performed over a broad frequency range by varying f_1 and f_2 together while maintaining a constant difference frequency of 30 MHz. Diode bias was maintained at .02 mA per diode pair for maximum nonlinear output. The frequency response of Fig. 3-5 is plotted versus input signal frequency, f_1, and is weighted predominantly by the input transducer frequency response. Relative to the single sided tap, the balanced configuration exhibits a fundamental frequency suppression in excess of 18 dB over the bandwidth measured. In theory, the suppression would be perfect for equal amplitude and zero phase error at the fundamental frequencies; however, slight diode and transducer nonuniformities versus dc bias and input frequency contribute to the degree of suppression achieved. For example, a 6 degree phase error alone, or a one dB amplitude error alone would result in 18 dB suppression.

Tap output power level versus dc bias current is shown in Fig. 3-6 for both tap configurations for the magnitude of dc bias current greater than I_{bo}, i.e., that required for maximum nonlinear output. This bias range appears to provide greater tap programming dynamic range and weighting accuracy than for bias $\leq I_{bo}$, particularly for the balanced configuration. Data for both positive and negative bias polarity is presented. The residual spurious signal level at the difference frequency caused by mixing within the $LiNbO_3$ delay line itself is also noted. This residual level was measured with the diode mixers electrically bypassed. It is particularly interesting to note the effect of the residual level at f_3 on the single sided tap response. As the tap output is decreased with increasd bias current, the bias dependence for positive and negative current separate, and do not follow the $(1/I_b)^4$ output power dependence predicted theoretically. A null is observed for negative bias when the difference frequency output from the diode mixer is equal in amplitude to the out-of-phase residual level. For positive bias, the tap output smoothly approaches the spurious level because of the nearly in phase addition of the diode mixed and spurious components at f_3. However, for the balanced mixer tap, the residual level is suppressed beyond the measurement noise level, resulting in a near theoretical $(1/I_b)^4$ output power bias dependence over a programming dynamic range of greater than 40 dB. The response for both bias polarities nearly overlay allowing accurate tap weighting via the theoretical bias law.

FIG. 3–4

NONLINEAR OUTPUT VERSUS INPUT POWER LEVELS

(M382 , f_1 = 70 MHz, f_2 = 100 MHz, f_3 = 30 MHz, I_b = 0.02 ma / DIODE PAIR)

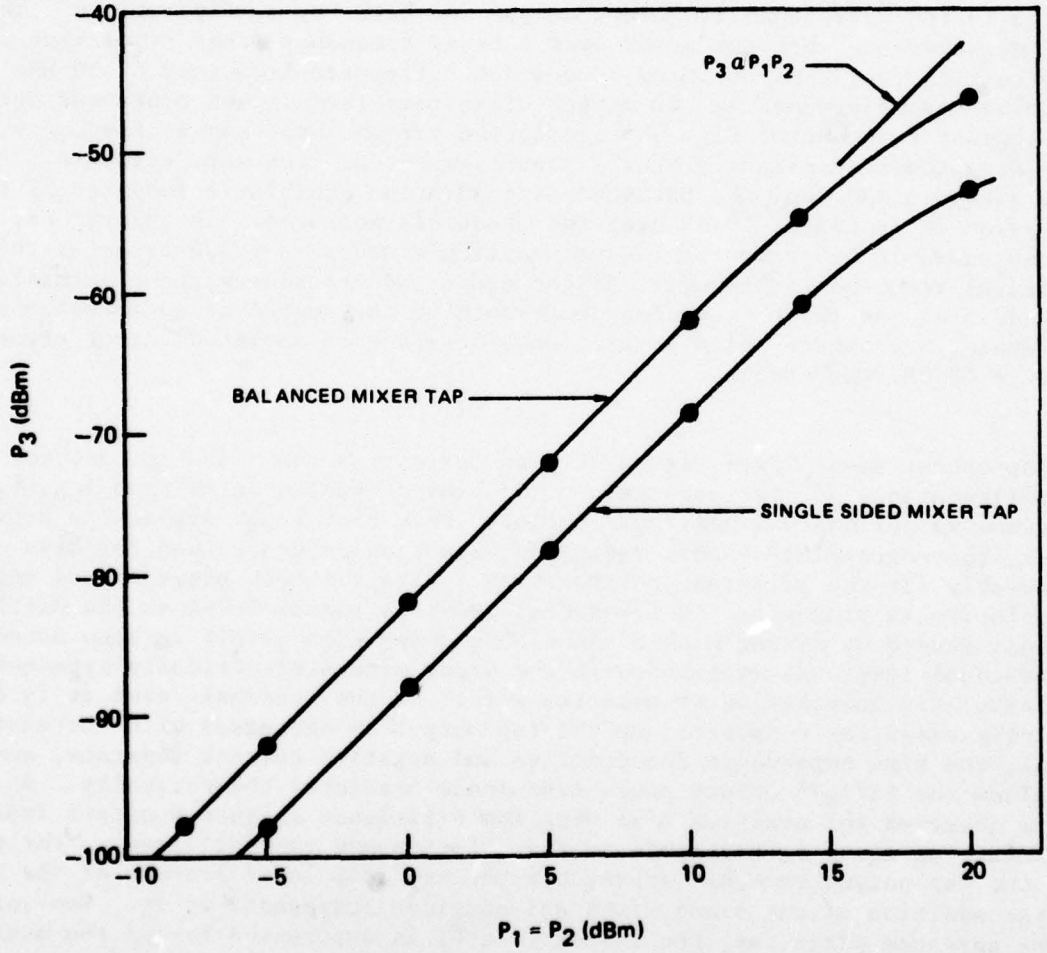

77–07–210–3

FUNDAMENTAL AND DIFFERENCE FREQUENCY TAP OUTPUT LEVELS

(M382, $P_1 = P_2 = 14$ dBm, $f_3 = 30$ MHz, $I_b = 0.0\ 2$ mA/DIODE PAIR)

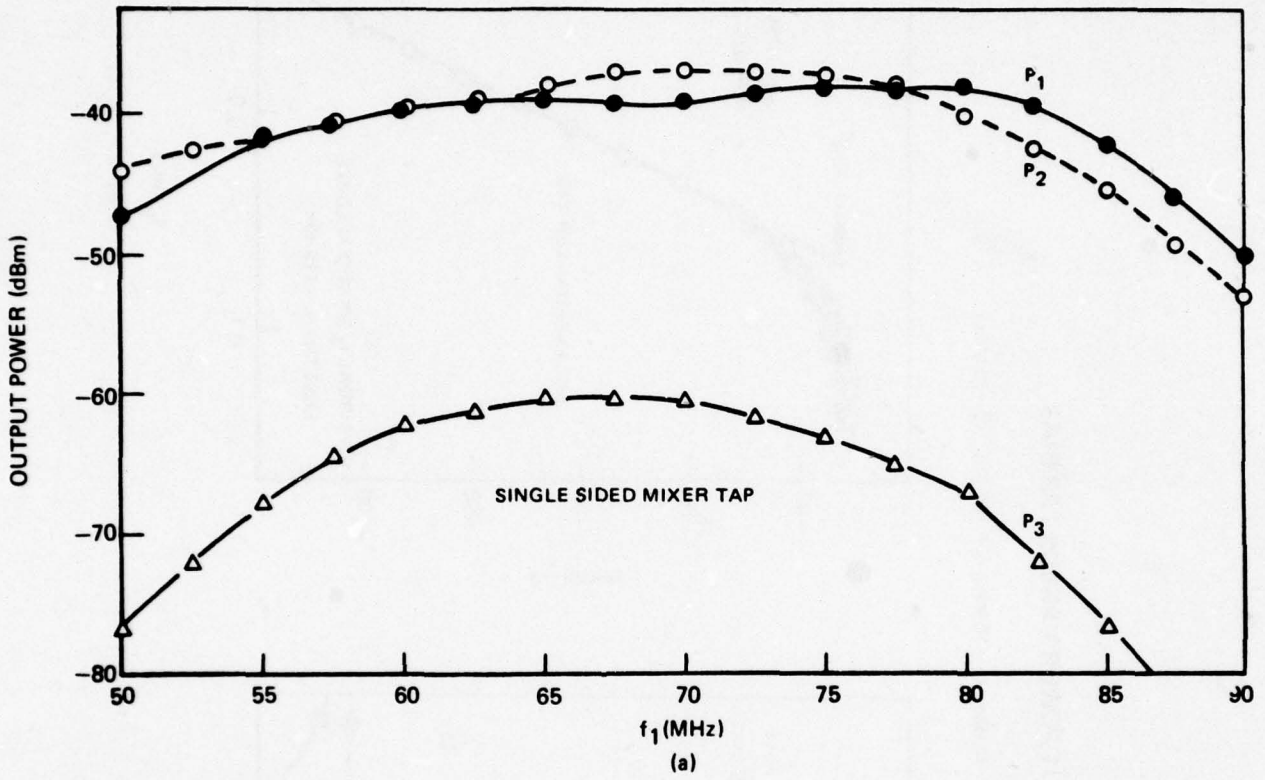

(a)

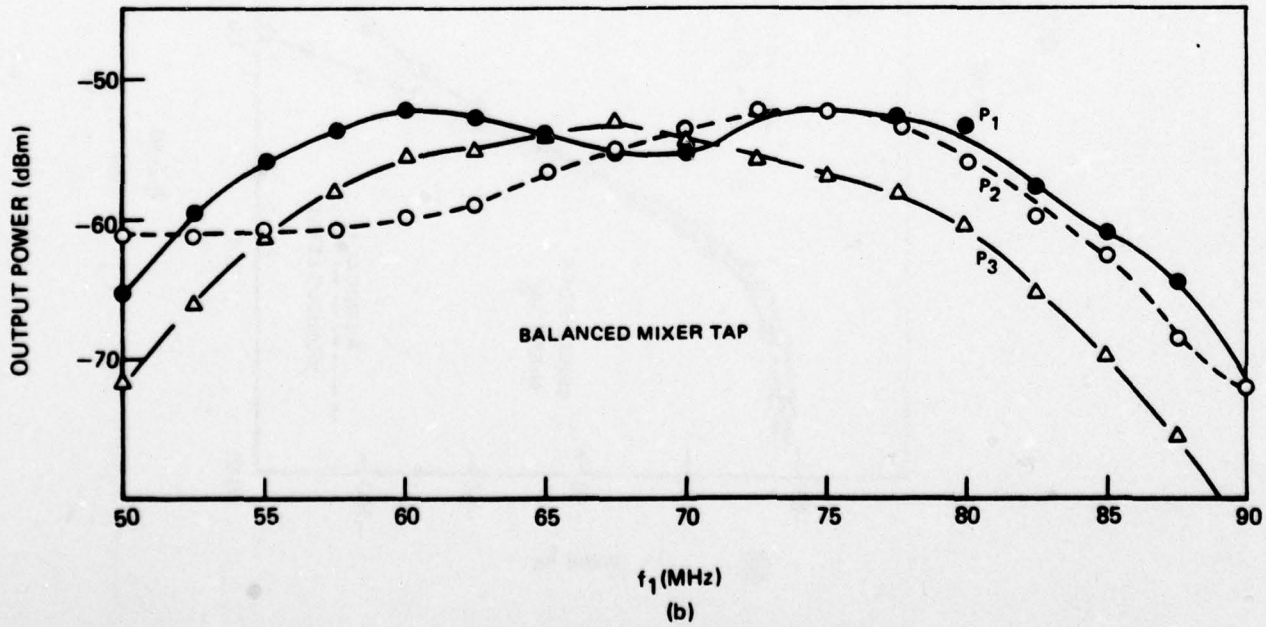

(b)

77–07–210–5

FIG. 3-6

OUTPUT POWER VERSUS TAP BIAS

(M 382. $P_1 = P_2 = 14$ dBm, $f_1 = 70$ MHz, $f_2 = 100$ MHz, $f_3 = 30$ MHz)

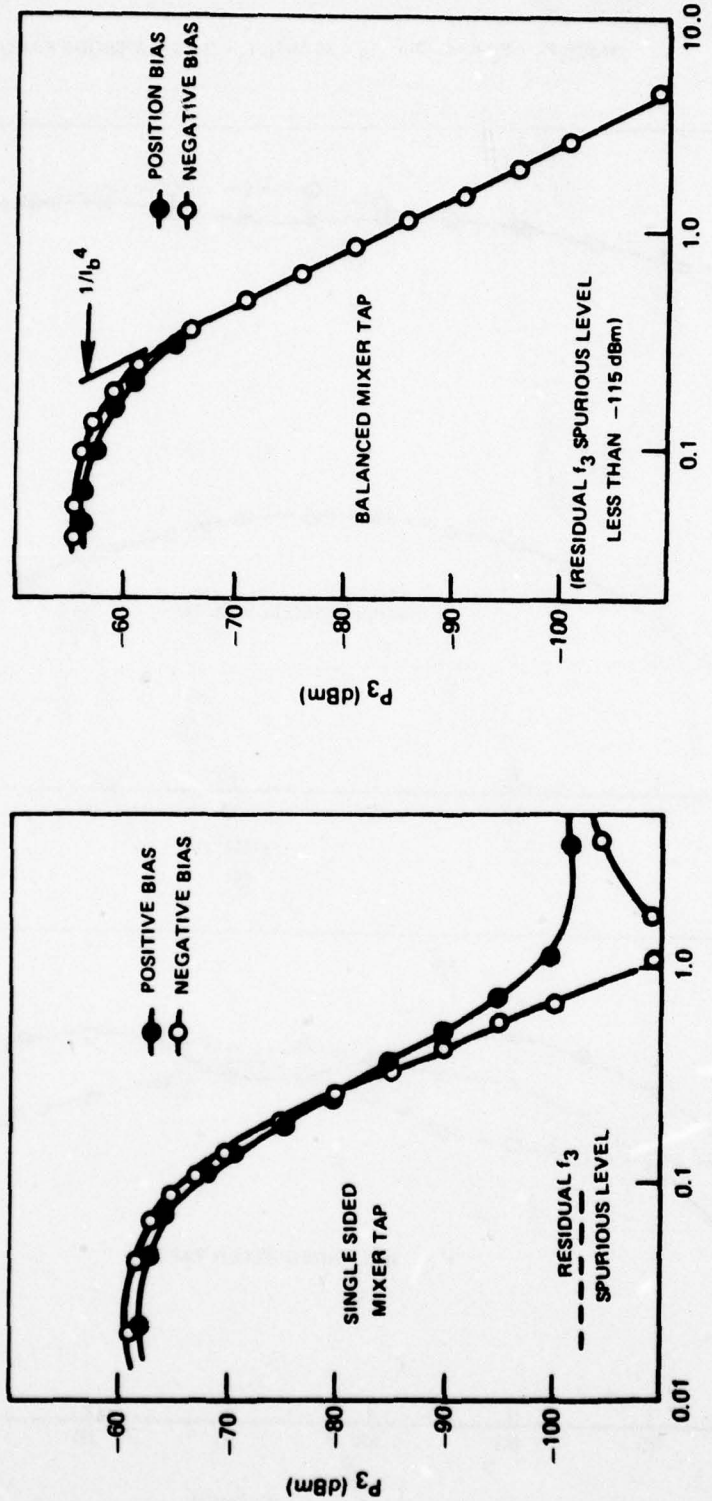

77-07-210-2

The phase dependence on tap weighting, corresponding to the amplitude dependence of Fig. 3-6, is shown in Fig. 3-7. The effect of the residual spurious difference frequency signal is also observed here for the single sided tap at low tap weighting. As the tap weighting is lowered, the phase for both positive and negative bias tends toward a common value, i.e., that of the residual signal. Suppression of the residual level within the balanced mixer tap removes this error source. As shown in Fig. 3-7, a phase reversal of 178 to 180 degrees over a 40 dB tap weighting range is observed when changing the bias polarity, as compared with 134 degrees for the single varying phase variation versus tap weighting due to the bias dependent change in diode impedance relative to tap capacitance. However, for tap weighting less than -6 dB, the relative phase error lies within 15 degrees over a 35 dB dynamic range.

The predicted phase dependence on tap weight, as obtained from analysis of Eq. 3-7, is in close agreement with the experimental results of Fig. 3-7b. The predicted phase variation over the 40 dB programming range is near 20 for the experimental tap parameters and results primarily from the variation of the diode rf conductance with dc bias as compared to the fixed tap reactance. Techniques for reducing this phase error can be considered, for example, by placing a shunt element in parallel with the diode, however, at the expense of reduced tap efficiency. However, since the phase error is predictable, as described in Section 3.4, we may use perturbation techniques to compensate for this error source. Measurements of tap to tap uniformity, i.e., output power versus applied dc bias current, have been performed for 26 representative taps of the two 128 tap PSK Diode-Correlators (Ref. 1) (devices M229 and M230) which have been employed for prototype PFFM demonstration.

The data taken for device M230 for positive tap bias and 15 dBm input power levels is shown in Fig. 3-8. Good repeatability of the tap to tap bias dependence is observed when the output of each tap is normalized to its maximum output. Random variations of $\pm$ 1.5 dB in maximum output are observed. This data was taken using short acoustic input pulses and recording the tap weighting bias dependence for every 5th tap while all other taps are turned off with 0 applied bias. The data for device M230 was essentially identical. For the device operation described in Section 5, each tap is individually programmed by setting its measured impulse response level to the prescribed value, thus minimizing tap nonuniformity effects.

3.4 Perturbation Techniques for Reducing Tap Phase Errors

As described in Section 3.3, a moderate phase error of within 20 degrees over a 40 dB programming range is found both experimentally and theoretically for the balanced mixer tap. Since this error is caused by fundamental parameters of the tap circuit, it is predictable and can be corrected using perturbation techniques. If we assume that the tap amplitude can be programmed to a high degree of accuracy, which is a reasonable assumption for the balanced mixer tap, the tap amplitude weighting may be controllably perturbed from the ideal, zero phase error case. For eventual microprocessor control of the tap coefficient programming, the error correction law may be incorporated with the $1/I_b^2$ tap weighting law to directly compensate for the inherent tap phase dependence on bias current.

FIG. 3-7

EXPERIMENTAL TAP PHASE VERSUS AMPLITUDE WEIGHTING

(M382, $P_1 = P_2 = 14$ dBm, $f_1 = 70$ MHz, $f_2 = 100$ MHz, $f_3 = 30$ MHz)

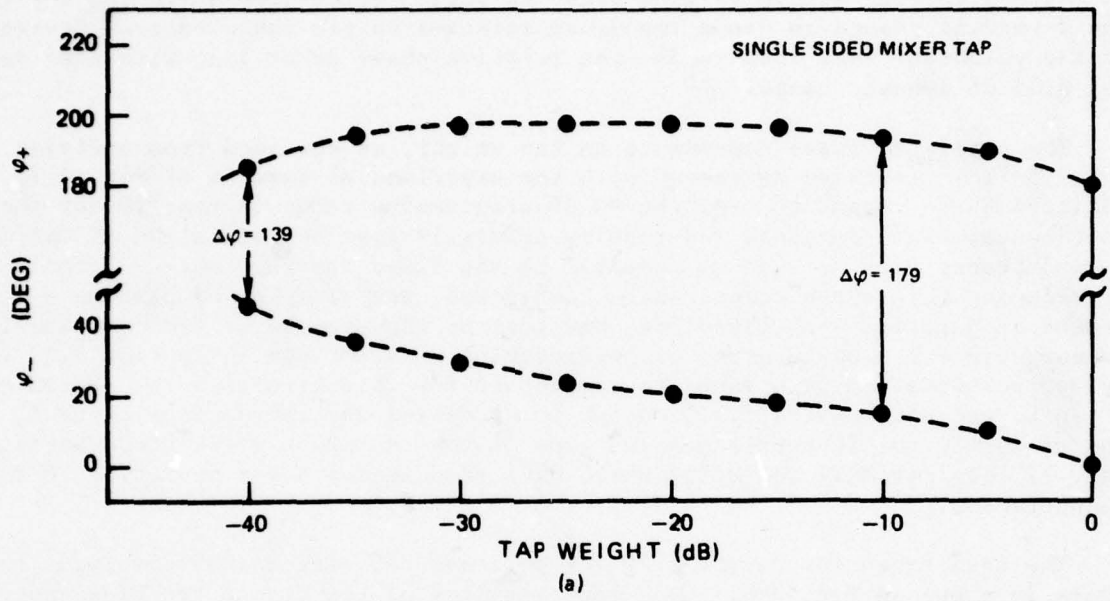

(a)

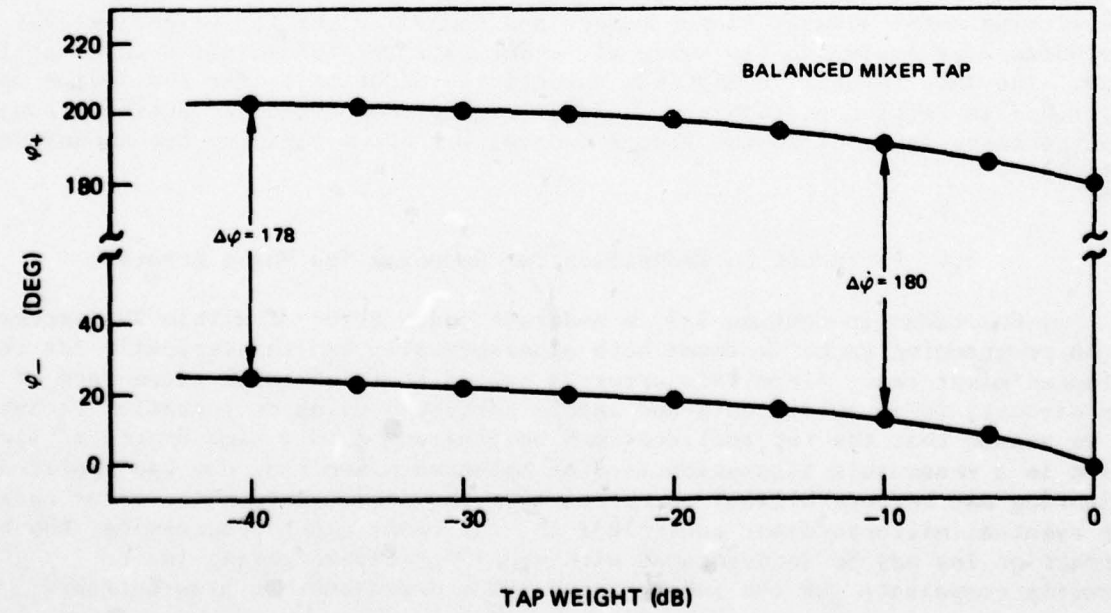

(b)

77-07-210-4

FIG. 3-8

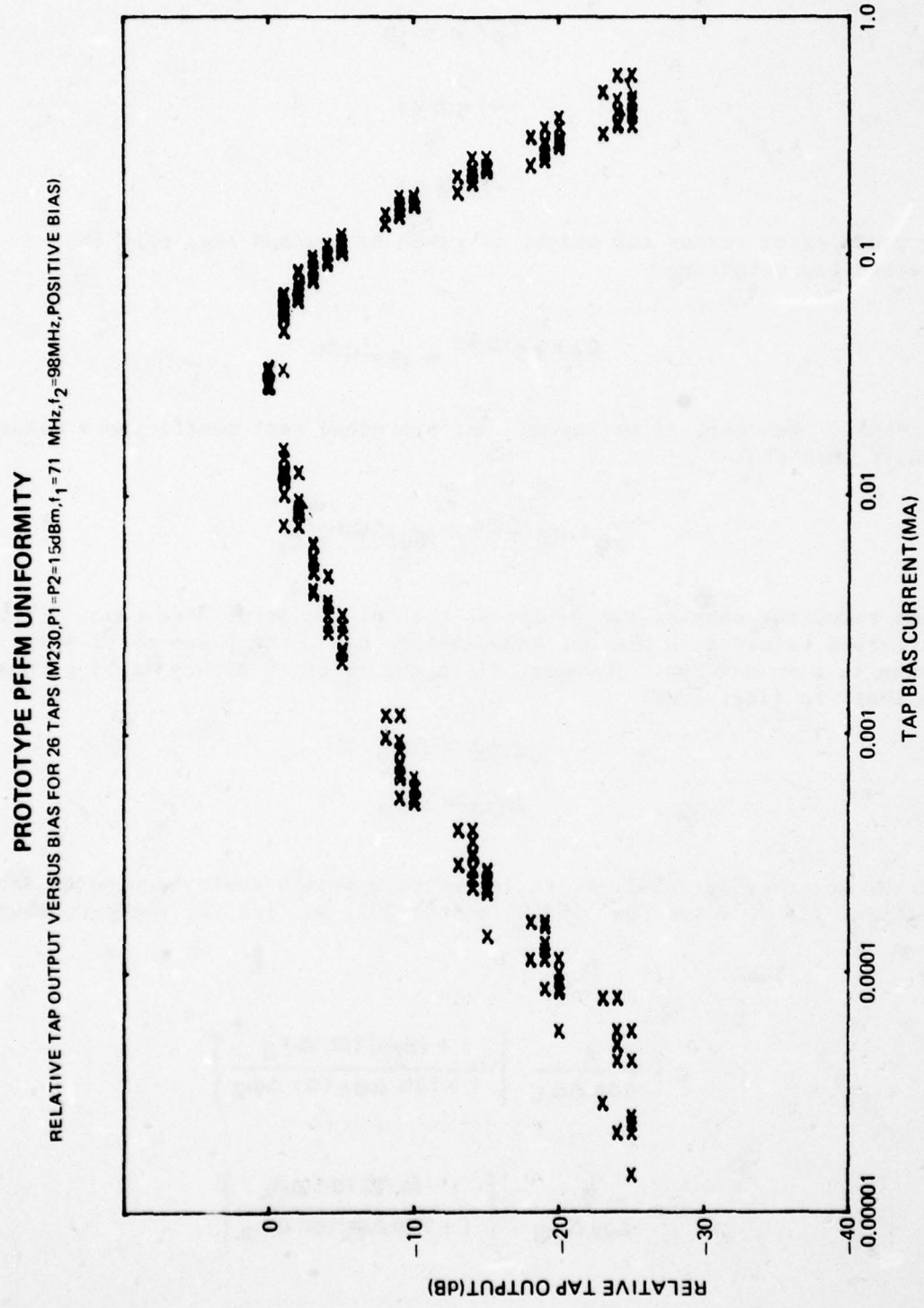

77-02-237-3

In the ideal, zero phase error case, the pth complex tap weighting coefficient values of the dual acoustic channel PFFM is given as

$$C_p = A + jB \tag{3-18}$$

where $-1 \leq A \leq 1$

and $-1 \leq B \leq 1$

If the phase error versus tap weight is given by $\Delta\varphi_A$ and $\Delta\varphi_B$, then the uncorrected tap weighting

$$C'_p = Ae^{j\Delta\phi_A} + jBe^{j\Delta\phi_B} \tag{3-19}$$

would result. However, if we assume that perturbed real coefficients values a, b exist such that

$$C'_p = ae^{j\Delta\phi_a} + jbe^{j\Delta\phi_b} = C_p \tag{3-20}$$

then the resulting complex tap weight is that of the error free case. Since the perturbed values a, b are not known before hand, the phase error associated with them is also unknown. However, since the error is slowly varying, one could assume that, to first order

$$\Delta\phi_b \simeq \Delta\phi_B \tag{3-21}$$

and $$\Delta\phi_a \simeq \Delta\phi_A$$

If further accuracy is required, an iterative approach could be used to determine $\Delta\varphi_a$ and $\Delta\varphi_b$. If we solve Eqs. (3-18) and (3-20), we find for the perturbed tap

$$a = \frac{A}{\cos\Delta\phi_A}\left[\frac{1 + (B/A)\tan\Delta\phi_B}{1 + \tan\Delta\phi_A \tan\Delta\phi_B}\right] \tag{3-22}$$

and

$$b = \frac{B}{\cos\Delta\phi_B}\left[\frac{1 - (A/B)\tan\Delta\phi_A}{1 + \tan\Delta\phi_A \tan\Delta\phi_B}\right] \tag{3-23}$$

4.0 EXPERIMENTAL PFFM DESIGN AND CHARACTERIZATION

4.1 Introduction

In this section, the design and fundamental operating characteristics of the experimental PFFM's are described. The 128 tap PSK Diode-Correlator devices developed previously (Ref. 1) have been utilized as prototype PFFM's and their construction and characteristics are reviewed. These prototype devices have the single sided diode mixer tap design described in Section 3. The design and operation of the two deliverable 64 tap dual acoustic channel PFFM's are described. These dual channel devices utilize the improved balanced diode mixer tap design also described in Section 3. This improved design has been shown in Section 3 to increase the single tap programming dynamic range to near 40 dB while minimizing the tap phase errors.

4.2 PFFM Configuration and Design Parameters

4.2.1 Prototype PFFM Design

A schematic diagram and photograph of one of the prototype 128 tap PFFM is shown in Figs. 4-1 and 4-2. Both the signal and reference waves are launched from the same side of the nonlinear diode-tapped interaction region. The input transducer comprising Ports 1 and 2 were series tuned and represented schematically in Fig. 4-1 by three quarter wavelength electrode lines. The actual transducer design used for f_1 and f_2 was more complex; parallel segments having split eighth wavelength electrode design and low series resistance loss were used to achieve low conversion loss.

A slanted tap configuration (Ref. 12) was adopted which differs from the in-line tap geometries used in previous Diode-Correlators. The prior in-line tap design suffered from excessively high intertap reflection and wave propagation losses because of the large number of electrodes in the acoustic wave path. Even with reflection cancelling eight wavelength fill-in electrodes located between taps (Ref. 13) the in-line geometry on $LiNbO_3$ resulted in losses as high as 0.15 to 0.20 dB per tap for wave frequencies near 100 MHz. Losses of this magnitude result in severe nonuniformity of the signal processing interaction and are unacceptable for the present application.

The taps are spaced by $\Delta L = .014$ inch corresponding to an intertap sampling frequency of $f_s = 9.81$ MHz. This spacing is chosen equal to an odd number of quarter wavelengths at the signal and reference transducer center frequencies so that acoustic reflections would cancel. Each broadband tap consisted of four eighth wavelength electrodes and had a center operating frequency of 85 MHz.

The taps were successively offet in the transverse direction by an amount $\Delta W_t = .004"$ so that that tap width, $W_t = .087"$, was a fraction of the input transducer beam width, $W_0 = 0.61"$. A given tap experiences decreasing reflections from 22 following taps, or only 11 on the average. This reduction in

FIG. 4–1

PROTOTYPE 128 TAP PFFM CONFIGURATION

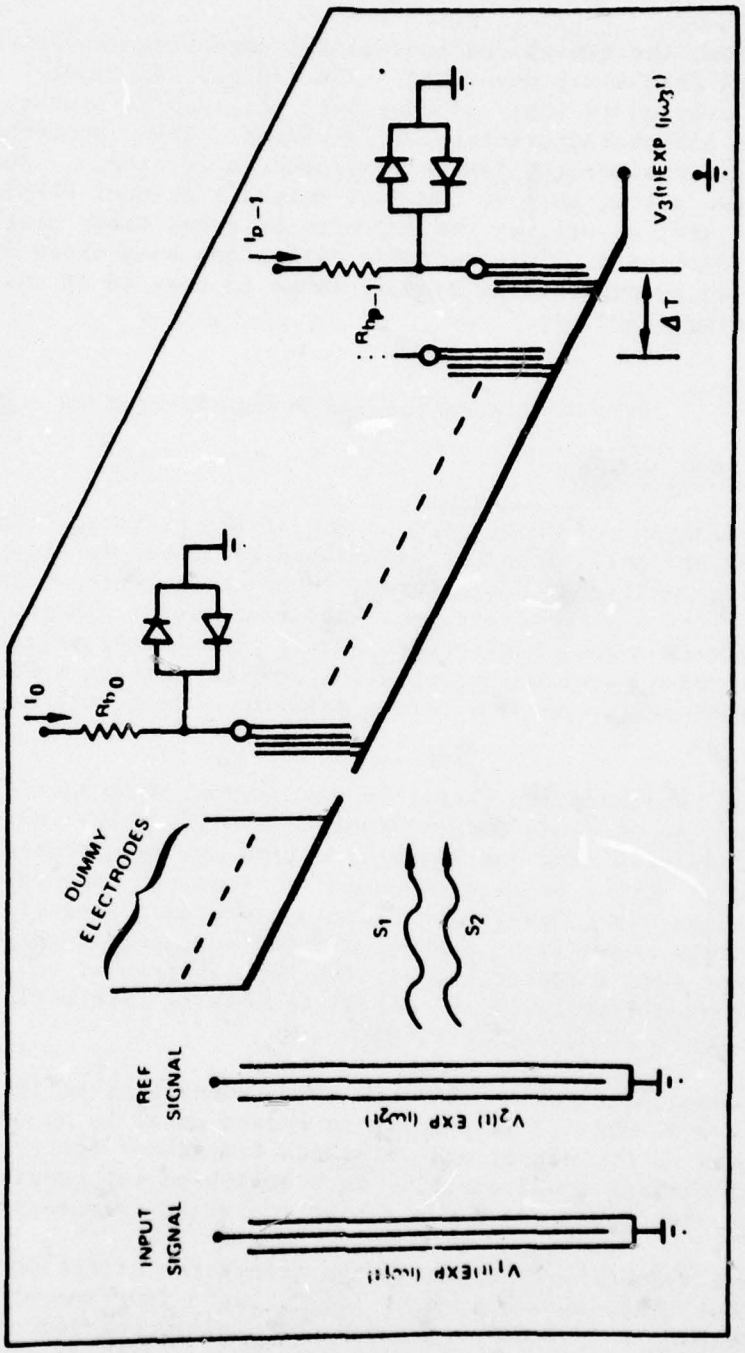

78–04–311–1

FIG. 4–2

CLOSE UP VIEW OF 128 TAP PSK DIODE CORRELATOR MODULE M230

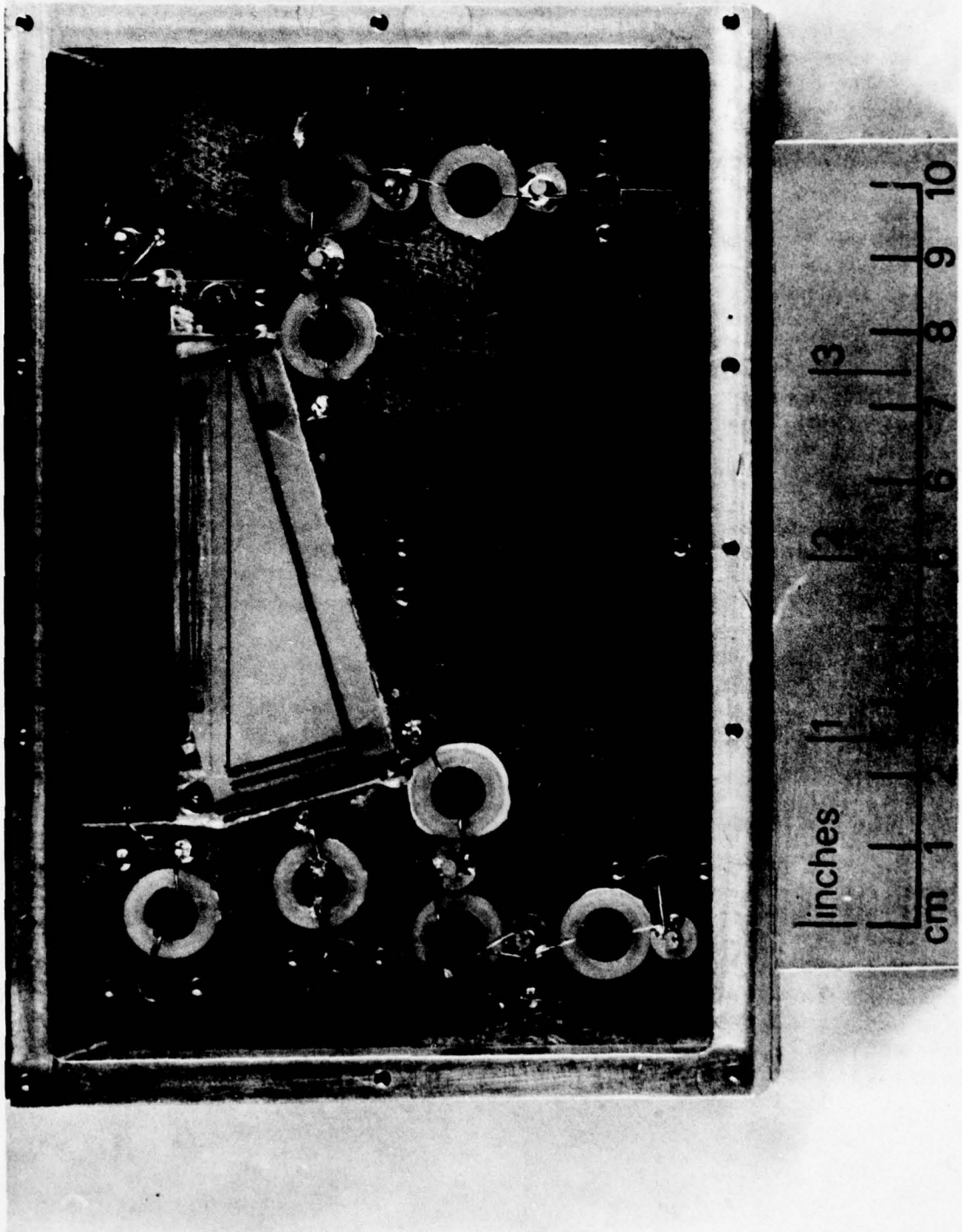

propagation losses was countered by increased input transducer losses since the taps intercept only a fraction of the input acoustic beam width. However, the overall correlation insertion loss was still reduced relative to an equivalent in-line geometry since the total power division loss for both input and reference waves, given by 20 LOG W_t/W_O = 17 dB was lower than the in-line propagation losses for 128 taps.

The active tapped interaction region was preceded by a series of dummy taps so that wave propagation characteristics prior to each active tap would be identical. The difference frequency output at $f_3 = f_2 - f_1 = 29.4$ MHz was taken at the common bus electrode comprising Port 3. Tap to tap phase coherence was satisfied with $f_3 = nf_s$ corresponding to n = 3 cycles per intertap transit time at the difference frequency.

Nonlinear mixing of the signal and reference waves occurs within the silicon on sapphire diode array mounted on the delay line adjacent to the tap electrodes. Each nonlinear tap is phase coded by means of the polarity of diode bias current applied through its bias resistor R_{bp} = 3000 ohms. Silicon-On-Sapphire (SOS) has been chosen for the substrate material in order to provide high diode isolation and to simplify the thin film resistor fabrication. For the 128 tap devices considered here, the .010" element spacing requires a 1.3" array length possessing highly uniform diode and resistor characteristics. This requirement has been satisfied with measured diode characteristics uniform to + 1/2 percent and typical bias resistors R_b = 3000 ohms + 6 percent. The detailed fabrication process of these and similar arrays has been previously reported (Refs. 1, 5, 6).

The SOS diode array elements were ultrasonically wire bonded to the adjacent delay line taps using .001 inch aluminum wire. The associated SOS bias resistor array was bonded to the multiconductor printed circuit board shown in the upper portion of Fig. 4-2. A matching connector was developed to allow individual bias control of each diode tap.

In addition to the signal processing region described above, a separate delay channel was fab ricated on the same 2.5 x 1 x .040 inch yz lithium niobate substrate as shown in Fig. 4-2. This delay channel permits cascading of modules thus extending the time-bandwidth product signal processing capabilities (Ref. 1).

4.2.2 Dual Acoustic Channel PFFM Design

As described in Section 2, the dual acoustic channel PFFM consists of two separately programmable single acoustic channel devices having their nonlinear output signals summed through a quadrature hybrid connector. The new single channel design developed under this program is shown schematically in Fig. 4-3. This design differs from that of the prototype PFFM in that a balanced mixer tap configuration is used to achieve the improved tap weighting characteristics which were described in Section 3. The reference frequency transducer at f_2 in this case consisted of N = 3 interdigital periods. In other respects, the design geometries and operating parameters are as described for the prototype devices.

SINGLE CHANNEL PFFM USING BALANCED MIXER TAP DESIGN

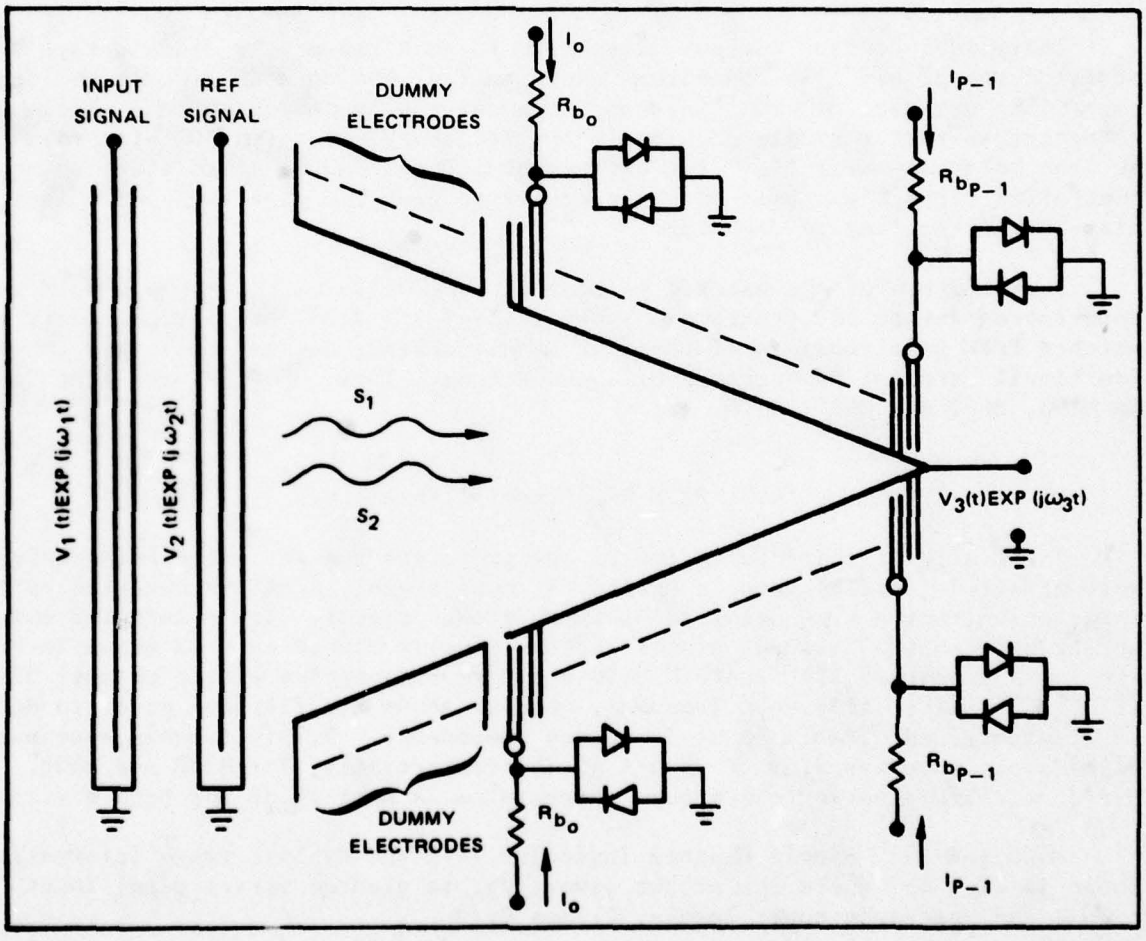

78–04–262–4

A photograph of one of the 32 tap single acoustic channel PFFM is shown in Fig. 4-4. The device is constructed on a 1 x 1 x .040 inch yz lithium niobate substrate. Each of the four single channel devices constructed under this program was fabricated on precisely oriented substrates which were obtained from the same lithium niobate boule.

The orientation of the thin film metallized pattern to the crystal x reference edge was matched for substrate pairs to within 2 minutes of arc. All substrates were metallized with 1500 Å of aluminum during the same sputtering run in order to further match the individual substrate properties.

The summing lines of each half of the balanced mixer tap array, as shown in Fig. 4-4, are electrically connected at a single output port. An additional single balanced mixer tap is located between the arrays and is positioned at the phase center of the tapped interaction region. This additional tap is included for bandstop filter applications, as described in Section 2, and also provides diagnostic information concerning tap performance.

Individual dc bias current is applied to each tap of the diode arrays by means of the 32 pin bias connectors shown in Fig. 4-4 on each side of the delay line. The two sets of bias lines are then externally connected to a single 32 pin connector so that a single dc bias is applied equally to both SOS bias resistors at each balanced mixer tap. For experimental convenience, a miniature potentiometer controlled circuit was used to individually program the magnitude and polarity of bias current applied to each tap.

A photograph of the matched pair of 64 tap dual acoustic channel PFFM's constructed during the program is shown in Fig. 4-5. As described earlier, the matched PFFM pair consists of the four single channel devices described above with additional external 90 degree hybrid connectors. These devices have been designated as M406, M407 and M415, M416.

4.3 PFFM Experimental Parameters

The nonlinear characteristics of the prototype and optimized PFFM devices were measured first by using a pulsed CW input signal, equal in duration to the interaction region time delay and a CW reference signal. The triangular correlation output between the CW input signal and the equally biased taps is shown in Fig. 4-6 for a prototype 128 tap PFFM M230 and a representative single channel 32 tap PFFM, M406. The difference frequency outputs shown are filtered prior to detection to eliminate undesirable input frequency components. Triple transit spurious signals are suppressed by 50 dB and 40 dB, respectively, for M230 and M406. Direct electromagnetic feedthrough suppression is near 60 dB for both devices.

M406 and M229 Single Channel insertion loss and dynamic range information are shown in Fig. 4-7 where the output power, P_3, is plotted versus equal input signal and reference power levels, P_1 and P_2.

PHOTOGRAPH OF ONE OF FOUR 32 TAP SINGLE CHANNEL PFFMs
DELIVERED UNDER THIS PROGRAM

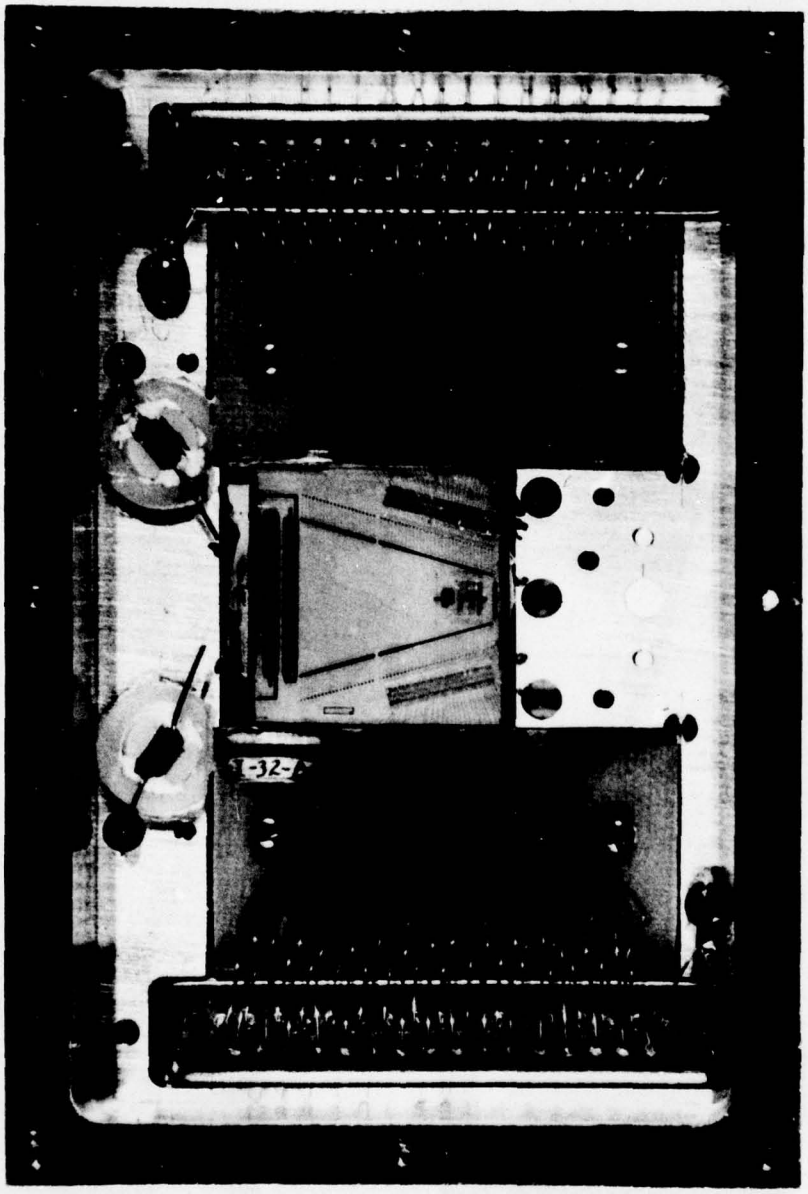

FIG. 4–5

PHOTOGRAPH OF THE 64 TAP PFFM MATCHED PAIR

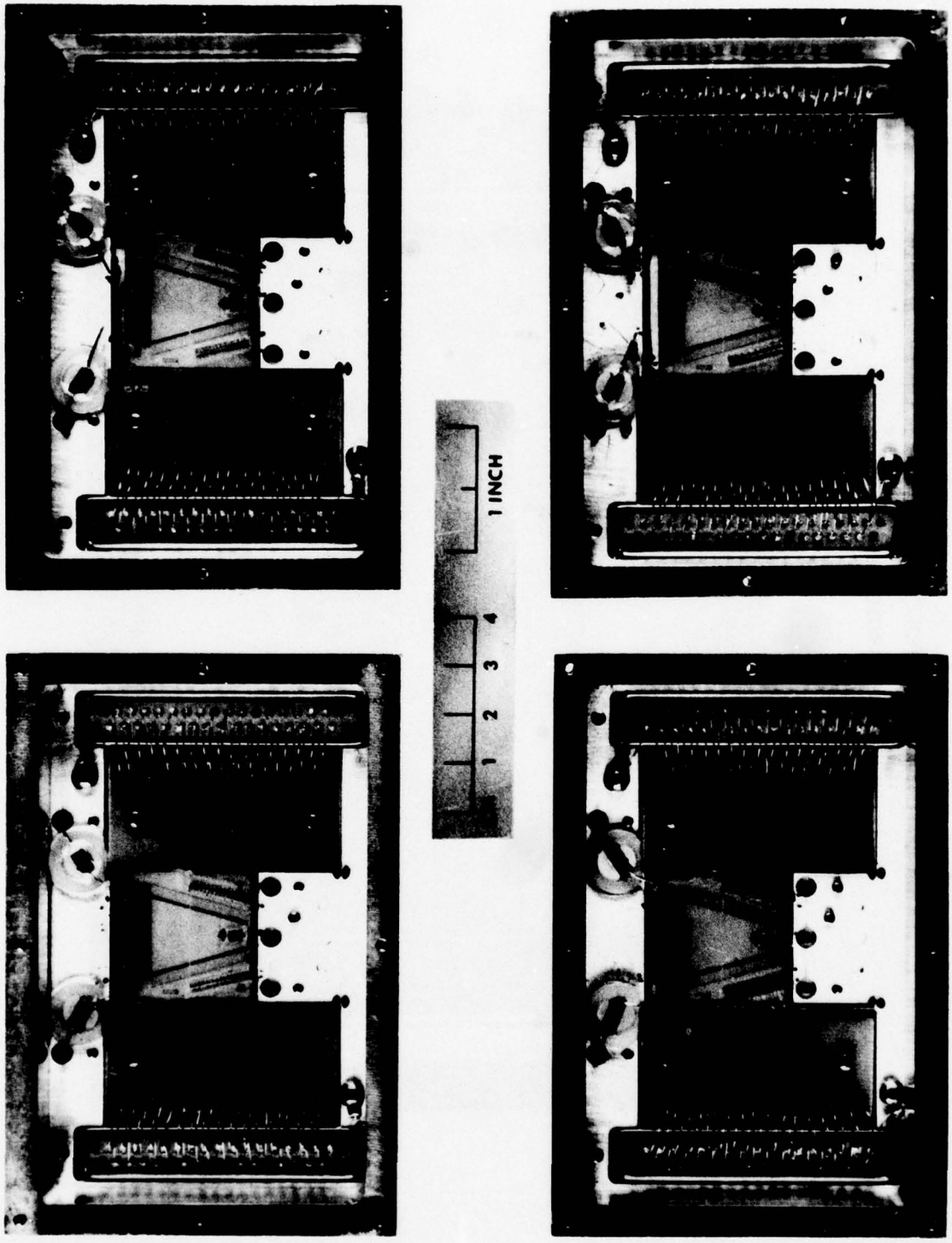

78–161–D

128 TAP PROTOTYPE AND 32 TAP PFFM CORRELATION RESPONSE

(f_1 = 71.1 MHz, f_2 = 100.5 MHz, f_3 = 29.4 MHz)

$P_1 = P_2$ = 24 dBm

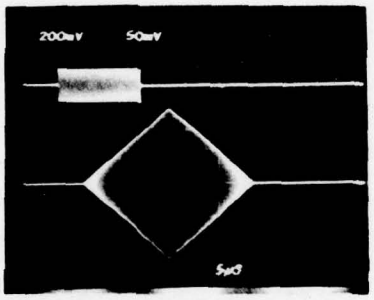

f_1 INPUT

f_3 OUTPUT

PROTOTYPE
M230

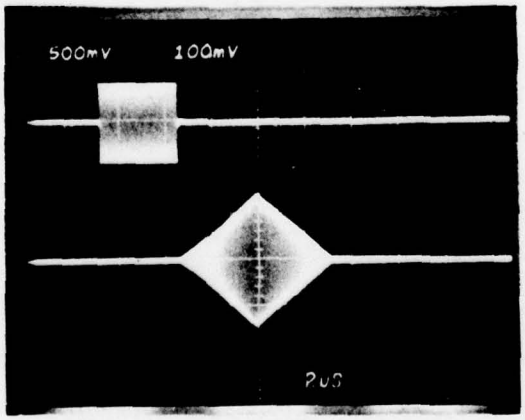

f_1 INPUT

f_3 OUTPUT

PFFM M406

78–04–262–6

128 TAP PROTOTYPE AND 32 TAP PFFM EFFICIENCIES

POWER OUTPUT VS. POWER INPUT

(f_1 = 71.1 MHz, f_2 = 100.5 MHz, f_3 = 29.4 MHz)

I_{bp} = 0.02 mA PER DIODE PAIR

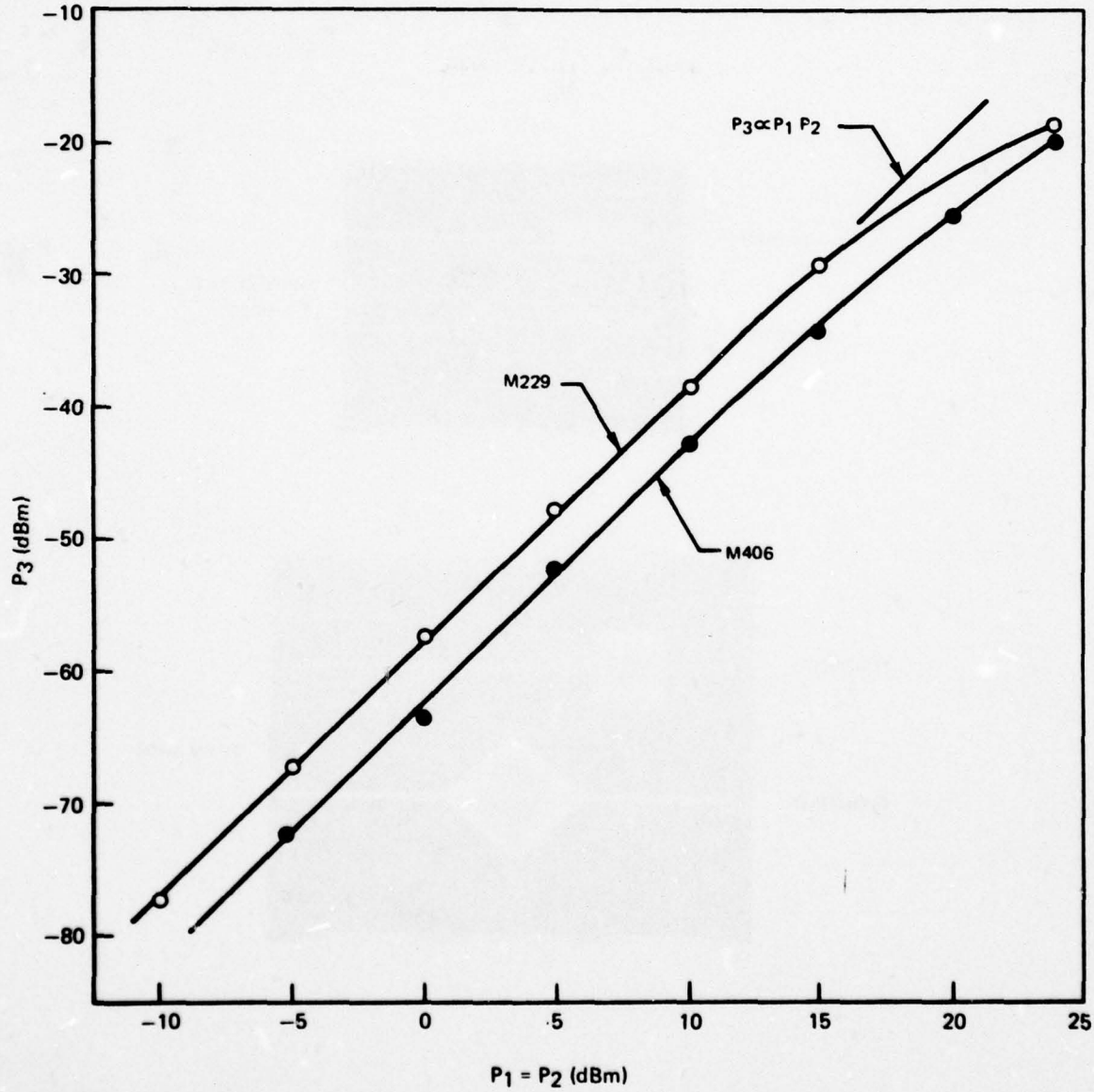

78–04–262–2

Diode tap bias of I_{bp} = .02 mA per diode pair is chosen for maximum output under nonsaturating small signal conditions. The bilinear relationship, $P_3 = F_t P_1 P_2$ (Ref. 14), is seen to be well satisfied for both devices over a output dynamic range in excess of 40 dB. The output to input signal insertion loss, P_3/P_1 is minimized by increasing the local oscillator power level P_2. At P_2 = 24 dBm, the insertion loss of the 128 tap and 32 tap devices are 40 dB and 45 dB, respectively, at input signal power levels below 15 dBm. At large input power levels, the insertion loss increases slightly due to diode saturation.

The actual filter insertion loss depends on the particular application and tap amplitude weighting which reduces the filter output power level from its maximum value. As discussed in Section 5, the broad bandwidth filters have higher insertion loss than the narrow bandwidth filters because of the greater amplitude weighting required in the broad bandwidth filter case.

5.0 EVALUATION OF THE EXPERIMENTAL PROGRAMMABLE FREQUENCY FILTER MODULES

5.1 Introduction

In this section, the performance of the experimental programmable frequency filters are described. Results are presented for several representative filter applications. These include programmable bandpass filtering with adjustable bandpass and center frequency, tunable bandstop filtering, and correlation matched filtering and encoding of PSK and chirp signals. The application to Chirp Z Transform (CZT) processing is also described and experimental transforms are presented.

5.2 Experimental Bandpass and Bandstop Filtering

Two classes of bandpass filters have been synthesized. The first of these is a Hamming, or cosine on a pedestal, weighted filter for which all the taps are amplitude weighted but possess the same phase. The weighting distribution has the form (Ref. 15)

$$g_p = w(p) = 0.54 + 0.46 \cos t(p) \tag{5-1}$$

where

$$p = 0 \rightarrow P-1$$

and

$$t(p) = \pi + \frac{\pi}{P}(1+2p) \tag{5-2}$$

Equation (5-2) is appropriate for an even number of P taps.

The second class of filter has amplitude and biphase weighted taps is a Hamming ·Sin X/X distribution (Ref. 9) with

$$g_p = w(p)\frac{\sin x(p)}{x(p)}, \tag{5-3}$$

where

$$x(p) = -2\pi + \frac{2\pi}{P}(1+2p). \tag{5-4}$$

The individual tap weighting was accomplished by varying the tap bias currents through miniature potentiometer circuits in a special purpose variable bias connector constructed for this application. Bias could be varied continuously from positive to negative values appropriate to the desired tap weight distribution. For a given filter experimentally synthesized, the theoretical response of the ideal filter having the same tap weights has been computed. The response for the nonideal filter having the amplitude and phase characteristics of the experimental devices

has also been simulated on the HP 9830 computer. A functional relationship between the experimental tap amplitude and corresponding phase error has been obtained using a least square polynominal fit to the data. Each tap is thus assigned the phase error appropriate for the computed amplitude and polarity. For ideal tap weights lower than the minimum experimental weight, the minimum weight appropriate to the tap polarity is used.

Figure 5-1 shows the computed filter frequency response for a 128 tap Hamming weighted filter with and without tap errors. The response with tap errors included is based upon the experimental tap characteristics of device M230. As a result of these errors, a degradation in sidelobe response to 33 dB from 42 dB for the ideal filter is predicted, however, the fractional bandwidth is unaltered. The experimental tap weighting and optimized frequency response is shown in Figs. 5-2 and 5-3. The near-in sidelobe level of 32 dB compares well with the predicted response, however, additional sidelobes located near $\pm f_s/2$ relative to the center frequency are only 21 dB down. In comparison, the response for device M229 showed near-in sidelobe levels of 27 dB for negative bias. This higher sidelobe level is partially caused by 3 inactive taps of M229. The experimental 3 dB filter bandwidth of 100 kHz, equal to 13 percent of the filter input frequency, f_1 = 71.9 MHz, is equal to the theoretical 3 dB bandwidth of the ideal Hamming weighted filter.

The computed response for a 32 tap Hamming·Sin X/X weighted filter is shown in Fig. 5-4 for the ideal and nonideal tap characteristics. This filter has a 3 dB bandwidth ten times that of the previous example. A predicted near-in sidelobe response of 50 dB for the ideal case is degraded to 25 dB with tap errors included. The experimenal tap weights and frequency response for this filter is shown in Fig. 5-5. A 20 dB near-in sidelobe response is experimentally found, with further out sidelobes of 16 dB. The 3 dB bandwidth of 1.0 MHz is in agreement with the predicted bandwidth and results in a fractional bandwidth, $\Delta f/f_1$ = 1.4 percent.

In addition to the variable passband characteristics of the PFFM, the filter center frequency is also continuously variable by tuning the reference oscillator f_2. Filter tuning over an 8 MHz range is shown in Fig. 5-6 for the two bandpass filters decribed above. The bandpass characteristics remain essentially unaltered when tuning, however, optimum sidelobe response is found near the design center frequencies of 71 and 100 MHz corresponding to odd multiple of quarter wavelengths between taps at f_1 and f_2, respectively. The filter response at frequencies corresponding to exactly full wavelength multiples between taps, i.e., f_1 = 68.7 and 78.5 MHz, tap reflections add up coherently resulting in severe distortions of the bandpass response.

A calculation of the response for a 128 tap tunable notch filter having the configuration shown in Fig. 2-1 is plotted in Fig. 5-7 for the case of Hamming weighting. A 3 dB notch bandwidth of $\Delta f/f_1$ = .019 is predicted for both the ideal and nonideal tap weighting. Passband ripple of .047 and.212 dB are predicted for the ideal and nonideal filter, respectively.

COMPUTED FREQUENCY RESPONSE OF PROTOTYPE PFFM
128 TAP HAMMING WEIGHTED FILTER

(M230, $P_1=P_2$=15 dBM, I_{bp}=0.02 mA, NEGATIVE BIAS, f_s=9.870 MHz)

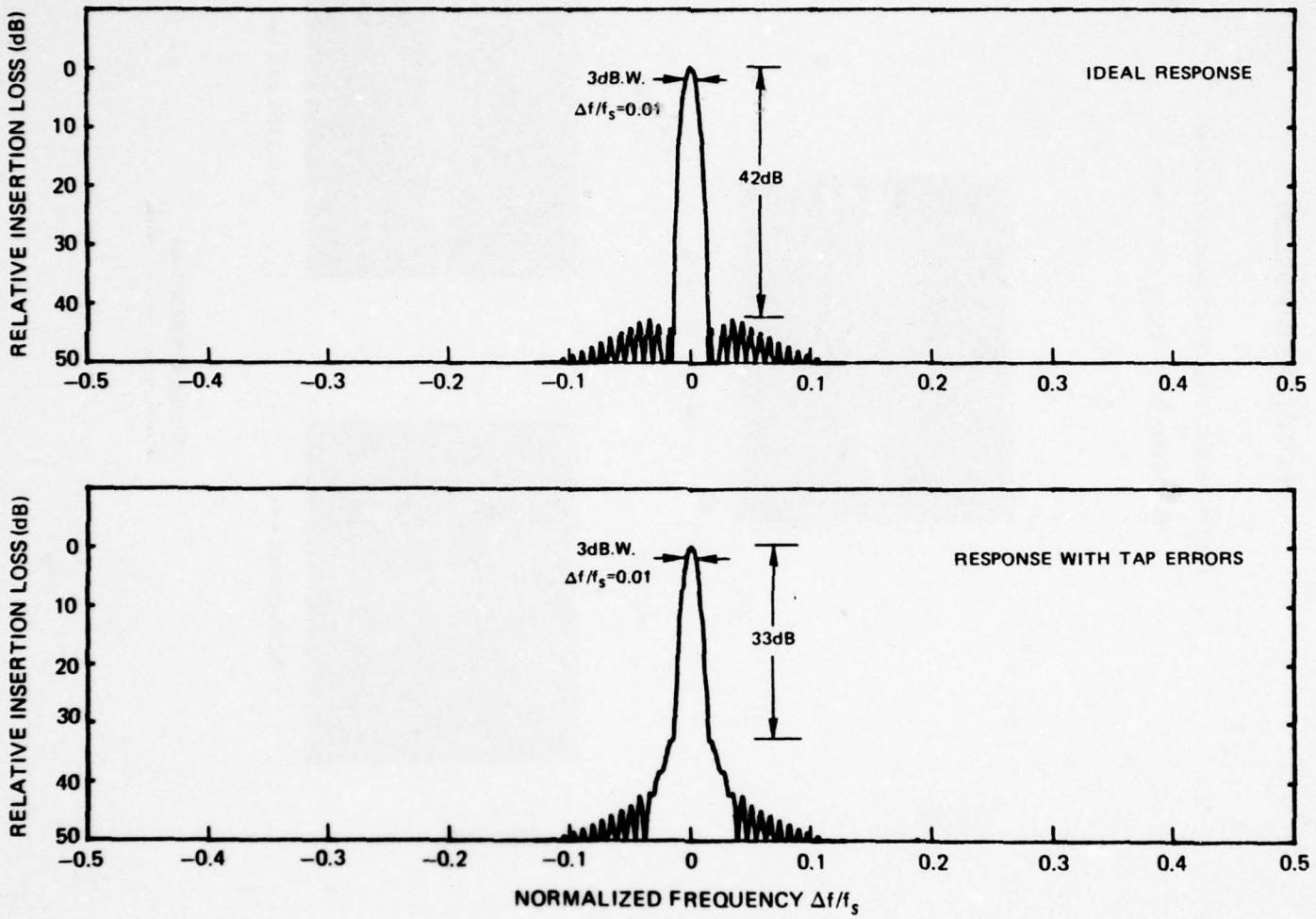

FIG. 5–1

R78–922667–18

5–3

77–02–237–4

PROTOTYPE PFFM M230

128 TAP HAMMING WEIGHTED BANDPASS FILTER

(P_2 = 15 dBM, P_1 = 0 dBM, f_2 = 101.3 MHz)

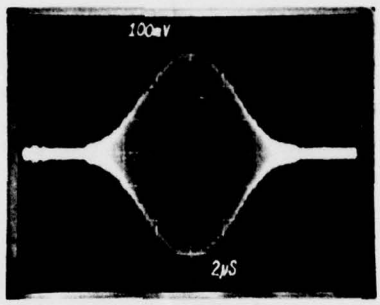

IMPULSE RESPONSE

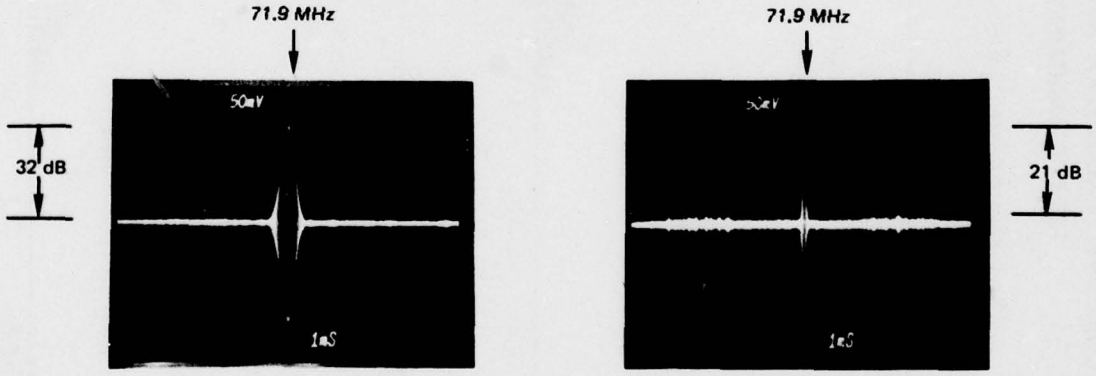

FREQUENCY RESPONSE

77–02–212–1

FIG. 5–3

PROTOTYPE PFFM M230

128 TAP HAMMING WEIGHTED BANDPASS FILTER

(P_2 = 15 dBM, P_1 = 0 dBM, f_2 = 101.3 MHz)

71.9 MHz

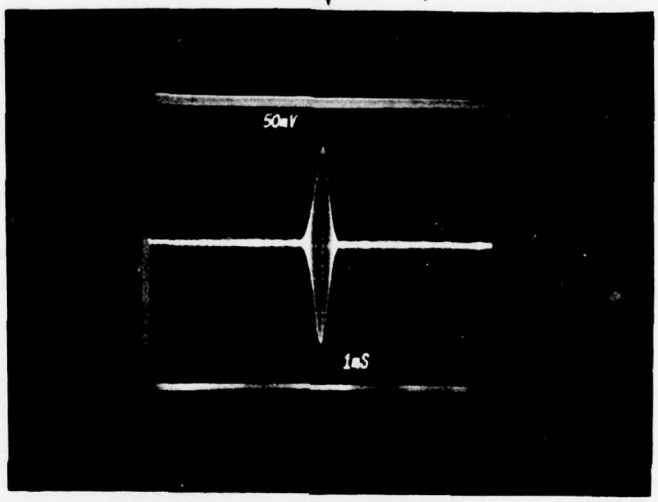

f_1 ⟶

71.9 MHz

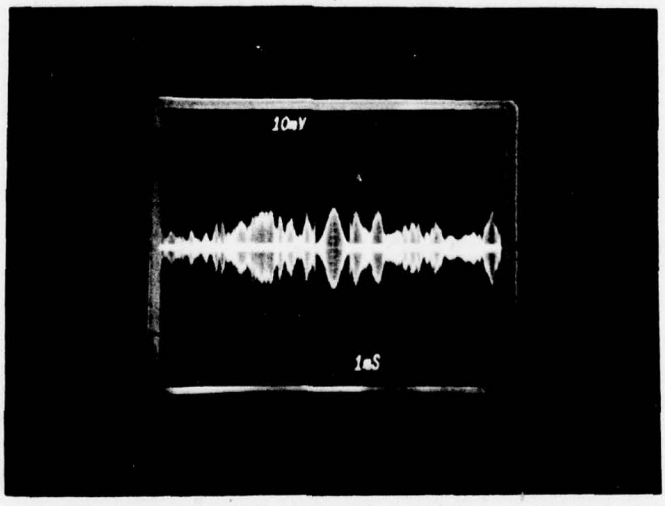

f_1 ⟶

32 dB
DOUBLE
EXPOSURE

FREQUENCY RESPONSE (0.3 MHz/DIV.)

77–02–212–2

FIG. 5-4

COMPUTED FREQUENCY RESPONSE OF PROTOTYPE PFFM 32 TAP HAMMING·SIN X/X WEIGHTED FILTER

(M230, $P_1 = P_2 = 15dBm$; $I_{bp} < 0.02mA$, $f_s = 9.807MHz$)

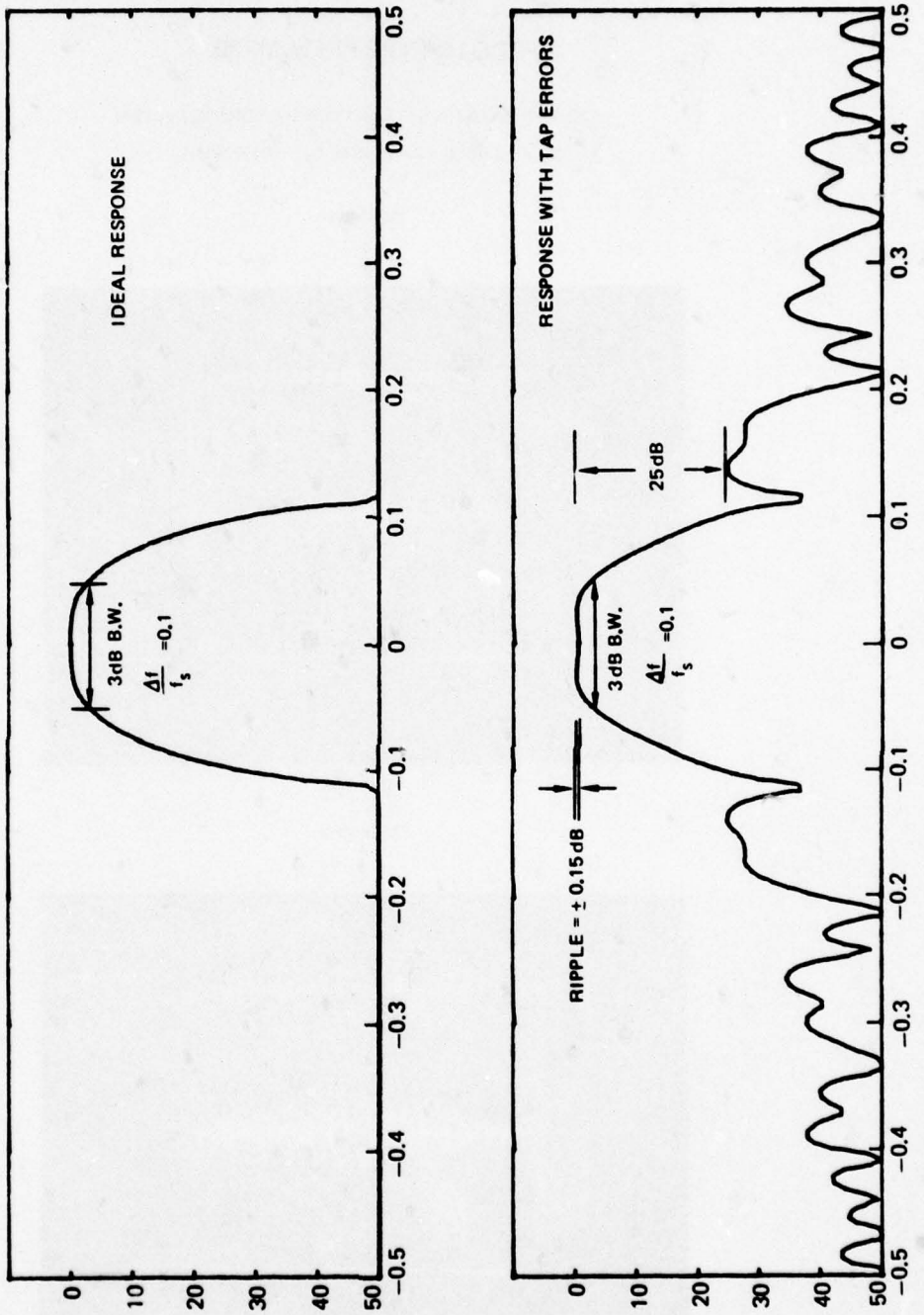

77-02-237-1

PROTOTYPE PFFM M230

32 TAP HAMMING · SIN X/X BANDPASS FILTER

(P_2 = 10 dBM, P_1 = 10dBM, f_2 = 101.6 MHz)

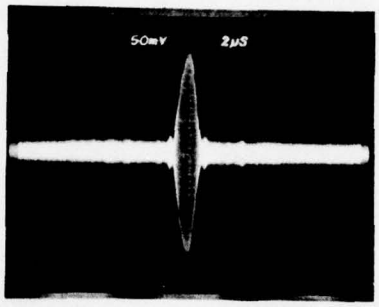

IMPULSE RESPONSE

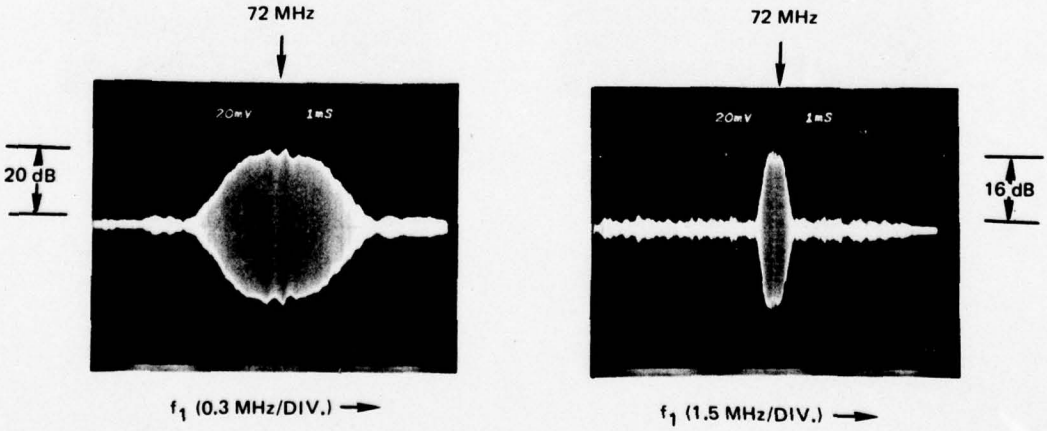

FREQUENCY RESPONSE

77-02-212-3

FIG. 5–6

PROTOTYPE PFFM M230

TUNABLE BANDPASS FILTER FREQUENCY RESPONSE

(REFERENCE FREQUENCY f_2 VARIED FROM 97.4 TO 105.4 MHz)

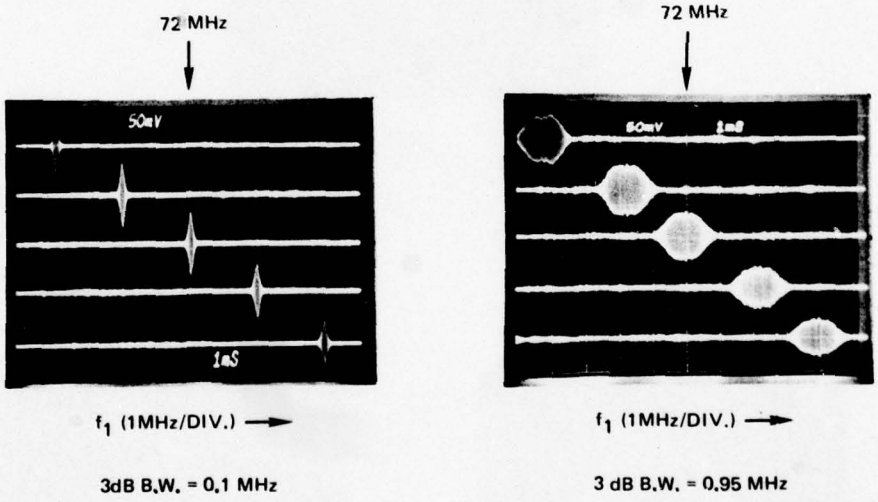

f_1 (1MHz/DIV.) ⟶

3dB B.W. = 0.1 MHz

f_1 (1MHz/DIV.) ⟶

3 dB B.W. = 0.95 MHz

77–02–212–4

FIG. 5–7

DUAL CHANNEL PROTOTYPE PFFM

128 TAP HAMMING WEIGHTED NOTCH FILTER (COMPUTED) (M230, $P_1 = P_2 = 15$dBm, $I_{bp} < 0.02$mA, $f_s = 9.807$ MHz)

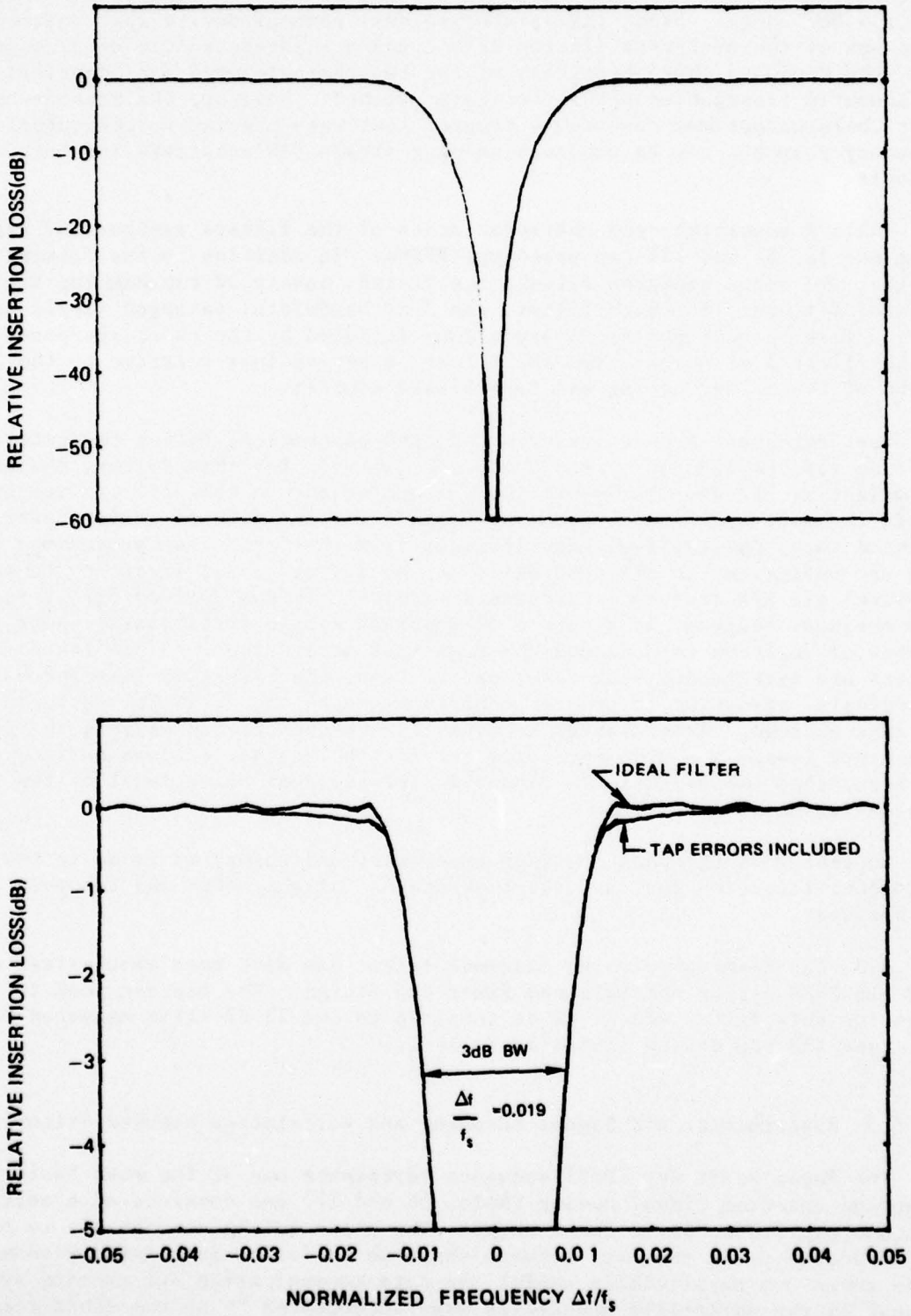

77–02–237–2

The experimental notch filter response is shown in Fig. 5-8. At 71 MHz, a notch of 30 dB is found. The 3 dB notch bandwidth of .18 MHz agrees with the predicted bandwidth. Variable notch frequency control is also shown in Fig. 5-8 over a 4 MHz range. Since this prototype dual channel device was constructed using one of the prototype 128 tap PFFM's and a separate single diode-tapped delay line, the bandpass characteristics of the two channels were not identical nor were the acoustic propagation paths precisely matched. However, the results obtained under these nonoptimum conditions suggest that very precise notch control and frequency response can be achieved using a single SAW substrate for both acoustic channels.

Table I summarizes the characteristics of the filters synthesized experimentally using the 32, 64 and 128 tap prototype PFFMs. In addition to the filters described earlier, two other bandpass filters are listed, namely 32 tap Hamming·Sin X/X weighted filters. For each filter, the 3 dB bandwidth, passband ripple and near-in peak to sidelobe ratio are given, followed by the skirt steepness measured at the filter 3 dB points, and the filter insertion loss relative to the peak output of the filter having all taps biased equally.

Best agreement between experimental and theoretical filter characteristics is found for the 128 tap 1 MHz bandwidth filter. For this filter, the minimum tap weight is -22 dB relative to the maximum weight so that all tap weights lie within the most accurate programming range. For the filters having fewer actively weighted taps, the residual contributions from the "off" taps programmed with 0 bias are sufficient to add coherently at the filter center frequency to produce a low level sin X/X frequency response in addition to the desired filter response. This residual response is a source of passband ripple particularly where the nummber of inactive taps exceed the number of active taps. Since the boader band filters are synthesized with fewer active taps, the insertion loss increases accordingly, resulting in greater contributions to the frequency response from spurious sources. Inaccuracies in manually setting the tap weights to their prescribed levels are also more apparent for the broader bandwidth filters since the prescribed tap weights lie closer to the residual noise level of the filter impulse response.

General good agreement between experiment and theory is found in the filter bandwidth, insertion loss and skirt steepness for the notch and bandpass filters synthesized.

A 32 tap Hamming weighted bandpass filter has also been synthesized using a 32 tap PFFM having the balanced mixer tap design. The near-in peak to sidelobe ratio for this filter was 27 dB as compared to the 22 dB ratio measured for the prototype 128 tap device listed in Table I.

5.3 Experimental PSK Signal Encoding and Correlation Matched Filtering

The Phase Shift Key (PSK) sequence represents one of the most basic forms of spread spectrum signal coding (Refs. 16 and 17) and consists of a series of constant amplitude, phase coded chips. The phase coding corresponds to relative 0 or 180 degree phase reversal between chips which follow in a pseudorandom sequence. These codes are particularly useful for data communication and ranging systems because of the noise-like properties when intercepted by an unmatched receiver.

FIG. 5–8

DUAL CHANNEL PROTOTYPE PFFM

TUNABLE 128 TAP HAMMING WEIGHTED NOTCH FILTER

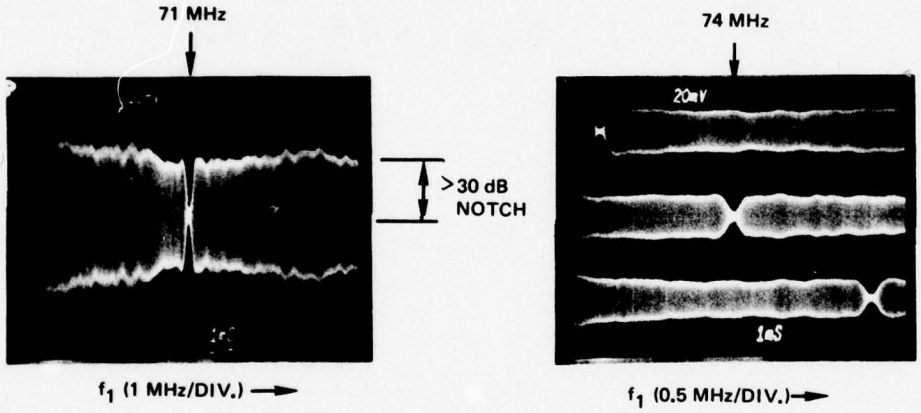

77–02–212–5

TABLE I

SUMMARY OF THEORETICAL AND EXPERIMENTAL PROTOTYPE
PFFM FILTER CHARACTERISTICS

Filter		Number of Taps	3 dB B.W. (MHz)	Passband Ripple (dB)	Near-In Peak/Sidelobe Ratio (dB)	Skirt Selectivity @ 3dB Point (dB/MHz)	Relative Insertion Loss † (dB)
	IDEAL		.1	0	42	117	5.4
HAMMING	EXP.**	128	.1	0	32	112	6
	THEORY*		.1	0	33	117	-----
	IDEAL		.4	0	42	29	17.4
HAMMING	EXP.**	32	.47	.36	22	24	18
	THEORY*		.4	0	33	29	-----
HAMMING	IDEAL		.49	0	50	44	18
.	EXP.**	64	.55	.7	20	47	20
SIN X/X	THEORY*		.45	.3	28	44	-----
HAMMING	IDEAL		.97	0	50	22	24
.	EXP.***	32	.95	.76	20	23	26
SIN X/X	THEORY*		.98	.3	25	22	-----
	IDEAL		.182	.047	--	157	null
HAMMING	EXP.**	128	.177	.74	--	130	> 30
NOTCH	THEORY*		.182	.212	--	157	null

*Including Experimental Tap Characteristics I_{bp} < .02 mA, M230

**Negative Tap Bias

***Bias for taps within main sin x/x lobe

†Relative to peak output with all taps biased equally

The single channel PFFM of Fig. 1-3 is ideally suited to PSK signal processing because of its capability for constant amplitude phase reversal of the tap output signal by revising the polarity of the dc bias current applied to the diode tap.

Programmable PSK signal encoding is accomplished by applying positive and negative bias current along the tapped diode array for the desired phase coded sequence. The tap phase is then scanned using a CW reference signal at frequency f_2 and a short input signal, at frequency f_1. The encoded PSK signal is that obtained at the difference frequency, f_3, after bandpass filtering to eliminate interfering input and sum frequency components. For PSK signal correlation, the matched filter taps are programmed in the reverse coded sequence. The input PSK signal at center frequency f_1 is then applied to Port 1 of the matched filter and the CW local oscillator reference frequency is applied to Port 2.

The experimental arrangement used for demonstrating 128 chip PSK signal encoding and matched filter correlation is shown in Fig. 5-9. Input and reference frequencies applied to the encoder are f_1 = 71.1 MHz and f_2 = 100.5 MHZ, respectively. The encoded difference frequency output signal is obtained at f_3 = 29.4 MHz. After amplification, mixing with the encoder reference frequency, f_2 = 100.5 MHz, and transmission through a 15 MHz bandwidth bandpass filter, the encoded signal is translated to f_1 = 71.1 MHz and is fed to the matched PSK correlator. The CW correlator reference is derived from the same f_2 source used to encode the signal waveform. The correlation output, after filtering and amplification is displayed on an oscilloscope. Both the encoder and correlator codes may be arbitrarily programmed in the desired PSK sequences. The PSK code sequence for this experiment was a 127 chip M-sequence which is defined using a 7 stage shift register having feedback taps 6 and 7 (Ref. 18). The biphase signal produced by the encoder at the difference frequency f_3, and after mixing to the input frequency f_1 are displayed in Fig. 5-10. Note that at f_1 and f_3 each chip contains 7 and 3 rf cycles, respectively. Phase reversal between chips at the input carrier frequency f_1 is shown in Fig. 5-10(b).

With input power levels of +24 dBm applied at frequencies f_1 and f_2, the encoded output power level at f_3 is -20 dBm. This level is 42 dB lower than the correlation output with all taps summed coherently and compares well with the 20 Log (128) = 41 dB loss predicted.

The matched filter response for both encoder and correlator programmed with the 127 chip M-sequence code is shown in Fig. 5-11(a). An expanded view of the correlation peak is given in Fig. 5-11(b). The experimental 21 dB peak to sidelobe ratio of the correlation response is close to the ideal 23 dB response for this code sequence. The matched filter triangular response for both encoder and correlator taps programmed with a constant phase is given in Fig. 5-11(c). These results demonstrate that the matched encoder-correlator pair performs as an accurate PSK transmission system and can be programmed for arbitrary PSK sequences. The individual tap reprogramming speed of 100 nsec has been experimentally measured.

FIG. 5-9

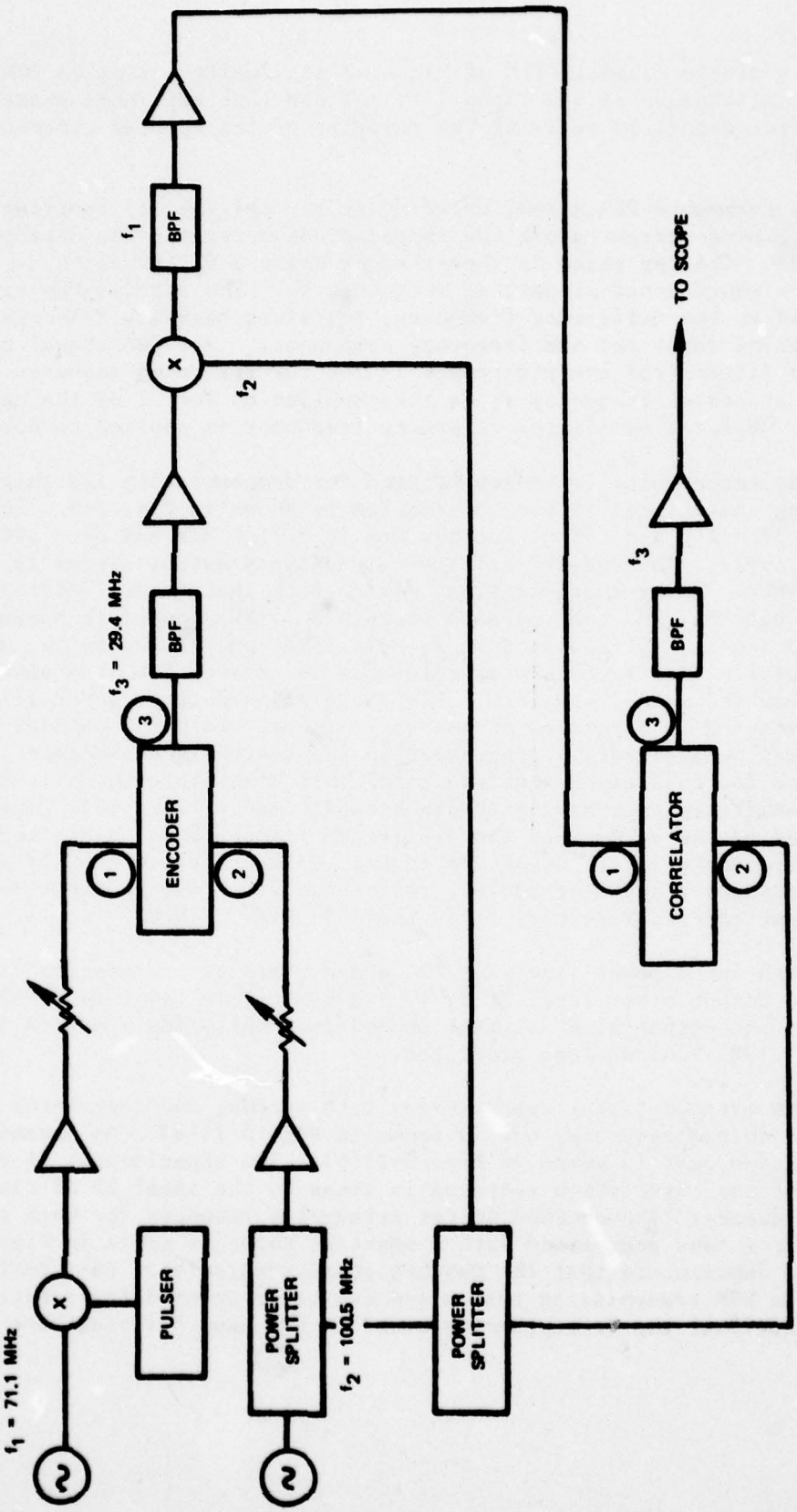

78-09-229-10

127 CHIP PSK M–SEQUENCE ENCODED WAVEFORMS

($P_1 = P_2 = 24$ dBm)

(a)

$f_3 = 29.4$ MHz

$f_1 = 71.1$ MHz

(b)

FIG. 5–11

128 TAP PSK DIODE CORRELATOR PAIR ENCODING–CORRELATION EXPERIMENT

AUTO CORRELATION WAVEFORMS

(f_1 = 71.1 MHz, f_2 = 100.5 MHz, f_3 = 29.4 MHz)

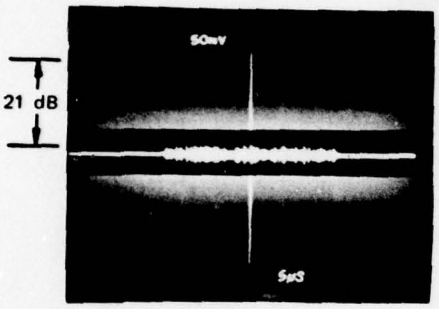

a)

127 CHIP M–SEQUENCE
(6,7 FEEDBACK TAPS)

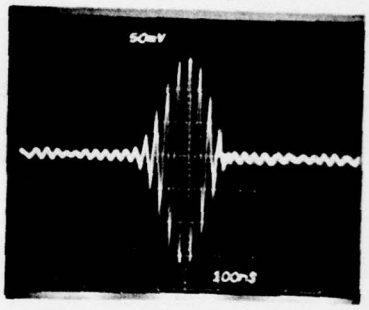

b)

EXPANDED VIEW OF M–SEQUENCE
CORRELATION PEAK

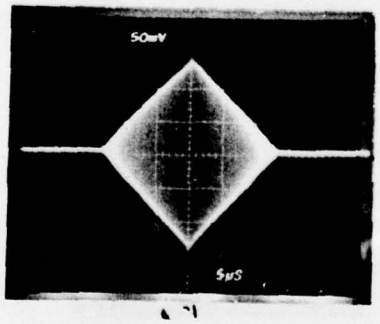

CONSTANT PHASE TAPS

5.4 Experimental Chirp Signal Encoding and Correlation Matched Filtering

While the single channel PFFM is limited to the processing of amplitude and biphase weighted codes, the duel channel PFFM of Fig. 1-4 can be programmed for processing arbitrarily phase and amplitude phase and amplitude coded waveforms lying within the device time bandwidth capabilities. For example, chirp waveforms may be processed by programming the PFFM taps in an equal amplitude, quadratic phase sequence which matches that of a discretely sampled chirp. Either positive or negative going chirp sweeps having chirp bandwidth varying from zero to the PFFM sampling frequency, f_s, may be processed with appropriate tap programming. The required complex tap coefficient values which permit continuous tap phase weighting are achieved by using the dual acoustic channel approach. Real and imaginary channels are separately programmed in the required amplitude and positive or negative relative phase sequence, and combined in a 90 degree hybrid connection.

Experimental results are presented using a dual acoustic channel PFFM as a matched filter for actively generated chirp signals of varying chirp bandwidth. The response of a matched PFFM chirp encoder-correlator pair is then described. These experiments represent a unique state-of-the-art capability in programmable SAW signal processing.

The experimental complex tap weighted chirp filters have been synthesized by combining two 32 tap devices in phase quadrature to form a 64 tap filter with 32 complex weighted taps. The chirp matched filter is obtained by programming the tap weights with quadratic phase of the form

$$g_p = e^{\pm j\pi(\frac{B}{f_s})p^2/P} \tag{5-5}$$

where B is the input chirp signal bandwidth and p = 0 to 31 is the tap number. The input chirp duration is chosen equal to the filter time delay $P\Delta T$, where $\Delta T = 1/f_s$ is the interlap time delay. Assuming that the input chirp is introduced at the signal Port 1 and a CW signal at ω_2 is applied to the reference Port 2, then the matched filter response at the difference frequency is given by

$$V_3(t) = H_t' \sum_{p=0}^{P-1} e^{j2\pi pBt/P} \tag{5-6}$$

where H'_t is a broad bandwidth proportionality constant. The present approach differs from other chirp processors (Refs. 19-21) in that the correlation output is completely asynchronous, i.e., the correlation peak will always be observed regardless of input signal timing. Additional flexibility is available by means of tuning the reference frequency, f_2, to accept chirps of equal chirp rate but varying center frequency.

The experimental circuit configuration used for PFFM correlation of actively generated chirps is shown in Fig. 5-12. The continuous chirp is generated using a Kruse-Stork sweep generator operating at a center frequency near 250 MHz and swept at the phase-lock input port by the IEC ramp generator. The swept output is down converted to the PFFM operating input frequency, f_1, and then pulsed to a

FIG. 5-12

64 PFFM CONFIGURATION FOR PROGRAMMABLE CHIRP MATCHED FILTER EXPERIMENTS

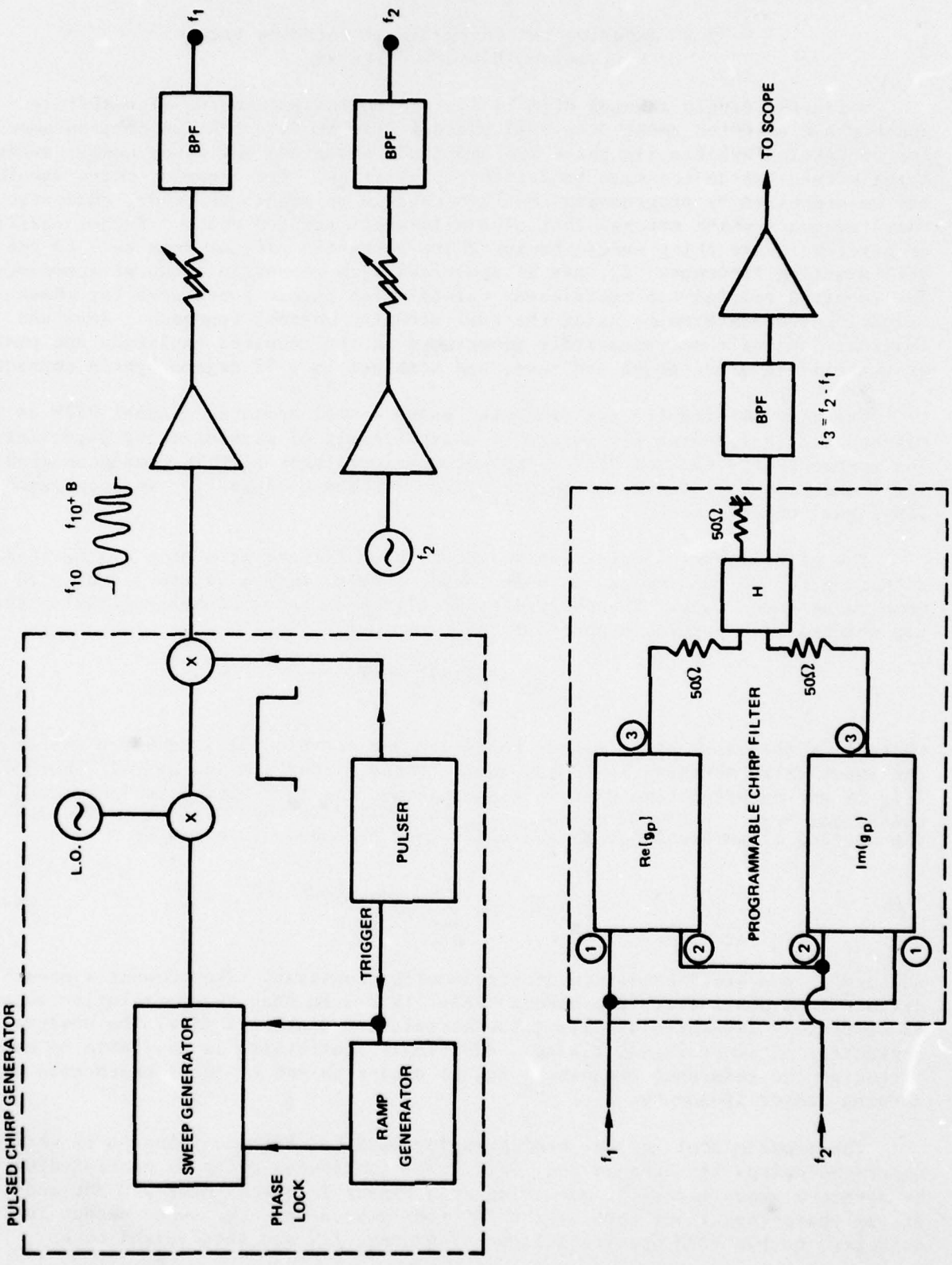

78-04-262-7

duration equal to the tapped interaction region time delay. The initial high frequency sweep generation and phase-lock input to the sweeper is chosen to provide the required 10 MHz chirp bandwidth and chirp linearity. However, imperfections of an input chirp may be alternatively compensated for by programming the PFFM taps to match a known chirp nonlinearity. The generated chirp is then amplified, bandpass filtered, and applied to the PFFM input port. A CW signal at frequency f_2 is applied to the PFFM reference port.

The PFFM real and imaginary channels are driven and their outputs combined as shown in Fig. 5-12. The input and output cables which connected the corresponding ports of the two channels were precisely matched to preserve the phase equality of the channels. After summing through a quadrature hybrid, the difference frequency output was bandpass filtered, amplified, and displayed.

Asynchronous operation as a chirp signal matched filter was tested using a linear chirp geneator to provide a 3.3 μs, 9.8 MHz sweep which matched the transit time and maximum sampling frequency of the filter. With $B = f_s$, the matched filter coefficients are given by

$$\mathrm{Re}(g_p) = \cos(\pi p^2/P + 0.2) \tag{5-7}$$

and

$$\mathrm{Im}(g_p) = \sin(\pi p^2/P + 0.2) \tag{5-8}$$

and are plotted in Fig. 5-13. The constant phase factor of .2 radians ued in Eqs. 5-7 and 5-8 was arbitrarily chosen to remove nulls from the filter impulse response and does not affect filter performance. The experimental impulse response for the cosine and sine channels, obtained by applying a 100 nsec rf pulse at the input port, is also shown in Fig. 5-13. The combined impulse respone, $g_p = e^{j\pi p^2/P}$, of the matched filter is shown in Fig. 5-14a.

Close examination of the combined response reveals a varying null between successive tap outputs which is reminiscent of the quadratic phase dependence of the coefficients. The filter response at f_3 = 29.8 MHz is shown in Fig. 5-14b for an input chirp sweep of f_1 = 74 MHz to 64 MHz and a CW local oscillator frequency of f_2 = 104 MHz.

The correlation peak to sidelobe ratio of 12.5 dB is within 1 dB of the ideal sidelobe level. The peak width at half maximum of 100 nsec agrees with the expected pulse compression ratio.

A second chirp filter was synthesized for correlating a 2 MHz bandwidth, 3.3 μsec chirp. The real and imaginary tap weights in this case are given by

$$\mathrm{Re}(g_p) = \cos(0.2\pi p^2/P + 0.2) \tag{5-9}$$

and

$$\mathrm{Im}(g_p) = \sin(0.2\pi p^2/p + 0.2) \tag{5-10}$$

64 PFFM PROGRAMMABLE CHIRP MATCHED FILTER B = 9.8 MHz, T = 3.3 μS

(DEVICE M406, M407, f_1 = 70 MHz, f_2 = 105.5 MHz, P_1 = 20 dBm, P_2 = 24 dBm)

a)

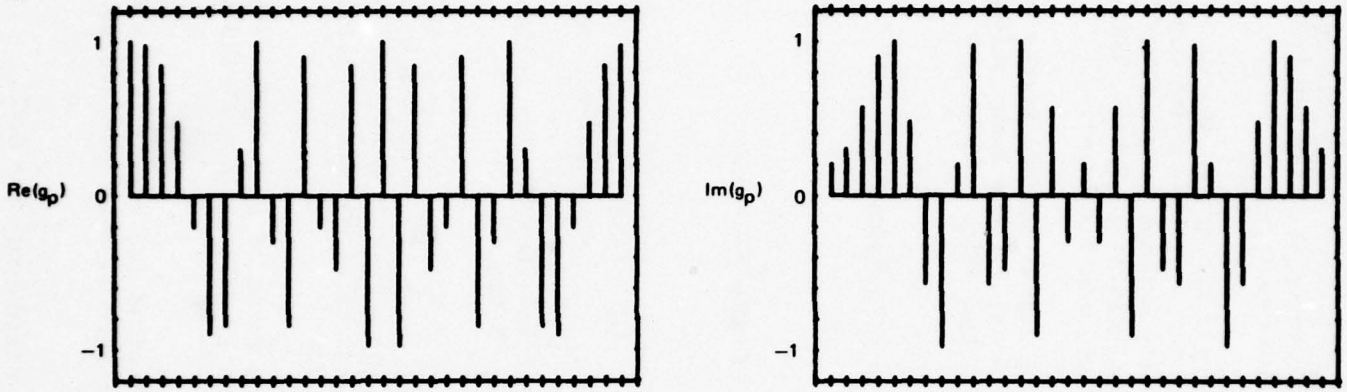

IDEAL TAP WEIGHTS

b)

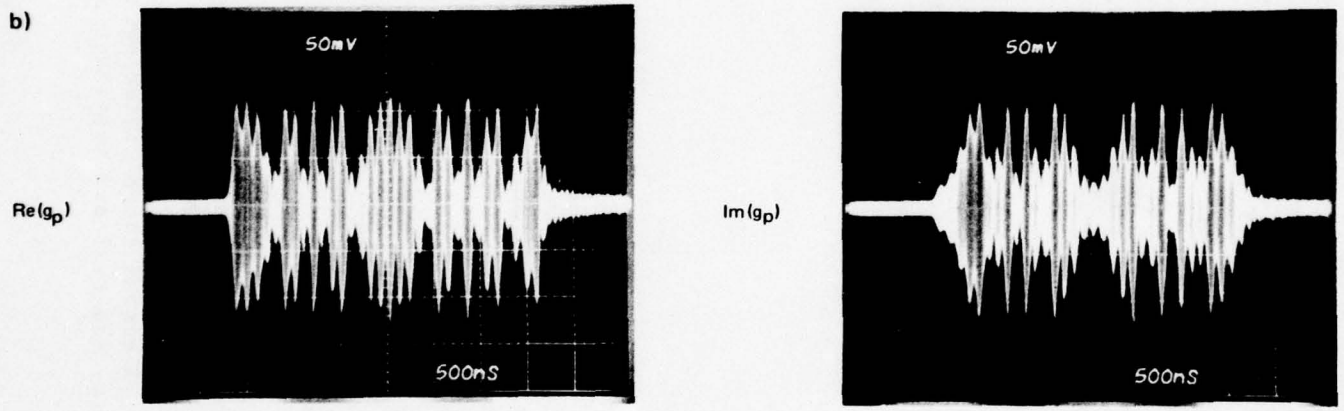

IMPULSE RESPONSE

R78-922667-18

FIG. 5-13

64 PFFM PROGRAMMABLE CHIRP MATCHED FILTER, B = 9.8 MHz, T = 3.3 μS

(DEVICE M406, M407, f_2 = 104 MHz)

P_1 = +20dBm, P_2 = 24 dBm

a)

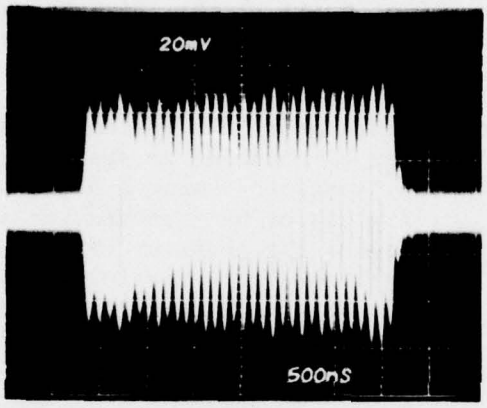

f_3 IMPULSE RESPONSE

$g_p = e^{-j\pi p^2/P}$

b)

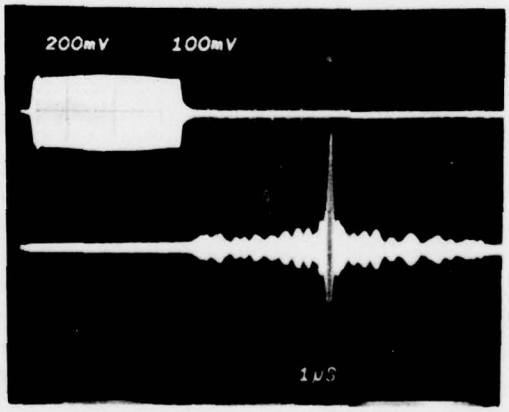

CHIRP INPUT

f_1 = 74 MHz ⟶ 64 MHz

f_3 CORRELATION OUTPUT

77–11–209–3

and plotted in Fig. 5-15a. The experimental real and imaginary filter impulse response is shown in Fig. 5-15b. Figure 5-16 gives the combined impulse response and matched filter response to a 2 MHz, 3.3 μsec input chip. The response shown for this case is also close to theoretical.

In the next experiment, the active chirp generator is replaced by a second dual channel PFFM. The experimental configuration for this matched pair encoder-correlator system is shown in Fig. 5-17. The 32 complex tap weights of both the encoder and matched filter are programmed with the same quadratic phase sequence given by Eqs. (5-7) and (5-8) corresponding to a sample 9.8 MHz chirp bandwidth. However, the inputs to the quadrature hybrid of the encoder are reversed with respect to those of the correlator to preserve the correct phase sequence or equivalent chirp sense during correlation.

The encoded signal, after frequency translation to f_1 and filtered with a 70 MHz, 15 MHz bandwidth filter, is shown in Fig. 5-18. Also shown in the figure is the correlation response of the matched PFFM. A 13 dB peak to sidelobe ratio is observed which is within one dB of the ideal response.

The correlation waveform of the matched pair PFFM system is similar to the waveform previously shown in Fig. 5-14 for the case of an actively generated input chirp. The deviation of the experimental sidelobe response from the theoretical sin x/x waveform is believed to be chiefly caused by inaccuracies in manually setting the tap weights and from the residual tap phase errors for the balanced mixer taps as discussed in Section 3. While the perturbation techniques described in Section 3 would eliminate the tap phase errors, it was beyond the scope of the program to experimentally evaluate such methods. Direct Hamming weighting of the filter taps would also provide a direct impact in reducing the correlation sidelobe response. These capabilities are straightforwad extensions of the present work which could be implemented for improved filter performance.

5.5 Operation as a Chirp-Z Transform Processor

In this section, we will describe the utilization of the PFFM for the performance of the Chirp-Z Transform (CZT) algorithm. The chirp transform has been demonstrated by a number of authors (Refs. 19-26) as a means for displaying the spectral components of an input rf waveform. The procedure usually employed requires the premultiplication of the input signal by a synchronized chirp using a discrete mixer, convolution of the premultiplied signal within a matched chirp filter, and post multiplication by a chirp. The post multiplication step is unnecessary when only the amplitudes of the spectral components are required. The transform is performed at a rate fixed by the predetermined chirp rate of the convolution filter.

The PFFM offers an alternative, more flexible approach to CZT embodiment. Unlike the fixed chirp filter used in prior CZT devices, the chirp rate of the PFFM may be programmed to accept a range of chirps lying within the time bandwidth product of the device. The transform coefficient rate may thus be varied to suit the particular system requirement. In addition, the internal nonlinear mixing

FIG. 5– 15

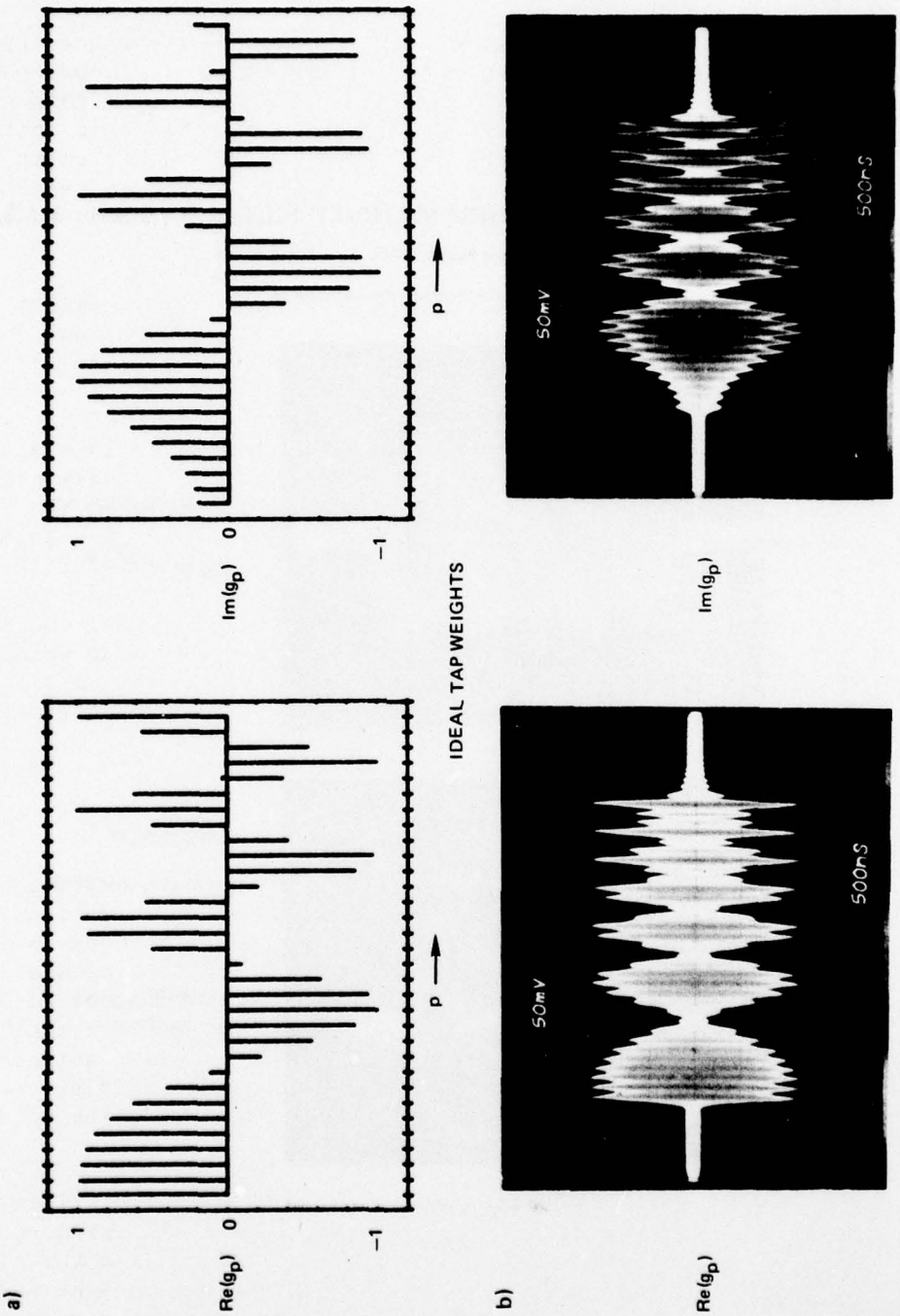
64 PFFM PROGRAMMABLE CHIRP MATCHED FILTER B = 2 MHz, T = 3.3 μS
(DEVICE M406, M407, f_1 = 70 MHz, f_2 = 105.5 MHz, P_1 = 20 dBm, P_2 = 24 dBm)
a)
b)
1
0
−1
Re(g_p)
Im(g_p)
p
IDEAL TAP WEIGHTS
50mV
500nS
IMPULSE RESPONSE

64 PFFM PROGRAMMABLE CHIRP MATCHED FILTER B = 2 MHz, T = 3.3 μS

(DEVICE = M406, M407, f_2 = 101.5 MHz)

P_1 = +20 dBm, P_2 = +24 dBm

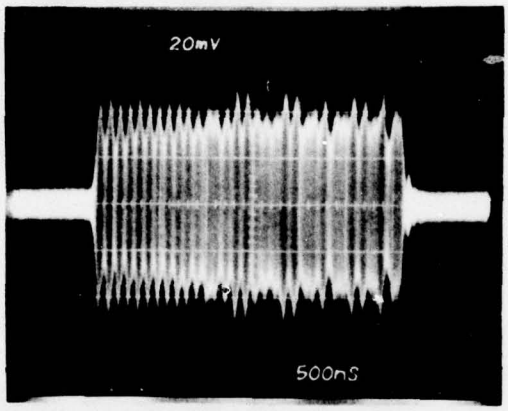

f_3 IMPULSE RESPONSE

$g_p = e^{-j\pi p^2/5P}$

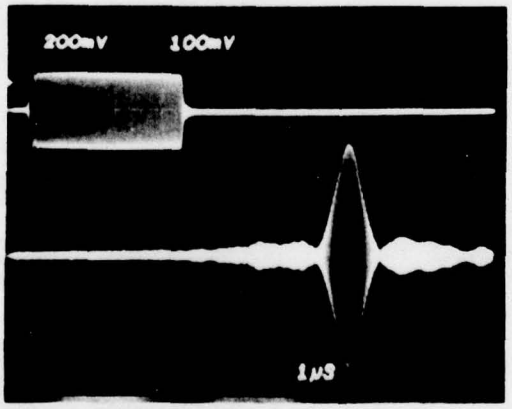

CHIRP INPUT

f_1 = 70 MHz ⟶ 72 MHz

f_3 = CORRELATION OUTPUT

77–11–209–4

FIG. 5–17

64 PFFM
CONFIGURATION FOR MATCHED PAIR ENCODER–CORRELATOR EXPERIMENT

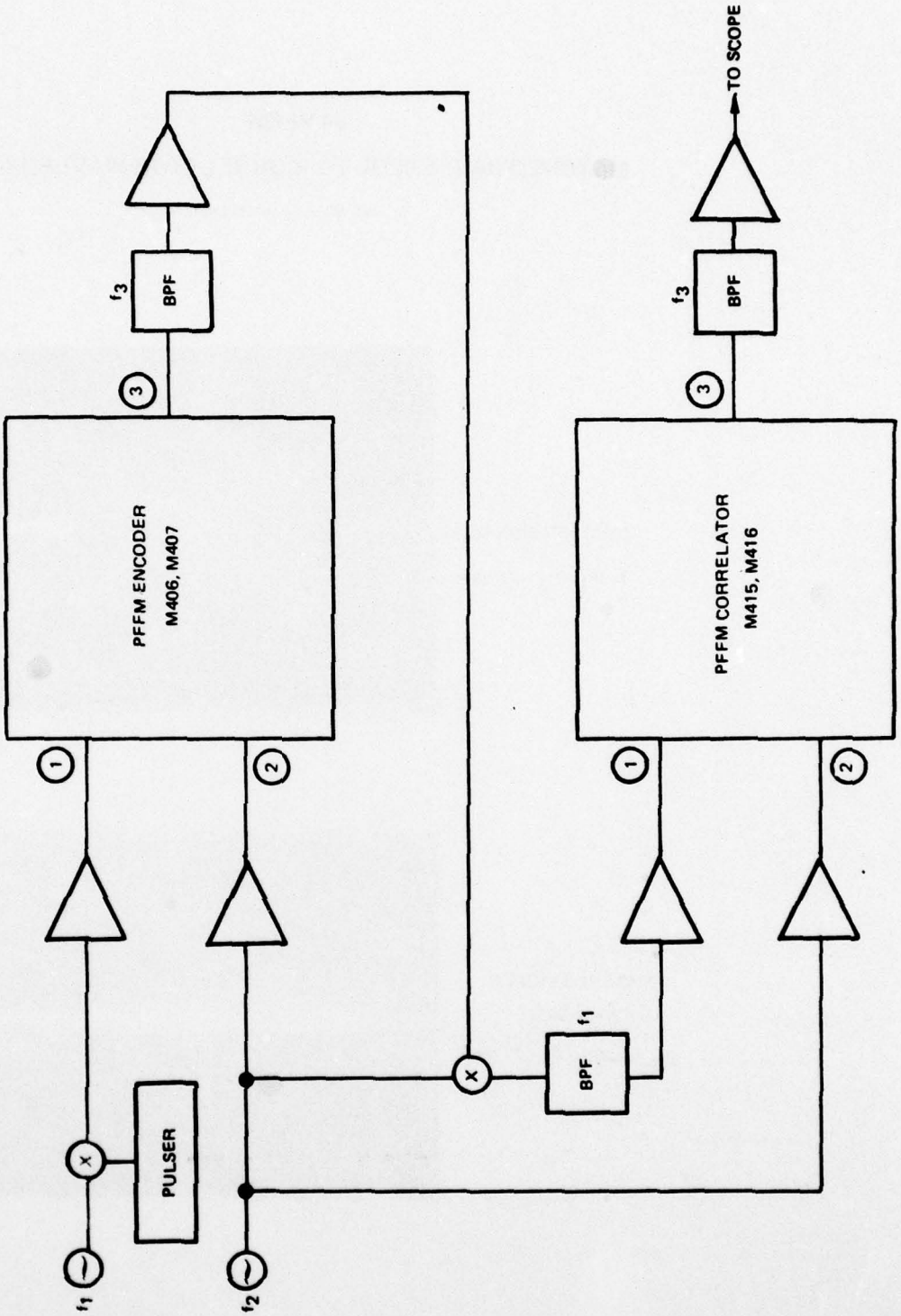

78–04–262–3

64 PFFM

MATCHED PAIR ENCODER–CORRELATOR WAVEFORMS

f_1 = 69 MHz, f_2 = 100 MHz

ENCODED SIGNAL AT

f_1 ($P_1 = P_2$ = 27 dBm)

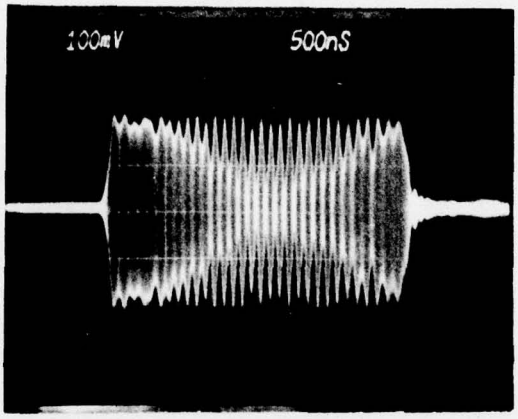

MATCHED FILTER

RESPONSE

(P_1 = 10dBm, P_2 = 27 dBm)

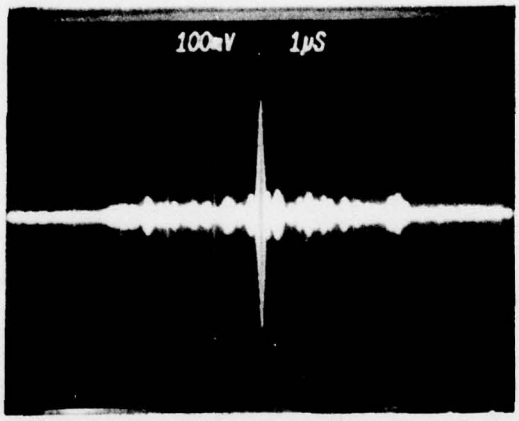

13 dB

78–04–262–1

performed within the programmable chirp filter itself accomplishes the premultiplication step, so that the need for an external premultiplying discrete mixer is eliminated. In the following, the application of the PFFM to CZT processing is developed and the experimental performance of the 64 tap PFFM is demonstrated.

The difference frequency output voltage of the dual acoustic channel PFFM is, in general, given by

$$V_3(t) = A\sum_{p=0}^{P-1} g_p V_2(t-t_p)\, V_1(t-t_p) \tag{5-11}$$

where A is a proportionality constant, g_p is the complex tap weight of the pth tap positioned at time $t_p = p\Delta t$, annd ΔT is the intertap time delay. We shall assume that the input chirp is applied to Port 1, and the signal to be analyzed is applied to Port 2. These waveforms then have the form

$$V_2(t) = M(t)\, e^{j\omega_2 t} \tag{5-12}$$

and

$$V_1(t) = e^{j(\omega_1 t - \mu_1 t^2)} \tag{5-13}$$

where μ is the input chirp rate. The instantaneous angular frequency of the chirp is given by $\omega = \omega_1 - 2\mu t$.

Substituting Eqs. (5-12) and (5-13) into Eq. (5-11) we find

$$V_3 = A\, e^{j\omega_3 t} \sum_{p=0}^{P-1} g_p\, M(t-t_p)\, e^{j\mu(t-t_p)^2} \tag{5-14}$$

Difference frequency operation and phase matching has been assumed with

$$\omega_2 - \omega_1 = \omega_3$$

and

$$\omega_2 - \omega_1 = 2\pi n\, f_s$$

where n is an integer and $f_s = 1/\Delta T$ is the intertap sampling frequency. By programming the complex tap coefficients, g_p, to match the input chirp rate, such that

$$g_p = \bar{e}^{j\mu' t_p^2} \tag{5-15}$$

the sampled quadratic phase factor within the summation of Eq. (5-14) is removed. The tap coefficient values may be rewritten in terms of the PFFM programmed bandwidth, $B = 2\mu P \Delta T$, over the total filter length,

$$g_p = \cos\left[\pi\left(\frac{B}{f_s}\right)p^2/P\right] - j\sin\left[\pi\left(\frac{B}{f_s}\right)p^2/P\right] \qquad (5\text{-}16)$$

The real and imaginary portions of g_p are programmed separately within each of the dual acoustic channels of the device and the channel outputs combined in phase quadrature.

The form of the CZT is apparent after substituting Eq. (5-15) into Eq. (5-14);

$$V_3 = A e^{j\omega_3 t} e^{j\mu t^2} \sum_{p=0}^{P-1} M(t-t_p)^{-j(2\pi B\, p/P)t} \qquad (5\text{-}17)$$

As pointed out by a number of authors, Refs. (19-21), the input chirp bandwidth and duration, must be less than or equal to half of the filter bandwidth, B, and time delay $P\ \Delta T$, respectively to avoid transform truncation errors.

Equivalent transform operation may also be achieved by interchanging the chirp and signal input ports and appropriately reversing the chirp sense.

The circuit configuration used in our CZT processing experiment is shown in Fig. 5-19. A 5 MHz, 1.6 μsec chirp at frequency f_1 is applied to port 1 of the dual acoustic channel PFFM. The signal to be processed is applied to port 2 and consists of CW carrier at frequency f_2 = 103.9 MHz which is modulated by the waveform M(t). The outputs from the 32 taps of each channel were combined in phase quadrature and bandpass filtered to pass the difference frequency transform output. The programmed chirp rate of μ = 3.1 MHz/μsec matched the input chirp rate and utilized the full 9.8 HHz bandwidth of the processor.

The experimental CZT results are shown in Fig. 5-20 for dc and sinusoidal modulation of the carrier at f_2. Input power levels of P_1 = dBm and P_2 = 25 dBm were applied to ports 1 and 2, respectively, from the input amplifiers. Each of the four photographs of Fig. 5-20 show the modulation M(t) in the upper trace and the transform output at 3.1 MHz/μsec in the lower traced. For the case of dc modulation applied as given in the upper left of Fig. 5-20, the dc transform coefficient is displayed with the characteristic sin x/x sidelobe distribution. With pure sinusoidal modulation as shown in Fig. 5-20 for the separate cases of f_m = 1 MHz and 2 MHz modulation frequencies, the corresponding transform coefficients occur at $\pm f_m$. The dc transform component is missing in these cases. In the lower right photograph of Fig. 5-20, a dc component is added to the 2 MHz modulation resulting in the additional dc transform coefficient observed.

FIG. 5-19

64 PFFM CHIRP Z TRANSFORM EXPERIMENT

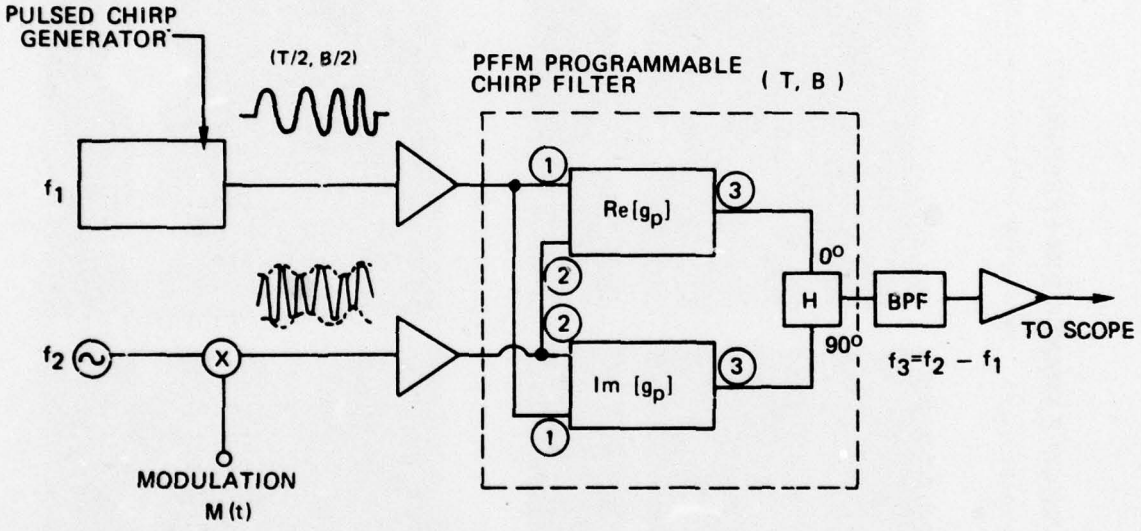

77-11-209-1

64 PFFM CHIRP Z TRANSFORM EXPERIMENT

(DEVICE M406, M407, PROGRAMMED PFFM DISPERSION = 10 MHz/3.3 μS ; INPUT CHIRP f_1 = 67 MHz ⟶ 72 MHz , 1.7 μS; f_2 = 103.9 MHz MODULATED)

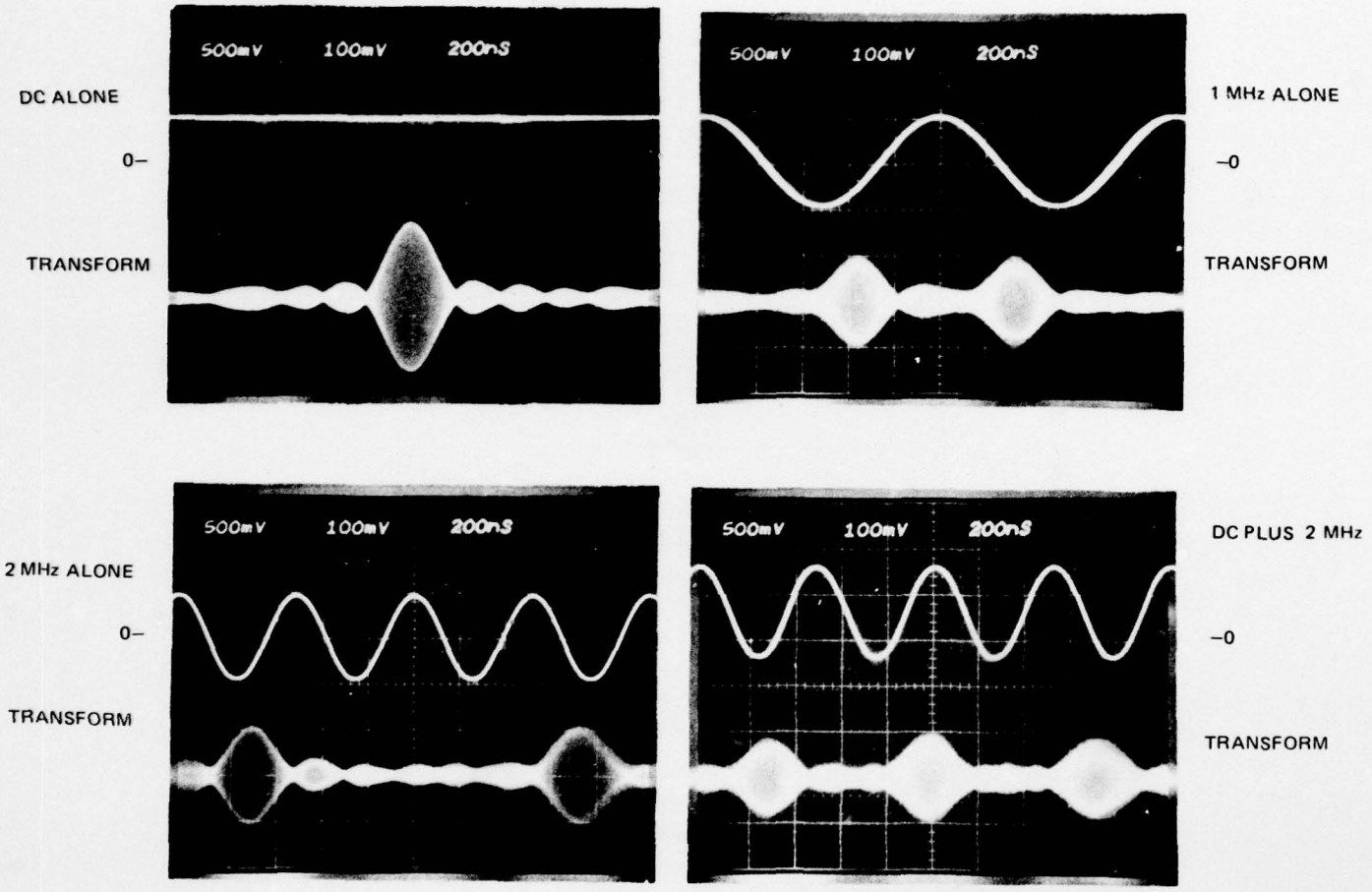

77–11–209–

FIG. 5-20

R78–922667–18

These experiments demonstrate that the PFFM is capable of programmable CZT operation. The nonlinear approach utilized here is more flexible than prior approaches which used fixed chirp delay lines since the transform rate may be varied by tap programming. The premultiplication function is performed within the PFFM itself by means of the tap nonlinearity so that the external premultiplication mixer is eliminated.

6.0 CONCLUSIONS AND RECOMMENDATIONS FOR FUTURE DEVELOPMENT

The Programmable Frequency Filter Module (PFFM) has been shown to provide state-of-the-art performance as an amplitude and phase programmable, 10 MHz sampled transversal filter. Several important filter types have been synthesized using prototype 128 tap devices having real tap coefficient values and 64 tap dual channel devices having complex tap weights. Programmable bandpass filtering has been demonstrated with bandpass variable from .1 to 1 MHz and center frequency tunable from 68 to 76 MHz. Adaptive bandstop filtering has been demonstrated with tunable notch control over a 4 MHz range. The application to programmable correlation matched filtering and encoding of arbitrarily phase and/or amplitude coded waveforms has also been demonstrated. The operation of a matched PSK encoder/correlator pair yielded a 21 dB peak to sidelobe response which was within 2 dB of the ideal correlation response. Variable chirp signal encoding and correlation was demonstrated by programming filter taps in a quadratic phase sequence which matched that of the sampled chirp waveforms. The acoustic filter performance for processing 2 MHz and 10 MHz chirp inputs has shown the capability for processing arbitrarily coded waveforms lying within the device time-bandwidth processing limits. Previous results (Ref. 1) have shown that the filter modules can be cascased for processing long code sequences. Additional application as a Chirp Z Transform processor was achieved by programming the PFFM taps as a chirp filter whose response is related to the discrete Fourier transform of the video modulation applied at an input port. Since the chirp slope of the filter may be electronically varied, the transform rate may be tailored to suit a particular system requirement.

A new balanced diode mixer tap configuration has been utilized which provides tap amplitude control over dynamic range exceeding 40 dB while minimizing tap phase errors. Perturbation techniques have been formulated which would remove the residual tap phase errors which are predictable as a function of tap weighting. The predicted perturbed tap weights applied to the real and imaginary filter channels could be directly incorporated within the tap programming law under eventual microprocesor control.

Although the present devices have been designed specifically for a 9.8 MHz tap sampling rate, extention to rates approaching 100 MHz is feasible without appreciable increase in device power consumption or complexity. While the lithium niobate delay lines utilized are capable of providing the high bandwidths desired, their inherent large temperature coefficient of time delay at first appears to be a significant disadvantage. However, the nonlinear approach utilized provides a method for directly compensating for the temperature induced linear phase errors along the delay line by offset of the CW reference frequency. For the correct frequency offset, the total phase error of the difference frequency tap outputs is nulled. The correct reference frequency offset versus temperature can be achieved by deriving the reference frequency from a SAW+ oscillator located on the lithium niobate substrate so that the oscillator frequency automatically satisfies the temperature compensation condition. Preliminary experimental verification of the basic approach has permittedd operation of a diagnostic lithium niobate correlator over a 100°C range with signal processing results comparable to those predicted for an equivalent ST quartz device.

While significant progress has been made during this program in the development of a high dynamic range, programmable balanced mixer tap configuration, further developmental work remains in the areas of device design and fabrication. Intertap mechanical reflections and electrical coupling, although reduced considerably through theuse of the inclined tap geometry and balanced mixer tap design, presently limit the control dynamic range of one tap of a P tap array to over 25 dB as compared to a control range of greater than 40 dB for a single isolated tap. Spurious reflection could be further reduced by offsetting the taps by a greater amount which in the limit would provide separate acoustic propagation paths for each tap. This approach is particularly applicable to devices having 64 or less programmable taps because of the corresponding increase in delay line dimensions and insertion loss. One method of achieving greater electrical isolation between taps is envisioned by providing integrated circuit buffer amplifiers between groups of taps. The balanced mixer configuration by itself provides significant electrical isolation by reducing the level of the fundamental frequency components at the p^{th} tap due to initial detection of the q^{th} tap. Further transducer design improvements are also warranted for reducing electromagnetic feedthrough and reflection between input ports.

In the area of device fabrication, the microelectronics wire bonds between the delay line taps and silicon on sapphire mixer arrays could be eliminated by a "flip chip" bonding technique which would provide a more rigid hybrid circuit structure. While little attempt has been made to reduce the overall package size of the devices developed under this program, the fundamental small delay line size and low device power dissipation inherent in the approach offers considerable advantage for mobile and expendable device applications. These advantages, coupled with development toward higher processing bandwidth, temperature compensation, and greater tap control accuracy, provide a programmable transversal filter technology which may satisfy diverse filter requirements of present and envisioned military systems.

7.0 REFERENCES

1. Grudkowski, T. W. and T. M. Reeder: Programmable PSK Correlators Utilizing Nonlinear SAW Delay Lines. Technical Report N00014-75-C-0978, Naval Electronics Systems Command, October 1976.

2. Reeder, T. M. and M. Gilden: Convolution and Correlation by Nonlinear Interaction in a Diode-Coupled Tapped Delay Line. Applied Physics Letters, Vol. 22, pp. 8-10, January 1973.

3. Reeder, T. M., J. M. Speiser, and H. J. Whitehouse: Real-Time Discrete Fourier Transforms Using a Programmable Diode-Convolver Module. Proceedings of the IEEE Microwave Symposium, pp. 365-367, IEEE Catalog No. 75 CH0955-5, May 1975.

4. Reeder, T. M. and T. W. Grudkowski: Real-Time Fourier Transform Experiments Using a 32 Tap Diode-Convolver Module. Proceedings of the IEEE Ultrasonics Symposium, pp. 336-339, September 1975.

5. Reeder, T. M. and J. L. Swindal: Variable Acoustic Surface Wave Correlator. Final Technical Report, Contract DAAB-07-73-C-0194, U. S. Army Electronics Command, Fort Monmouth, New Jersey, November 1974.

6. Reeder, T. M. and T. W. Grudkowski: Large Bandwidth Diode-Convolver Using An Exceptionally Uniform Silicon-On-Sapphire Diode Array. Electronics Letter, Vol. 11, pp. 530-532, October 1975.

7. Grudkowski, T. W. and T. M. Reeder: Programmable Transversal Filtering Using Nonlinear Tapped Delay Lines. Proceedings of the 1977 IEEE Ultrasonic Symposium, pp. 710-714, IEEE Publication No. 77CH1264-ISU, October 1977.

8. Grudkowski, T. W. and T. M. Reeder: Programmable PSK Diode Convolver. Electronics Letters, Vol. 12, pp. 186-187, April 1976.

9. Tancrell, R. H.: Analytical Design of Surface Wave Bandpass Filters. IEEE Transactions on Sonics and Ultrasonics, Vol. SU-21, pp. 12-22 (January 1974).

10. Rabiner, L. R., R. W. Schafer, and C. N. Rader: The Chirp-Z Transform Algorithm and Its Application. Bell System Technical Journal, p. 1249 (May/June 1969).

11. Lindmayer, J. and C. Y. Wrigley: Fundamentals of Semiconductor Devices, New York: Van Nostrand, Chapter 2, 1965.

12. Fisher, T. S, et al.: Surface Wave Correlator With Inclined Transducer. Electronics Letters 9, p. 55, February 1973.

13. Bristol, T. W.: Analysis and Design of Surface Acoustic Wave Transducers. Proceedings of the Aviemore SAW Device Seminar, IEE (British) Publicatin No. 109, pp. 115-129, September 1973.

REFERENCES (Cont'd)

14. Kino, G. S., et al.: Signal Processing by Parametric Interactions in Delay Line Devices, IEEE Trans. on Microwave Theory and Tech., MIT-21, pp. 244-254, (April 1973).

15. Cook, C. E. and M. Bernfeld: Radar Signals. Academic Press, 1967.

16. Cahn, C. R.: Spread Spectrum Applications and State of the Art Equipment. Spread Spectrum Communications, AGARD Lecture Series No. 58, Section 5, pp. 1-111, Hartford House, London, July 1963.

17. Dixon, R. C.: Spread Spectrum Systems. John Wiley and Sons, 1976.

18. Gold, R.: Optimal Binary Sequences for Spread Spectrum Multiplexing. IEEE Trans. on Information Theory, Vol. IT-13, pp. 619-621, October 1967.

19. Hayes, R. M., W. R. Shreve, D. T. Bell, Jr., L. T. Claiborne and C. S. Hartmann: Surface Wave Transform Adaptable Processor System. 1975 Ultrasonics Symposium Proceedings, IEEE Publication No. 75 CHO 994-4SU, pp. 363-370, September 1975.

20. Nudd, G. R. and O. W. Otto: Chirp Signal Processing Using SAW Filters. 1975 Ultrasonics Symposium Proceedings, IEEE Publication No. 75 CHO 994-4SU, pp. 350-354, September 1975.

21. Gerard, H. M. and O. W. Otto: A Programmable Pulse Compression Filter Utilizing Chirp Transform Correlation. 1976 Ultrasonic Symposium Proceedings, IEEE Publication No. 76, CH1120-5SU, pp. 371-381.

22. Alsup, J. M., R. W. Means, and H. J. Whitehouse: Real-Time Discrete Fourier Transforms Using Surface Acoustic Wave Devices. Proceedings Int. Seminar on Component Performance and Systems Applications of Surface Acoustic Wave Devices (Aviemore, Scotland), pp. 278-286, September 1973, IEE Publication 109.

23. Jack, M. A., P. M. Grant, and J. H. Collins: Real-Time Network Analyzer Employing Surface Acoustic Wave Chirp Filters. 1975 Ultrasonics Symposium Proceedings, IEEE Publication No. 75 CHO 994-4SU, pp. 359-362, September 1975.

24. Maines, J. D., G. L. Moule, C. O. Newton, and E. G. S. Paige: A Novel SAW Variable-Frequency Filter. 1975 Ultrasonics Symposium Proceedings, IEEE Publication No. 75 CHO 994-4SU, pp. 355-358, September 1975.

25. Atzeni, C., G. Manes, and L. Masotti: Programmable Signal Processing by Analog Chirp-Transformation Using SAW Devices. 1975 Ultrasonics Symposium Proceedings, IEEE Publication No. 75 CHO 994-4SU, pp 371-376, September 1975.

26. Gerard, H. M. and O. W. Otto: A Programmable Radar Pulse Compression Filer Utilizing Chirp Transform Correlation. 1976 Ultransonic Symposium Proceedings, IEEE Publication No. 76 CH1120-5SU, pp. 371-381.

Distribution List - R78-922667-18

	Number of Copies
Dr. Dennis C. Webb Program Scientific Officer Code 5257 (DODAAD Code N00173) Naval Research Laboratory S.W. 4555 Overlook Avenue Washington, D. C. 20375	(2)
AFPRO United Technologies Corporation Pratt & Whitney Aircraft East Hartford, Connecticut Code FY1715	(1)
Mr. Harold Belcher Code 2415-HB Naval Research Laboratory Washington, D. C. 20375	(1)
Office of Naval Research Branch Office DODAAD Code N62879 495 Summer Street Boston, Massachusetts 02210	(1)
Dr. Larry Summey Code 3042 Naval Electronics System Command Crystal City Washington, D. C. 20360	(1)
Mr. Elliott Ressler Naval Air Development Command Warminster, Pennsylvania 18974	(1)
Mr. Peter Bratt Mitre Corporation P. O. Box 208 - Mail Stop B-190 Bedford, Massachusetts 01730	(1)